SANDIA REPORT

SAND2015-10662
Unclassified Unlimited Release
Printed December 2015

Modeling of the Reactor Core Isolation Cooling Response to Beyond Design Basis Operations – Phase 1

Kyle Ross, Jeff Cardoni, Chisom Wilson, Charles Morrow, Douglas Osborn, and Randall Gauntt

Prepared by
Sandia National Laboratories
Albuquerque, New Mexico 87185-0748

Sandia National Laboratories is a multi-program laboratory managed and operated by Sandia Corporation, a wholly owned subsidiary of Lockheed Martin Corporation, for the U.S. Department of Energy's National Nuclear Security Administration under contract DE-AC04-94AL85000.

Issued by Sandia National Laboratories, operated for the United States Department of Energy by Sandia Corporation.

Available to DOE and DOE contractors from
U.S. Department of Energy
Office of Scientific and Technical Information
P.O. Box 62
Oak Ridge, TN 37831

Telephone: (865) 576-8401
Facsimile: (865) 576-5728
E-Mail: reports@adonis.osti.gov
Online ordering: http://www.osti.gov/bridge

Available to the public from
U.S. Department of Commerce
National Technical Information Service
5285 Port Royal Rd.
Springfield, VA 22161

Telephone: (800) 553-6847
Facsimile: (703) 605-6900
E-Mail: orders@ntis.fedworld.gov
Online order: http://www.ntis.gov/help/ordermethods.asp?loc=7-4-0#online

SAND2015-10662
Unclassified, Unlimited Release
Printed December 2015

Modeling of the Reactor Core Isolation Cooling Response to Beyond Design Basis Operations – Phase 1

Kyle Ross, Jeff Cardoni, Douglas Osborn, and Randy Gauntt
Severe Accident Analysis Department

Chisom Wilson
Technical Assessments Department

Charles Morrow
Advanced Nuclear Fuel Cycle Technologies Department

Sandia National Laboratories
P.O. Box 5800
Albuquerque, New Mexico 87185-0748

Abstract

Efforts are being pursued to develop and qualify a system-level model of a reactor core isolation (RCIC) steam-turbine-driven pump. The model is being developed with the intent of employing it to inform the design of experimental configurations for full-scale RCIC testing. The model is expected to be especially valuable in sizing equipment needed in the testing. An additional intent is to use the model in understanding more fully how RCIC apparently managed to operate far removed from its design envelope in the Fukushima Daiichi Unit 2 accident.

RCIC modeling is proceeding along two avenues that are expected to complement each other well. The first avenue is the continued development of the system-level RCIC model that will serve in simulating a full reactor system or full experimental configuration of which a RCIC system is part. The model reasonably represents a RCIC system today, especially given design operating conditions, but lacks specifics that are likely important in representing the off-design conditions a RCIC system might experience in an emergency situation such as a loss of all electrical power. A known specific lacking in the system model, for example, is the efficiency at which a flashing slug of water (as opposed to a concentrated jet of steam) could propel the rotating drive wheel of a RCIC turbine. To address this specific, the second avenue is being pursued wherein computational fluid dynamics (CFD) analyses of such a jet are being carried out. The results of the CFD analyses will thus complement and inform the system modeling. The system modeling will, in turn, complement the CFD analysis by providing the system information needed to impose appropriate boundary conditions on the CFD simulations. The system model will be used to inform the selection of configurations and equipment best suitable of supporting planned RCIC experimental testing.

Preliminary investigations with the RCIC model indicate that liquid water ingestion by the turbine decreases the developed turbine torque; the RCIC speed then slows, and thus the pump flow rate to the RPV decreases. Subsequently, RPV water level decreases due to continued boiling and the liquid fraction flowing to the RCIC decreases, thereby accelerating the RCIC and refilling the RPV. The feedback cycle then repeats itself and/or reaches a quasi-steady equilibrium condition. In other words, the water carry-over is limited by cyclic RCIC performance degradation, and hence the system becomes self-regulating. The indications achieved to date with the system model are more qualitative than quantitative. The avenues being pursued to increase the fidelity of the model are expected to add quantitative realism. The end product will be generic in the sense that the RCIC model will be incorporable within the larger reactor coolant system model of any nuclear power plant or experimental configuration.

ACKNOWLEDGEMENTS

This work is funded through the U.S. Department of Energy - Office of Nuclear Energy's Light Water Reactor Sustainability Program. Clinton Smith of Phoenix Analysis & Design Technologies (PADT) is acknowledged for providing assistance on the FLUENT efforts in this report, as well as modifying the geometry model of the Terry turbine to make it more amenable for FLUENT analysis with rotating reference frames.

TABLE OF CONTENTS

LIST OF FIGURES

LIST OF TABLES

NOMENCLATURE

AFW	Auxiliary Feedwater
BDB	Beyond Design Basis
BWR	Boiler Water Reactor
BWROG	Boiler Water Reactor Owners' Group
CAD	Computer Aided Drafting
CFD	Complex Fluid Dynamics
CST	Condensate Storage Tank
DOE-NE	U.S. Department of Energy's Office of Nuclear Energy
ELAP	Extended Loss of AC Power
EOP	Emergency Operating Procedure
INL	Idaho National Laboratory
MSL	Main Steam Line
NPSH	Net Positive Suction Head
PRA	Probabilistic Risk Assessment
PWR	Pressurized Water Reactor
RCIC	Reactor Core Isolation Cooling
RCS	Reactor Coolant System
RPV	Reactor Pressure Vessel
SAMGs	Severe Accident Management Guidelines
SBO	Station Blackout
SNL	Sandia National Laboratories
SOARCA	State-of-the-Art Reactor Consequence Analyses
SRV	Safety Relief Valve
TAMU	Texas A&M University
TDAFW	Turbine-driven Auxiliary Feedwater
USNRC	U.S. Nuclear Regulatory Commission
WW	Wetwell

1 INTRODUCTION

This section provides the motivation for Sandia National Laboratories' (SNL) efforts to assist the world-wide commercial nuclear power community in characterizing the behavior of the reactor core isolation cooling (RCIC) system under beyond design basis operations. Also, this section provides background information, the analytical models used for this work, and discussion of the data needs and additional precursors to the modeling efforts.

1.1 Purpose and Motivation

The Fukushima accident demonstrated both the challenges associated with severe accident management, and the importance of understanding the behavior of critical equipment under beyond design basis conditions. The purpose of this project is to improve reactor safety for emergency and severe accident management by understanding real-world performance of critical components (i.e., experimental testing and analytical modeling will allow for RCIC to be more accurately characterized under beyond design basis (station blackout-like and extended loss of AC power) conditions). The current use of conservative assumptions regarding equipment functioning as found in probabilistic risk assessment (PRA) applications limits the anticipated prevention and mitigation options considered for emergency operation procedures (EOPs) and severe accident management guidelines (SAMGs). This work is part of an overall project (***Terry Turbine Expanded Performance Operations Test Program***) that would experimentally test and analytically verify the RCIC steam-driven turbine pump performance under beyond design basis (BDB) conditions. This project would be jointly funded through support from the U.S. Department of Energy's Office of Nuclear Energy (DOE-NE), U.S. nuclear industry, and international stakeholders.

The overall goal of the project is to understand the real-world behavior of RCIC operation under BDB conditions in order to advance our predictive fidelity and applicability in emergency and severe accident prevention and mitigation. Accurate characterization of the RCIC system could have fleet-wide impacts in how EOPs and SAMGs will be implemented (e.g., knowing a RCIC pump will last longer than an hour or two after DC power is lost will allow operators to consider other options for plant recovery or accident mitigation). Further, investigation of severe accident performance may also provide insights into means to improve severe accident performance.

The purpose of this research is to develop a dynamic and mechanistic system-level model of the RCIC turbine/pump system capable of predicting the system performance under BDB conditions that include two-phase water ingestion into the Terry turbine at various potential reactor operating pressures, and to characterize its ability (or not) to maintain adequate water injection with sufficient pump head under degraded operating conditions. This model will also demonstrate the self-regulating mode of operation as was observed in the Fukushima Daiichi Unit 2 accident, where RCIC ran uncontrolled and successfully maintained reactor water inventory for nearly three days. The following sections describe aspects of two-phase flow anticipated to be important in the turbine nozzles and solid wheel turbine buckets, computational tools such as CFD that will support system-level modeling of the RCIC system, and a provisional MELCOR implementation of impulse turbine dynamic models into the MELCOR code to be used in analysis of RCIC operation in beyond design basis conditions.

This work is the first step towards developing a thermodynamically-based analytical model of the steam-driven RCIC system operation with mechanistic accounting of liquid water carryover and pump performance degradation, to be used in codes like MELCOR or MAAP. These insights will provide the basis for experimental design to operate a RCIC pump under extended uncontrolled operating conditions. The full-scale RCIC experiments will support an improved understanding of plant risk, improve plant operations, and provide the technical basis for improving the reliability of an essential plant system as shown in the three main categories below[1]:

1. **Regulatory/Risk:** Test data can reduce plant operational risk and improve regulatory compliance
   - Improved incident response timing and prediction of RCIC performance to determine staffing needed to implement beyond design basis mitigation activities
   - Improved response to regulatory changes associated with post Fukushima Lessons Learned
   - A better prediction of the core damage frequency reduction associated with implementation of beyond design basis mitigation activities
2. **System Improvement:** Improve system reliability; operation of an essential system needed to mitigate/prevent risk dominate accidents
   - Identifies RCIC enhancements and changes in maintenance practices to meet Fukushima Lessons Learned
   - Provides performance data on refurbished hardware (including I&C)
   - Provides for system performance conditions for station blackout (SBO)-like conditions to allow for proper quantification of needed system margins
3. **Plant Operations:** Improves operations during an beyond design basis (BDB) event to mitigate the accident under a wide range of plant conditions
   - Identifies optimal approaches to operate RCIC during a long term station blackout and loss of heat sink
   - Provides data to support identification of RCIC performance conditions could complicate or challenge FLEX implementation
   - Identification of proper handoff conditions from RCIC to FLEX

[1] Letter from BWROG to DOE-NE Federal Programs Manager Richard A. Reister, BWROG-14066, November 21, 2014.

1.2 Background

Prior to the accidents at Fukushima Daiichi, modeling of the performance of key critical components such as the RCIC steam-driven turbine pump and safety relief valves (SRVs) are based mostly on design basis conditions. Their performance under severe accident conditions is poorly known and largely based on conservative assumptions used in PRA applications. For example, common PRA practice holds that battery power (DC) is required for RCIC operation to control the boiling water reactor (BWR) vessel water level, and that loss of DC power results in RCIC flooding of the steam lines. The flooding of the steam lines is assumed to lead to a subsequent failure of the RCIC system due to two-phase water ingestion into the turbine-side of the pump. This assumption for accident analysis implies that RCIC operation should terminate on battery depletion which can range from between 4 hours and 12 hours [1.1]. In contrast, real-world observation from Fukushima Unit 2 shows that RCIC function was affected but not terminated by uncontrolled steam line flooding, and in fact provided coolant injection for three days [1.2].

Similar issues and uncertainties exist for pressurized water reactors (PWRs) as well with the use of the turbine-driven auxiliary feedwater (TDAFW) system to feed steam generators (i.e., the same steam-driven turbine pump is used for RCIC and AFW systems).

Use of conservative assumptions regarding equipment functioning as found in PRA applications may limit the anticipated mitigation options considered for emergency operations and severe accident management procedures. Improvements to reactor safety can be realized for severe accident management if real-world performance of critical components such as the RCIC steam-driven turbine pump can be more faithfully characterized. Improved understanding of this critical component can be realized through a combination of advanced modeling methods such as embodied in the DOE/Industry sponsored CASL project and through large scale testing.

The purpose of this research is to develop a dynamic and mechanistic system-level model of the RCIC turbine/pump system capable of predicting the system performance under beyond design basis conditions that include two-phase water ingestion into the Terry turbine at various potential reactor operating pressures, and to characterize its ability (or not) to maintain adequate water injection with sufficient pump head under degraded operating conditions. This model will also demonstrate the self-regulating mode of operation as was observed in the Fukushima Daiichi Unit 2 accident, where RCIC ran uncontrolled and successfully maintained reactor water inventory for nearly three days. The following sections describe aspects of two-phase flow anticipated to important in the turbine nozzles and solid wheel turbine buckets, computational tools such as CFD that will support system-level modeling of the RCIC system, and a provisional MELCOR implementation of impulse turbine dynamic models into the MELCOR code to be used in analysis of RCIC operation in beyond design basis conditions.

1.3 Analytic Tools

Several analytical tools are being applied to investigate RCIC behavior for severe accidents. The tools include reactor system modeling codes such as MELCOR and RELAP, in addition to computational fluid dynamic (CFD) codes such as FLUENT and SolidWorks Flow. The primary

goal is a mechanistic, system-level model that permits fast execution of long transient simulations (i.e. several hours to days for severe accidents). This will enable simulation capabilities for Fukushima forensic analyses, the development of technically-defensible SAMG/FLEX strategies, and design analysis of potential upcoming RCIC experiments. The intent of using several codes, both system-level and CFD, is to inform and enhance the system-level modeling efforts using focused CFD analyses of key components, particularly where lumped-parameter methods and simple hand calculations have limited capability. An example is CFD analysis of the steam nozzles that drive the RCIC turbine.

The computer codes being applied in the RCIC modeling are briefly described in the following subsections.

1.3.1 MELCOR

MELCOR is a fully integrated, engineering-level computer code that models the progression of severe accidents in light-water reactor nuclear power plants [1.3]. MELCOR is being developed at SNL for the U.S. Nuclear Regulatory Commission (USNRC) as a second-generation plant risk assessment tool, and the successor to the Source Term Code package. A broad spectrum of severe accident phenomena in both BWRs and PWRs is treated in MELCOR in a unified framework. These include thermal-hydraulic response in the reactor coolant system, reactor cavity, containment, and confinement buildings; core heat-up, degradation, and relocation; core-concrete attack; hydrogen production, transport, and combustion; fission product release and transport behavior. MELCOR applications include estimation of severe accident source terms, and their sensitivities and uncertainties in a variety of applications. Design basis accidents in advanced plant designs (e.g., the Westinghouse AP-1000 design and the GE Hitachi Nuclear Energy ESBWR design) have been analyzed with MELCOR.

Current applications of MELCOR include the USNRC sponsored State-of-the-Art Reactor Consequence Analyses (SOARCA) [1.1], and the U.S. Department of Energy (DOE) sponsored Fukushima Daiichi accident analyses [1.2].

1.3.2 RELAP5-3D

RELAP5-3D[2] is a system-level two-phase thermal hydraulic code used in transient analyses of nuclear power plant systems. RELAP5-3D has been developed by Idaho National Laboratory (INL) for the DOE's Office of Nuclear Energy (DOE-NE) to simulate BWR and PWR thermal hydraulic responses during nominal and off-nominal operation.

1.3.3 SolidWorks

SolidWorks [1.5] is a commercially available computer aided drafting (CAD) and analysis software package. SolidWorks is a product of Dassault Systemes SolidWorks Corp. It is being used to generate 3D CAD models of key RCIC components, such as the Terry turbine wheel, buckets, nozzles, and turbine casing. CAD models are essential for proper conceptualization of

[2] In this document, RELAP5-3D is simply referred to as "RELAP."

system-level models. For example, they provide insights into the configuration of buckets and nozzles (e.g. number of buckets and nozzles, nozzle-bucket angle) that can fit on a turbine wheel of a given size–these quantities are 'model parameters' that are required inputs for the system-level MELCOR and RELAP models. The CAD models are also integral to the CFD analyses of RCIC using SolidWorks Flow and Fluent.

1.3.4 Fluent

FLUENT [1.6] is a commercially available CFD code that is currently developed and distributed by ANSYS, Inc. FLUENT is used to investigate key components of the RCIC system, such as the nozzles of the Terry turbine.

1.4 Modeling Needs

As part of this work, SNL determined what information was currently available for modeling, what additional information would be needed, and initial failure modes for the RCIC system. From this, the following post-Fukushima questions and inspections were determined:

Questions for TEPCO:

- Had the original mechanical turbine governors been replaced on the Fukushima Daiichi Units 2 and 3 RCIC systems?
- Where are the Fukushima Daiichi Unit 2 and 3 torus RCIC turbine exhaust and pump suction locations?

Post-accident inspections:

- Does the Unit 2 RCIC over-speed mechanism show to have engaged?
- What is the status of the D/P strainer indicator?
- What is the status of the D/P strainer indicator?
- Does a vibration sensor exist?
    - If so, what is its indication?

SNL realizes that post-accident inspections will not be available for years due to the location of the RCIC pump room. Both rooms are currently buried under debris and are highly contaminated.

Additional information identified as needed for further modeling includes:

- RCIC system elevations and where it taps off the main steam piping
    - Isometric Drawings for one or two BWR/PWR plants
- RCIC turbine exhaust and pump suction locations for multiple BWR plants
    - PWR plants exhaust the turbine to the environment
- Detailed lube oil system drawing/water cooling of turbine-pump bearings
    - Identify which plants in the U.S. use RCIC/AFW pumps with a lube oil system

- Identify which plants in the U.S. use RCIC/AFW pumps with an integral water cooling system

SNL theorizes various potential failure modes for the RCIC pump. The component failure modes were broken into three and the following scenarios were developed:

1. Turbine-side failure scenarios
   - Manual Speed Control – over-speed trip
   - Electrical control with manual over-speed trip
     - Look for cyclic drivers in steam supply
   - Failure / lack of steam drains / rotor damage
   - Metal fatigue failure of the rotor
   - Start/stop of rotor with coast down

2. Pump-side failure scenarios
   - Cavitation damage
     - Time vs NPSH
     - Flow fall off with cavitation damage
   - Plugging of inlet strainer
   - If a multi-stage pump, inter-stage seal failure

3. Lube Oil system failure scenarios
   - Bearing failure
   - Lube oil failure due to water ingress

While this list is not exhaustive, it does provide a first-order look into the development of an experimental testing plan for expanding the operational band for Terry turbines. As an example, Appendix A provides additional discussions and hand calculations on cavitation damage which is deemed likely for each pump-side failure.

Additionally, recent work at Texas A&M University (TAMU) through the sponsorship of the USNRC and a DOE Nuclear Energy University Programs initiative indicates potential pump-side failure due to cavitation. Experimental tests at TAMU indicated thermal stratification occurring within the wetwell [1.7]. TAMU initial experimental results would indicate the entire thermal capacity of the wetwell is not being used during prolonged RCIC operations and could cause higher than expected water temperatures (e.g., at or near saturation temperature) at the suction of the RCIC pump.

1.5 Document Outline

The primary thrust of this report is the documentation of a mechanistic, system-level model that is amenable to coupling with existing transient codes like MELCOR and RELAP. Section 2 describes the development and testing of governing equations for a RCIC (Terry) turbine. CFD analyses of the Terry turbine are provided in Section 3, which provide some novel findings on the operation of the Terry nozzles. Key results from the CFD calculations are integrated into expanded system-level models presented in Section 4. Improved RCIC pump models via

homologous curves are also implemented for the analyses in Section 4. Finally, Section 5 provides a summary of the work and recommended future efforts.

1.6 Section 1 References

[1.1] SNL, NUREG/CR-7110 Volume 1, "State-of-the-Art Reactor Consequence Analyses Project Volume 1: Peach Bottom Integrated Analysis," USNRC, Washington, DC, 2012.

[1.2] R.O. Gauntt, et al., SAND2012-6173, "Fukushima Daiichi Accident Study (Status as of April 2012)," SNL, Albuquerque, NM, 2012.

[1.3] R.O. Gauntt, et al., NUREG/CR-6119, "MELCOR Computer Code Manuals, Vol. 2: Reference Manuals, Version 1.8.6 (Vol. 2, Rev. 3)," Sandia National Laboratories, Albuquerque, NM, 2005.

[1.4] INL, INEEL-EXT-98-00834 Rev. 4, "RELAP5-3D Code Manual Volume 1: Code Structure, System Models, and Solution Methods," INL, Idaho Falls, ID, 2012.

[1.5] Dassault Systems, http://www.solidworks.com/.

[1.6] Ansys, Inc., "ANSYS FLUENT User's Guide," Version 16.2, July, 2015, Canonsburg, PA, http://www.ansys.com.

[1.7] Solom, M., Vierow, K., Nosek, A., "Experimental Investigation of Thermal Hydraulic Limits of BWR RCIC System Operation under Long-Term Operation - DRAFT," 16th International Topical Meetiong on Nuclear Reactor Thermalhydraulics, Chicago, IL, September, 2016.

2 SYSTEM-LEVEL MODEL DEVELOPMENT

Derivation of a novel RCIC model is described here for use in system-level codes such as MELCOR and RELAP. Modern thermal-hydraulic codes (including MELCOR and RELAP) do not have internal models dedicated to simulating the RCIC system in a mechanistic fashion[3]. This is mainly due to the unique Terry turbine used in the RCIC system. Therefore, the RCIC model development in this section concentrates on the Terry turbine more so than the pump. Test calculations are used to gauge the utility of the Terry turbine equations, and these test calculations implement simplified treatments of the RCIC pump. However, the ultimate intent is to couple the Terry turbine governing equations to more comprehensive plant models that use higher-fidelity pump treatments, such as homologous pump curves. Such efforts are described later in Section 4.

A mechanistic model is required for predictability of RCIC behavior in the context of supporting future FLEX/SAMG strategies for severe accidents. This entails the consideration of the dynamic forces imparted to the Terry turbine in order to predict how the system operates outside its design envelope. The Terry turbine operates on an impulse principal where high velocity jets of steam impinge onto rotating buckets imparting momentum to the turbine wheel. Analysis of this type of turbine, akin to a water wheel, amounts to applying Newton's Laws for a rotational system where the forces on the turbine include impulses from water and steam, friction losses (windage), shock losses in the buckets, and torque from the pump shaft. The control volume formulation of angular momentum conservation is used to derive an equation of motion that is being implemented via control functions in MELCOR. The control volume approach readily lends itself to integration with MELCOR or other system codes, and allows for easy identification of model parameters that require derivation through other means such as CFD and experimental measurements. Alternatively, these parameters may simply be used as tuning variables through benchmarking against operating data (e.g., Fukushima data and RCIC startup test data).

A necessary literature review of Terry turbine design is first presented in Section 2.1. The development of a novel and mechanistic RCIC model is discussed in Section 2.2. Test calculations of the Fukushima Daiichi Unit 2 accident sequence are presented in Section 2.3 that show promising initial results.

2.1 Terry Turbine Literature Review

An overview of Terry turbine design is presented here to provide context for the modeling approach. Thorough review of more system-oriented RCIC aspects can be found in other sources [2.1][2.2]. For this work it is sufficient to note that RCIC is a steam-turbine-driven pump that

[3] The term 'mechanistic' is used here and throughout the report literally, i.e. in the sense that the actual working mechanisms of Terry/RCIC turbine are considered by the system-level model. For instance, given that RCIC uses a Terry impulse turbine, RCIC models actually calculate the momentum of the fluid jets exiting the nozzles in order to calculate the torque developed by the turbine. The term mechanistic is not used here to signify the use of very high fidelity methods. Instead, it conveys the fact that simplified (lumped-parameter) but mechanistic models are being used to facilitate the simulation of long transients of large systems.

provides makeup water to the reactor pressure vessel (RPV) following core isolation events. The turbine consumes steam delivered from the RPV via relatively small piping tapped off a main steam line (MSL), and drives a pump by means of a common shaft. The pump takes suction from the condensate storage tank (CST) or the wetwell (WW) of the containment. The turbine discharges steam to the wetwell.

2.1.1 Reaction vs. Impulse Turbine

The Terry turbine is a small, single-stage, compound-velocity impulse turbine [2.3] originally designed and manufactured by the Terry Steam Turbine Company purchased by Ingersoll-Rand in 1974. Terry turbines are currently marketed by Dresser-Rand. Terry turbines were principally designed for waste-steam applications with the following key attributes [2.3]-[2.7]:

1. The turbine and casing are not pressurized out of necessity: it may be at low or even atmospheric pressure;

2. Rapid startup (less than 60 s) is of primary importance;

3. Reliability, resilience under off-nominal conditions[4], and low maintenance are of primary importance;

4. Efficiency is of secondary importance.

The features listed above are quite opposite those of large, multi-stage, high-pressure, high efficiency turbines (for electrical power generation) that are typically considered in thermal-hydraulic codes. For example, RELAP has a turbine component model. Such turbines are generally described as 'reaction turbines' since their operation is strongly dictated by steam expanding through long blades that comprise the various stages of the turbine. The blades form flow channels that act as nozzles. The reaction turbine is effectively comprised of many rotating nozzles, and several stages of the reaction turbine may be at elevated pressure out of necessity. Despite the reaction and impulse monikers, turbines often differ more by degree than by type, since many large turbines incorporate both reaction and impulse stages [2.3]. The Terry turbine is a unique exception to this rule: Technical literature always describes it as a single-stage, 'pure-impulse' machine, where the steam has completely expanded before it enters the turbine [2.3]-[2.9]. Figure 2.1 illustrates the difference between a reaction force and an impulse force.

[4] It is known that Terry turbines can ingest and work through liquid slugs. However, depending on the (automatic) operation of the governor valve, there is a potential for turbine overspeed. The ingress of liquid slows the turbine, which causes the governor valve to open excessively in an attempt to compensate. Upon clearing of the liquid slug, steam flow through the wide-open governor can transfer too much momentum to the turbine, thereby causing it to overspeed [2.5]. For a severe accident scenario like Fukushima unit 2, the functioning of the governor valve after loss of power can be uncertain, depending on the design of the valve and the circumstances of the accident.

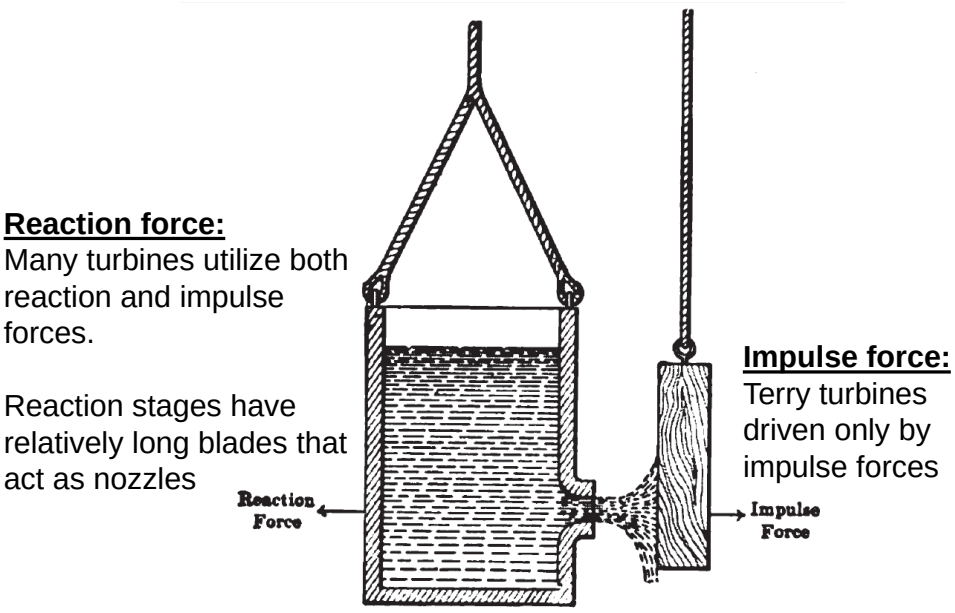

Figure 2.1. Reaction vs. impulse forces [2.4]

In Figure 2.1, the orifice that ejects fluid on the block to the right is equivalent to a *stationary* nozzle in a turbine. The Terry nozzles are detached from the turbine and stationary, much like how the left reservoir with the orifice is detached from the target block on the right (so they move independently). Hence, there is no reaction force on the Terry turbine; reaction forces on the nozzles, which are attached to the casing, also have no direct influence on the turbine. The reaction and impulse force are obviously related since both are manifestations of fluid accelerating through an orifice, and for some turbine applications the close differentiation of the two might be splitting hairs. Nevertheless, the pure-impulse function of the Terry turbine calls for a focused examination on the evolution of momentum from the nozzle and through the turbine during transient conditions (e.g., variable nozzle inlet pressure, two-phase composition, and turbine speed). The unique and simple design of the Terry turbine was probably necessary to satisfy the requirements for its intended applications (i.e. fast start up, reliable, low maintenance, etc.). It is rather commonsense that existing codes like MELCOR and RELAP have no existing physics capability to faithfully represent the Terry turbine, given its unique nature. This substantiates the need for a novel Terry turbine model.

2.1.2 Terry Turbine Overview

The Terry turbine is essentially a solid cylindrical wheel with several machined semi-circular 'buckets' that are shaped into the body of the wheel. All Terry RCIC applications in the US use a "G turbine frame size" [2.5] that denotes a 24 inch (0.61 m) diameter turbine wheel. Fixed nozzles and reversing chambers surround the wheel inside the turbine casing. Figure 2.2 illustrates the geometry and flow path of steam through the nozzle, turbine buckets, and reversing chambers. The small buckets of the Terry turbine bear little resemblance to the long blades used in multi-stage reaction turbines. Therefore, an effective reaction force cannot develop in such small buckets, even if the turbine was at high pressure and the steam had not fully expanded through the nozzles.

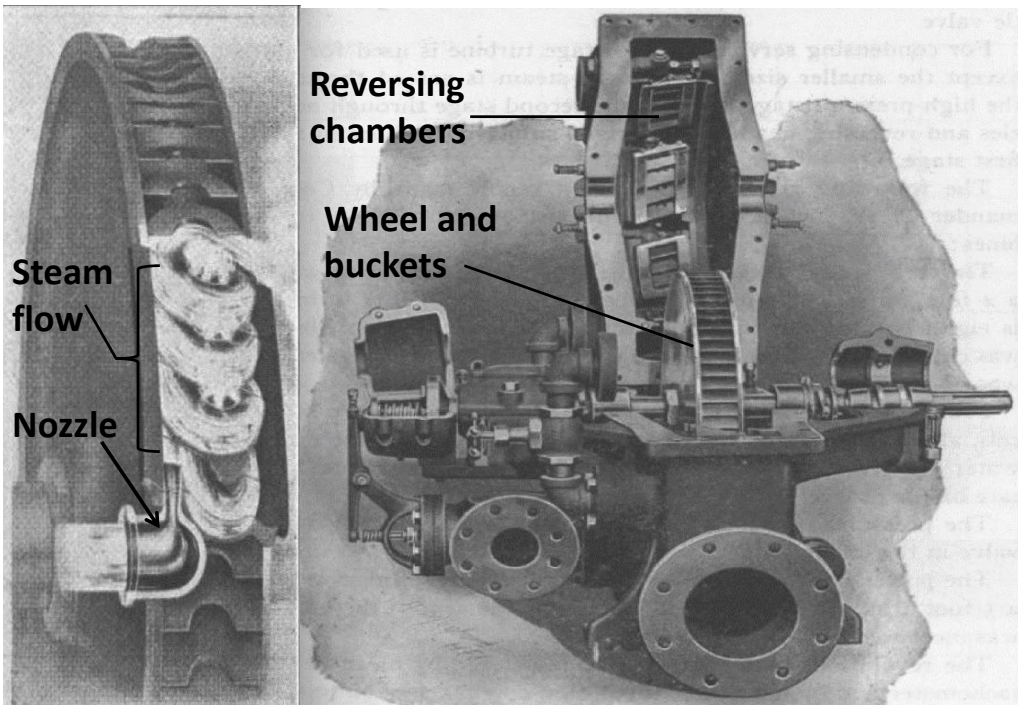

Figure 2.2. Terry turbine bucket flow (left) and interior view of turbine case (right) [2.8][2.9]

Steam enters the semi-circular buckets after expanding through five to ten nozzles that are fixed around the wheel; steam flow direction is reversed 180^{o} in the buckets. The nozzles are separated by at least three buckets to make room for reversing chambers that also surround the wheel. Since the steam is completely expanded after exiting the nozzles, which are fixed and detached from the turbine wheel, the expansion process itself imparts no energy on the turbine [2.6]-[2.8]. For this reason, the pressure drop and the enthalpy change over the RCIC turbine are essentially zero, especially if no phase change occurs after steam enters the turbine. This is in direct contrast to the operation of a reaction turbine where steam expands in the turbine blades, and the blades themselves act as nozzles. Hence, the typical formulas and relationships for multi-stage reaction turbines are not valid for mechanistic analyses of RCIC turbines. Being a pure impulse turbine, RCIC principally operates on the exchange of momentum and kinetic energy. Turbine motion is induced by means of steam acceleration in the buckets after it has been totally expanded through the nozzles.

The compound-velocity feature of the Terry design refers to the fixed reversing chambers that redirect ejected steam back into the buckets several times. The intent is to capture as much of the steam's kinetic energy as possible–steam is typically reversed three to five times at lower turbine speeds before it is finally ejected through small flow channels in the reversing chambers [2.5]-[2.7]. As shown in Figure 2.2, the reversing chambers are slightly angled to direct the steam forward (in the direction that the turbine spins) into the downstream buckets.

The fixed reversing chambers in Terry turbines are a proven design feature for lower turbine speeds (typically less than 1300 rpm [2.6]), but there is evidence that suggests the reversing chambers are of secondary importance for the higher speeds that RCIC operates [2.6][2.7]. An EPRI maintenance manual for RCIC states that the influence of the reversing chambers is

minimal for speeds above 2500 rpm [2.5]. The rated speed of a typical BWR Terry turbine is around 4000-4700 rpm [2.5]. Therefore, it is reasonable to assume that the reversing chambers are only important for the initial startup of the RCIC. This assumption is physically intuitive upon examination of the Terry turbine geometry: Fluid flow between the buckets and reversing chambers requires proper alignment that probably becomes 'out of phase' when the turbine is at high speed. During startup of the RCIC, the turbine buckets are effectively stationary relative to the steam velocity, and thus there is proper exchange of steam between the buckets and reversing chambers. For typical RCIC operation, the tangential velocity at the turbine radius (i.e. the bucket velocity) may be 20% to 50% (1:5 to 1:2) the steam velocity of steam entering the first bucket. Conversely, Terry turbines were originally designed to have a bucket to steam velocity ratio of about 1:8 to 1:10 [2.7]. The relatively slow bucket velocity of the original Terry applications (which date back over 100 years) supports the assertion that the reversing chambers were more important for low speed turbine applications.

2.1.3 Literature Review Key Findings

The model derivation in Section 2.2 makes use of the following set of assumptions/assertions that are based on literature review of design, operation, and maintenance of Terry turbines:

- RCIC uses a single-stage Terry impulse turbine that functions according to exchange of momentum and kinetic energy.
- Steam enters semi-circular buckets and reverses direction (~180^o).
- The reversing chambers are only important for low speed operation, such as during initial startup.
- The expansion of steam after the nozzles is total; the expansion process converts the static pressure (enthalpy energy) of the steam into kinetic energy to be imparted into the turbine buckets. No meaningful reaction force is developed by the Terry turbine.

2.2 Model Approach and Derivation

Rigorous assessment of RCIC operation for a wide range of accident conditions entails the use of a mechanistic model that dynamically considers the forces imparted on the turbine and predicts the integrated behavior of the turbine-pump. The RCIC model must also be amenable to coupling with system-level codes that simulate the thermal-hydraulics of the reactor coolant system (RCS) for long transients (i.e. several days for severe accidents). Such analyses inherently involve large uncertainties, so it is further desirable that the model be simple enough to facilitate fast computation of many different calculations. A lumped-parameter approach is therefore used to derive governing equations for RCIC.

2.2.1 Governing Equations for RCIC Model

The RCIC governing equation is based on a control volume formulation of the angular momentum equation where the control volume is an enclosure surrounding the turbine buckets

that slices through the shaft of the turbine-pump; the nozzles are outside the control volume. This approach is adapted from Reference [2.10] for a control volume analysis of a Pelton turbine, which is similar to a Terry turbine in theoretical and design aspects. The turbine responds principally to the impulses of vapor and liquid water that exit the nozzles. A key quantity is thus the momentum flux of the fluid delivered to the turbine buckets. The momentum flux of the fluid recirculated by the reversing chambers is probably only significant during system startup.

The main impedance to turbine acceleration is resistance from the centrifugal pump. The turbine and pump are connected by a common shaft. Therefore, the turbine speed must equal the pump speed at all times, and the forces resisting the pump are felt instantaneously by the turbine. The pump displaces volume of fluid (water) against head of fluid being pumped, i.e., losses in the RCIC injection piping and RCS, and the RPV pressure being pumped against. Other resistance forces on the turbine itself include friction losses (e.g., windage) and so-called shock losses [2.11] that are the result of fluid streams entering buckets at the wrong angle. Shock losses for the RCIC might be important for high speed operation where the reversing chambers no longer function ideally, especially under two-phase conditions where significant water flashing may disturb the nominal flow patterns; this is a potential avenue for future CFD and experimental investigations. However, these loss mechanisms are currently neglected, and only the first-order forces on the turbine are considered: the fluid impulses in the buckets and the pump resistance.

Equation 2.1 provides the pertinent scalar component of the angular momentum relationship for a control volume [2.10]. The turbine is assumed to be adiabatic, which is probably a good approximation for a pure impulse turbine. The turbine only spins in one direction along a stationary axis, which is the θ-coordinate for a cylindrical (r-θ) coordinate system. The control volume for the RCIC turbine is a cylindrical boundary about the wheel and buckets that intersects the shaft. The coordinate system for this control volume is centered at the axis of the wheel and is stationary; hence the coordinate system is inertial and Equation 2.1 is valid. An example of a non-inertial configuration would be a turbine inside a system that is accelerating, such as an airplane.

$$\oiint rT_\theta dA + \iiint rB_\theta dV = \oiint ru_\theta(\rho \boldsymbol{u} \bullet d\boldsymbol{A}) + \frac{\partial}{\partial t}\iiint ru_\theta \rho dV \tag{2.1}$$

In Equation 2.1, r is the radius of the turbine wheel, T_θ is a force function over the surface of the control volume (with area A and volume V), B_θ is a body force such as gravity, $\boldsymbol{u}$ is the velocity vector, u_θ is the tangential component of the outlet velocity of the fluid leaving the bucket, and ρ is the fluid density. The tangential outlet velocity introduces additional important variables such as the nozzle-bucket inlet and outlet angles, the bucket velocity, and the angular speed of the turbine. These relationships may be resolved using velocity triangles. Appendix B describes how the tangential outlet velocity for the Terry turbine can be written as:

$$u_\theta = r\omega - \left(V_j - r\omega\right)cos\beta \tag{2.2}$$

In Equation 2.2, ω is turbine speed ($r\omega$ is the bucket speed), V_j is the nozzle jet velocity, and β is the inlet/exit angle between the fluid velocity vectors and the horizontal/tangential direction of the turbine motion (i.e. the bucket velocity vector). This angle is discussed more in Appendix B.

Neglecting minor losses, the only torque that penetrates the boundary of the control volume is the shaft torque. The shaft torque, which is also the pump torque[5], must be equal and opposite to the torque developed by the fluid action on the turbine according to Newton's Third Law. Thus the first term in Equation 2.1 may be reduced to:

$$\oiint rT_\theta dA = -T_{shaft} = -T_{pump} \tag{2.3}$$

In Equation 2.3, T_{pump} is the pump torque that is generally a function of other variables including time.

The second term (with B_θ) in Equation 2.1 is zero because this analysis neglects gravity. For one-dimensional inlets and outlets, the third term in Equation 2.1 may be rewritten as:

$$\oiint ru_\theta(\rho \boldsymbol{u} \bullet d\boldsymbol{A}) = \sum_{out} |\boldsymbol{R} \times \boldsymbol{u}|_o \dot{m}_o - \sum_{in} |\boldsymbol{R} \times \boldsymbol{u}|_{in} \dot{m}_{in} \tag{2.4}$$

Equation 2.4 shows that this term represents the driving moment of the fluid flow in the buckets. The evaluation of this term for one-dimensional inlets and outlets is commonly demonstrated in introductory textbooks on fluid mechanics (e.g. References [2.10] and [2.12]). For the RCIC model, the cross products in Equation 2.4 can be simplified upon consideration of the Terry turbine geometry. For the Pelton turbine problem from Reference [2.10], where the fluid inlet and out velocities are parallel to the bucket velocity, Equation 2.4 reduces to:

$$\oiint ru_\theta(\rho \boldsymbol{u} \bullet d\boldsymbol{A}) = ru_\theta \dot{m} - rV_j \dot{m} = r\dot{m}\left(u_\theta - V_j\right) \tag{2.5}$$

Equation 2.5 is the difference between the moments of outlet and inlet momentum fluxes for the Pelton turbine, multiplied by the effective outlet and inlet flow areas. This equation neglects losses in the bucket and assumes that the bucket inlet and outlet mass flow rates are identical (given by $\dot{m}$), which reflects mass conservation for the bucket. The mass flow rate through the bucket is assumed to be the same as the mass flow rate exiting the nozzle. Hence at any given time it is assumed that $\dot{m}_{nozzle} = \dot{m}_{bucket}$ and the bucket velocities can be resolved using simple velocity triangles. The details of such pseudo-steady assumptions for the bucket flow may be revised pending CFD and experimental analyses of the RCIC turbine.

The fluid velocities for the Terry turbine are not parallel to the bucket velocity. The fluid enters the buckets from the nozzles at an angle that effectively reduces the moment arm of the momentum flux. From a design perspective, the reduced moment-arm is probably compensated for by the increased number of buckets that can fit into the wheel for the Terry configuration. Figure B.1 and Figure B.2 in Appendix B demonstrate this velocity orientation for the Terry turbine. Thus, Equation 2.4 and Equation 2.5 can be modified for the Terry geometry to become:

$$\oiint ru_\theta(\rho \boldsymbol{u} \bullet d\boldsymbol{A}) = r\dot{m}\left(u_\theta - V_j cos\beta\right) \tag{2.6}$$

[5] This is only true if the pump is perfectly efficient. For the purposes of the RCIC model development, pump efficiency is accounted for later using rather approximate techniques (see Sections 2.2.2 and 2.2.3). Pump modeling is improved through the use of homologous curves, which is described in Section 4 of this report.

Substituting the formula for u_θ (Eq. 2.2) into Equation 2.6 yields the following expression:

$$\oiint r u_\theta (\rho \boldsymbol{u} \bullet d\boldsymbol{A}) = r^2 \dot{m} \omega (1 + cos\beta) - 2r\dot{m} V_j cos\beta \tag{2.7}$$

Using Equations 2.1, 2.2, 2.3, and 2.7, the original governing equation can now be written as:

$$-T_{pump} = r^2 \dot{m} \omega (1 + cos\beta) - 2r\dot{m} V_j cos\beta + \frac{\partial}{\partial t} \iiint r(r\omega - (V_j - r\omega) cos\beta) \rho dV \tag{2.8}$$

Further formulation from this point depends on the implementation scheme into the thermal-hydraulic code. Two possible schemes are developed and described in Section 2.2.2 and Section 2.2.3.

2.2.2 Quasi-steady Scheme

Severe accident transients for LWRs, such as those at Fukushima Unit 2, are rather slowly evolving with respect to time. There are often time periods where important variables such as RPV pressure only change by about 1-10% over the course of several hours. Hence it is reasonable to presume that a quasi-steady form of the RCIC equation may be used to gradually 'steer' the transient thermal-hydraulic calculation. This neglects turbine-pump inertia and forces the RCIC to make instantaneous changes between quasi-equilibrium conditions every time the RCIC inputs (i.e. the momentum and mass fluxes) are updated by the thermal-hydraulic code; the frequency of the input updating is the coupling time step, which is currently set to be every thermal-hydraulic time step in this work.

The time derivative in Equation 2.8 is zero for the quasi-steady scheme. Therefore the angular momentum equation reduces to:

$$T_{pump} = 2r\dot{m} V_j cos\beta - r^2 \dot{m} \omega (1 + cos\beta) \tag{2.9}$$

The instantaneous power developed by the pump is equal to the product of pump torque and angular speed; pump power is also equal to the product of the head (h) and volumetric flow rate (Q) of the pump. Equation 2.10 can then be used to relate the pump torque to the pump head.

$$\text{Power} = T\omega = hQ. \tag{2.10}$$

The pump torque relationship from Equation 2.9 can be inserted into Equation 2.10 and then solved for the pump head. This pump head formula can implemented directly as input for common system thermal-hydraulic codes such as MELCOR.

Upon implementing the pump head formula into the MELCOR model, the relationship is expanded to consider the flow of two phases. The effects of steam and water jetting from the turbine drive nozzles and impinging on the turbine wheel are assumed to be fully distinct and additive in that separate mass flow rate and velocity terms are included for each of the phases in Equation 2.9. In reality there may be important joint influences. Flashing of the liquid and/or condensation of the vapor may be important. The MELCOR flashing model is employed at the

nozzles to capture to first order the deleterious effects of liquid flashing as it exits the nozzles, but this is an area where CFD investigations are expected to contribute important realism. The flashing would likely significantly decrease the energy and momentum available to drive the turbine wheel. This is fundamentally a three-dimensional problem that needs to be analyzed using CFD and/or experiments, which may then be used to introduce and quantify parameters that are applied to the liquid phase terms in the lumped parameter model. The intent is to quantify parameters in a CFD analysis that can be introduced to a MELCOR solution to better account for the reduction in drive potential attributable to flashing.

The pump head formula for two-phase flow that is incorporated into the MELCOR test problem in Section 2.3 is given by Equation 2.11, where v subscripts denote vapor flow and l subscripts denote liquid flow.

$$h = \frac{\eta(\omega,Q)}{Q}[2r\omega(\dot{m}_v V_v + \dot{m}_l V_l)cos\beta - r^2\omega^2(\dot{m}_v + \dot{m}_l)(1 + cos\beta)]. \quad (2.11)$$

Equation 2.11 introduces a parameter η for the pump efficiency, which is generally a function of both the pump speed and the volumetric flow rate (Q) developed by the pump. This term is evaluated using common relationships for centrifugal pumps. Upon implementation into MELCOR, Equation 2.11 is updated every MELCOR time step. In Equation 2.11, r and β are true constants, while the fluid velocities and mass flow rates are calculated by the thermal-hydraulic code, as is the pump volumetric flow rate. Because a differential equation is not being solved for the turbine speed, ω must be updated after evaluation of Equation 2.11. Likewise, the current time step solution of Equation 2.11 uses an 'old' value for ω. Turbine speed is calculated according to Equation 2.12, where ω_{rated} and h_{rated} are model input parameters for the rated pump speed and pump head.

$$\omega = \omega_{rated}\sqrt{\frac{h}{h_{rated}}}. \quad (2.12)$$

2.2.3 Time-dependent Differential Equation Scheme

The quasi-steady approach in Section 2.2.1 neglects the inertia of the turbine-pump. Even though LWR severe accidents generally evolve slowly with time, there are likely certain time periods that would benefit from the use of a differential equation for turbine speed. For instance, the Unit 2 accident sequence exhibits several time periods where the effects of turbine-pump inertia may be important; these include RCIC startup (near 1 hour after scram), the onset of two-phase flow into the RCIC (unknown timing), the pump suction switch from the CST to the WW (near 13 hours), and eventual system failure near 68 hours after reactor shutdown.

Equation 2.8 can be written as:

$$-T_{pump} = r^2\dot{m}\omega(1 + cos\beta) - 2r\dot{m}V_j cos\beta + I(1 + cos\beta)\frac{d\omega}{dt} \quad (2.13)$$

The time derivative term from Equation 2.8 has been replaced with $I(1+cos\beta)\frac{d\omega}{dt}$, where I is the turbine moment of inertia. Appendix C shows the derivation of this term. Equation 2.13 can be rearranged to be:

$$I\frac{d\omega}{dt} + r^2\dot{m}\omega(t) = \frac{-T_{pump}(t)}{1+cos\beta} + 2r\dot{m}V_j\frac{cos\beta}{1+cos\beta} \tag{2.14}$$

Equation 2.14 is a first-order differential equation for turbine speed. If the pump torque was a known function and the coefficients were constants or functions in time, then this equation would be readily solvable by Laplace transformation. Since this is not the case, a constitutive relationship is necessary to solve the equation. Centrifugal pump torque is proportional to the pump speed squared. Therefore the pump torque can be expressed as:

$$T_{pump}(t) = \eta(\omega(t), Q)\frac{T_o}{\omega_o^2}\,\omega^2(t) \tag{2.15}$$

In Equation 2.15, η is an efficiency term that is currently treated as the same pump efficiency defined for the pump head in Equation 2.11. In general, these two efficiencies may not be identical, but the assumption is thought sufficient especially given other known uncertainties. T_o and ω_o are the rated pump torque and speed, respectively. After putting Equation 2.15 into Equation 2.14, the final differential equation for turbine speed becomes:

$$I\frac{d\omega}{dt} + r^2\dot{m}\omega(t) = -\frac{\eta}{1+cos\beta}\frac{T_o}{\omega_o^2}\,\omega^2(t) + 2r\dot{m}V_j\frac{cos\beta}{1+cos\beta} \tag{2.16}$$

It is noted that the same differential equation for turbine speed could be derived directly from the cross product of Newton's Second Law (i.e. $\frac{d\boldsymbol{p}}{dt} = \sum \boldsymbol{F}$). This is consistent with the fact that the angular momentum equation is obtained from the cross product of the linear momentum equation, which is also a statement of Newton's Second Law. The familiar formula is $I\frac{d\omega}{dt} = \sum M$. The evaluation of this equation simply requires careful consideration of the appropriate signs and angles for the various terms that comprise $\sum M$, the summation of moments acting on the turbine.

The only true constants in Equation 2.16 are I, r, and β. The other terms are generally functions of several other variables. If these terms were constant or simply functions of time, Equation 2.16 would be a Riccati equation and an analytical solution might be possible. However, a simple time-discretization scheme is sought for the scoping calculations that can be advanced each time step in unison with a thermal-hydraulic code. The simplest coupling method between the RCIC equation and the thermal-hydraulic code is an explicit scheme where $\dot{m}$, V_j, and η are assumed to be constant between each coupling time step. Thus the equation can be advanced/integrated quite simply over each time step.

An example numerical solution is given here by assuming that $\dot{m}$, V_j, and η can be treated as pseudo-constants over each integration step. These terms are updated each time step by MELCOR for the test calculations in Section 2.3. A simple backward (implicit) Euler scheme is

derived by the following time-discretization of Equation 2.16, where Δt is the MELCOR time step size (alternatively it could be a coupling time step):

$$I\frac{\omega_{n+1}-\omega_n}{\Delta t}+r^2\dot{m}\omega_{n+1}=-\frac{\eta}{1+cos\beta}\frac{T_o}{\omega_o^2}\,{\omega_{n+1}}^2+2r\dot{m}V_j\frac{cos\beta}{1+cos\beta} \tag{2.17}$$

Equation 2.17 is a quadratic equation for ω_{n+1}, the new time step value of the turbine speed. Given the simplicity of this equation and the fact that it only models a single computational node, Equation 2.17 can be solved directly by the quadratic formula.

The implicit Euler solution for ω_{n+1} is given by Equation 2.18 and it depends on the previous time step value for turbine speed, ω_n. Hence for n = 1, ω_1 is the known initial condition and taken to be zero. The negative solution to the quadratic equation is neglected because it would yield negative turbine speeds, and this analysis only considers turbine motion in the positive direction.

$$\omega_{n+1}=\frac{-\left(I+r^2(\dot{m}_v+\dot{m}_l)\Delta t\right)+\sqrt{(I+r^2(\dot{m}_v+\dot{m}_l)\Delta t)^2+4\frac{\eta\Delta t}{1+cos\beta}\frac{T_o}{\omega_o^2}[I\omega_n+2r\psi(\dot{m}_vV_v+\dot{m}_lV_l)\Delta t]}}{2\frac{\eta\Delta t}{1+cos\beta}\frac{T_o}{\omega_o^2}} \tag{2.18}$$

The mass flow rate and momentum flux terms in Equation 2.18 have been expanded to include distinct terms for the liquid (subscript l) and vapor (subscript v) phases, as was done in the quasi-steady scheme (see Equation 2.11). For the differential equation scheme, the pump head quantity that couples to MELCOR is derived using Equation 2.12 in conjunction with the turbine speed from Equation 2.18. The angle ratio from Equation 2.18 is replaced by the constant variable $\psi=\frac{cos\beta}{1+cos\beta}$ for brevity.

2.3 Test Calculations

The RCIC governing equations are tested in a simplified MELCOR model of a generic 2000 MW_{th} BWR. MELCOR is used to simulate the thermal-hydraulic behaviors of the RPV and the two-phase flow through the RCIC steam piping. Because the RCIC turbine discharges steam to the wetwell, which is at a much lower pressure than the RPV, MELCOR must also model two-phase choked flow (as appropriate) at the governor valve and the turbine nozzles. The turbine dynamics are resolved using control functions (i.e. user-formulas that the code calculates each time step) containing the equations from Section 2.2. In this test model the turbine discharge flow to the wetwell is not modeled (although it could be), and hence the wetwell pressure must be imposed as a boundary condition. The wetwell pressure is most important in determining the wetwell pool temperature if CST-WW switchover is assumed to occur. If the wetwell pressure is known, the pool temperature can be easily resolved if saturated conditions are also assumed.

2.3.1 MELCOR Nodalization and RCIC Model Inputs

The MELCOR model has a basic nodalization of the RPV and RCIC piping. The RPV is a single control volume; two volumes are between the RPV and the governor valve for the RCIC steam piping; one volume is between the governor valve and the nozzles to represent the RCIC steam

chest, which is actually inside the turbine casing; and three volumes are used to model the pump and its piping. Main steam lines are not represented, and the steam piping from the RPV to the RCIC turbine is at a constant elevation. The turbine region after the nozzles is a time-independent volume that sees the wetwell pressure, which is input as a time-dependent boundary condition based on plant data from the Fukushima unit 2 accident. These model simplifications are chosen intentionally in order to expedite the testing of the RCIC equations and to demonstrate that the model can predict key features of the Fukushima unit 2 accident. A crucial goal of the MELCOR modeling is the demonstration of physically reasonable feedback between the RPV and the RCIC under SBO-conditions comparable to Fukushima Unit 2, i.e., where the RCIC overfills the RPV and a two-phase mixture spills over into the steam piping leading to the RCIC. A schematic of the RPV-RCIC coupling and feedback is given by Figure 2.3.

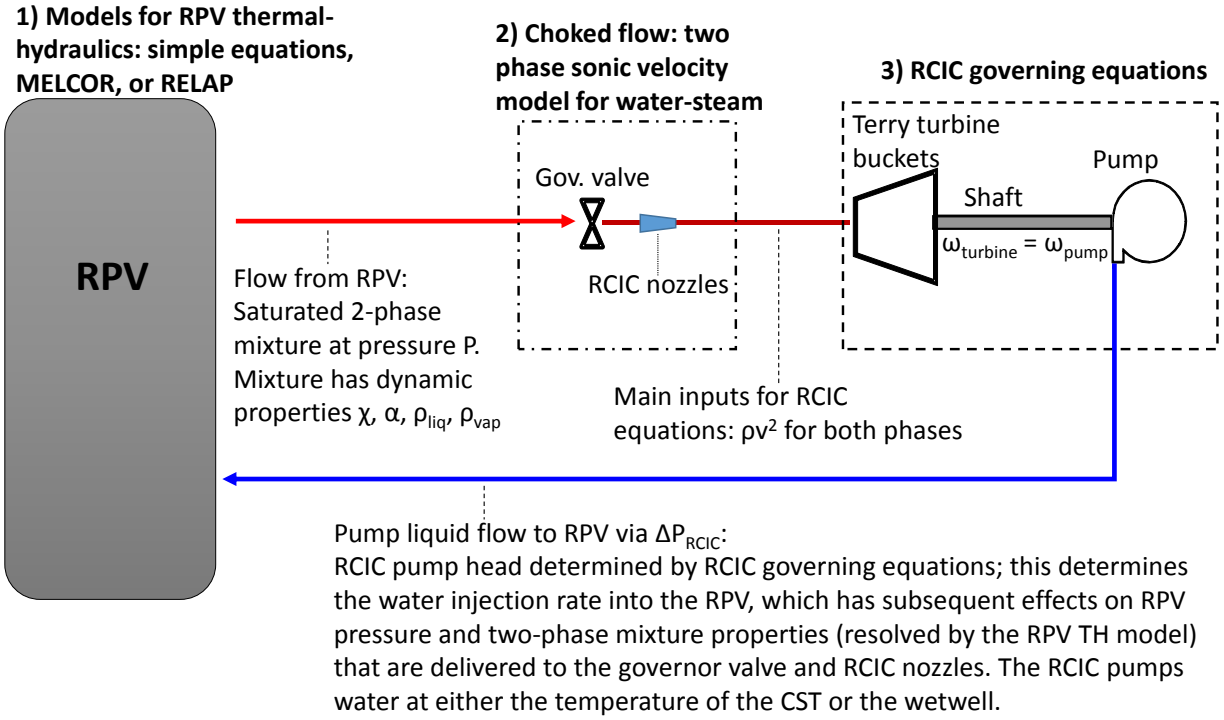

Figure 2.3. Simplified representation of physical coupling in MELCOR test model

A summary of the main inputs and boundary conditions employed in the test calculations is given by Table 2.1. The Fukushima test calculations use plant data of containment pressure to approximate wetwell temperature. The temperature of the wetwell pool is likely considerably higher than the CST temperature, and this has strong impacts on the RPV thermal-hydraulic response after the switch in pump suction. The calculations predict choked flow through the turbine nozzles. Liquid flashing at the nozzles is treated by MELCOR. MELCOR inherently treats the nozzles as converging and yields choked flow at the throats. In reality the nozzles appear to be of converging-diverging design that likely involves supersonic flow near design conditions, according to CFD calculations that are discussed in Section 3.

Table 2.1. Input values for MELCOR test calculations

Input variable	Value
Turbine radius (r)	0.3 m (12”)
Nozzle inlet/outlet angle ($\alpha=\beta$, see Appendix B)	$\pi/4$ radians
Nozzle width	0.01 m (0.39”)
Number of nozzles	5
Turbine moment of inertia (I)	10 kg m^2 (237 lb ft^2)
Rated RCIC speed (ω_{rated}, ω_o)	4300 rpm
Rated pump head (h_{rated})	7.52 MPa (1090 psi)
Rated pump torque (T_o)	449 N m (331 lb ft)
Pump injection flow area	0.0168 m^2 (0.18 ft^2)
CST-WW suction switch	14 hours
WW pool temperature at switch	387 K

2.3.2 Test Results for Fukushima-type Accident Scenario

The MELCOR model and RCIC equations are tested using an accident scenario that is comparable to Fukushima Unit 2. No ‘tuning’ or rigorous benchmarking against data is attempted here. There are still too many unknown and uncertain model parameters (e.g. bucket angles and velocity coefficients) for such an effort to be meaningful. Moreover, the available plant data is very sparse. The test calculations are instead deliberately performed for a non-Fukushima model to demonstrate that the models have not just been forced to agree with the Fukushima data. For example, the model has an arbitrary power level of 2000 MW and boiler properties from SNL’s Peach Bottom SOARCA model [2.13], including relatively high safety relief valve (SRV) setpoints (Peach Bottom is a larger 3500 MW reactor).

The test calculation is an extended station blackout where reactor scram occurs at t = 0. The only credited safety systems are RCIC and the automatic SRV operation. After t = 1 hour, the RCIC is allowed to run uninhibited by any controllers (i.e. no operator throttling or automated trips); its behavior is resolved entirely from the RCIC equations from Section 2 and the MELCOR thermal-hydraulic calculations. The calculation assumes that the governor valve is opened fully at 1 hour and all water injection by the RCIC pump flows to the RPV–no water is diverted back to the CST or wetwell. The RCIC pump initially takes suction from the CST, which has a water temperature of about 289 K, and switchover to the WW is assumed to occur at 14 hours in the test calculations. At this time, the WW pool water is assumed to have a temperature of 387 K. Thus the switchover manifests itself as a sudden and large increase in the water temperature that is injected into the RPV by the RCIC.

Figure 2.4 shows calculated RPV pressures compared to the plant data for Fukushima Unit 2. The models are predicting key features of the RPV pressure trend that are in reasonable, qualitative agreement with the plant data, despite the simple nature of the MELCOR model and the deliberate modeling of a non-Fukushima reactor. The first drop in RPV pressure in the models near 2 hours is the result of the RPV filling rapidly due to full RCIC operation, which is more than capable of handling the decay heat and refilling the vessel especially with the governor valve fully opened and no recirculation of injection water. RPV overfill is typically

prevented either by operator throttling (e.g. recirculation of water back to the CST or wetwell via the test and recirculation lines), or by automatic high-level detection that trips the RCIC, neither of which are included in the Fukushima test calculations. During the first hour of the Unit 2 accident, the RCIC was started and stopped at least two times, possibly due to high level and manual restarts, and the operators may have throttled injection before they lost all power due to the tsunami. The operators had restarted RCIC just before the tsunami arrived, after which they lost control of it and it appears to have run until at least 66 hours after scram. The calculations corroborate the notion that the system may have operated in a self-regulating fashion for most of this time period.

The calculations predict complete RPV flooding to the MSL elevation near 3 hours. After the RPV water level reaches the MSL elevation, significant saturated water is ingested by the turbine and void fraction at the nozzles decreases (Figure 2.5), which results in an immediate reduction in RCIC speed (Figure 2.6) and a sharp increase in RPV pressure back to the SRV setpoint. This trend is mainly the result of decreasing sonic velocity at the nozzles due to increased liquid content in the two-phase mixture. In general, the critical velocity for saturated water and steam (a two-phase, one-component system) decreases with increasing liquid fraction as the mixture expands through a nozzle. Thus, the momentum flux that drives the turbine (Figure 2.7) decreases considerably. The increased fluid density of the liquid is not as important since momentum flux is proportional to the square of the velocity.

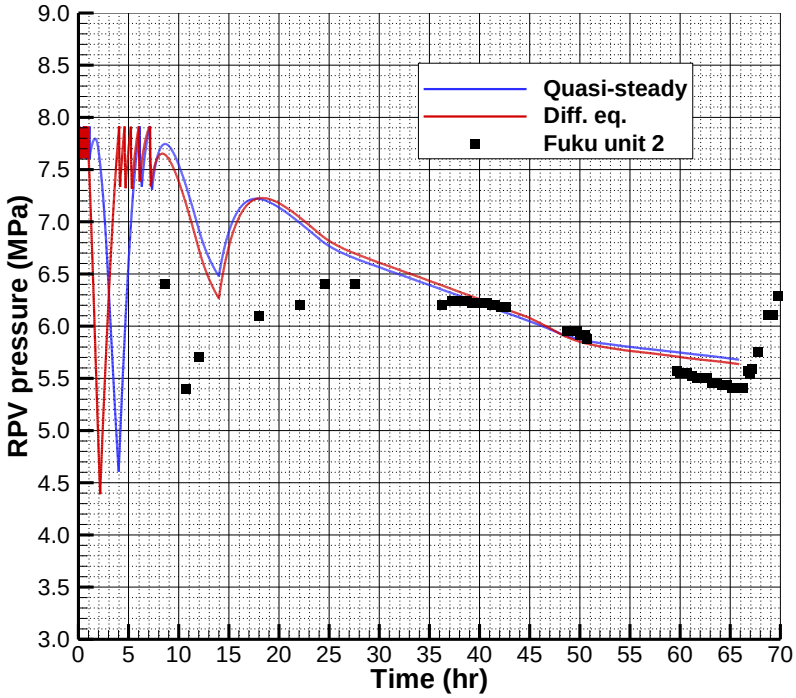

Figure 2.4. RPV pressure for MELCOR test model and Fukushima Unit 2 data

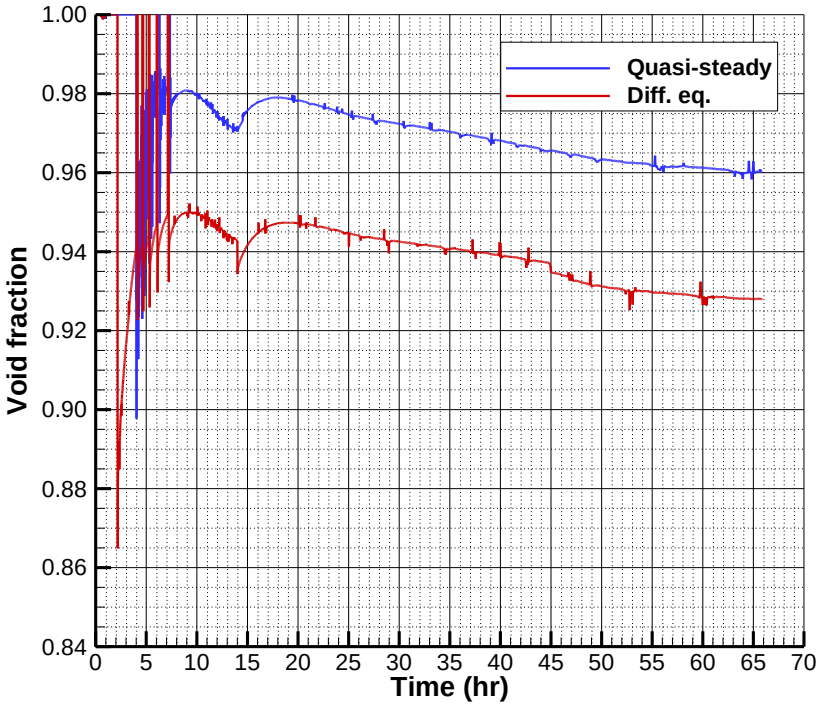

Figure 2.5. Void fraction into turbine nozzles for MELCOR test models

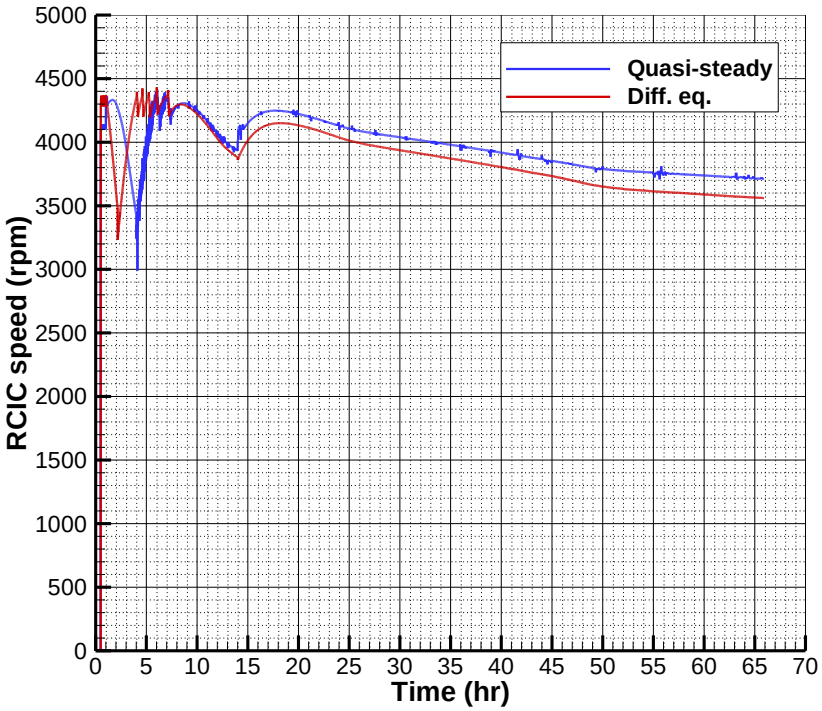

Figure 2.6. RCIC speed for MELCOR test models

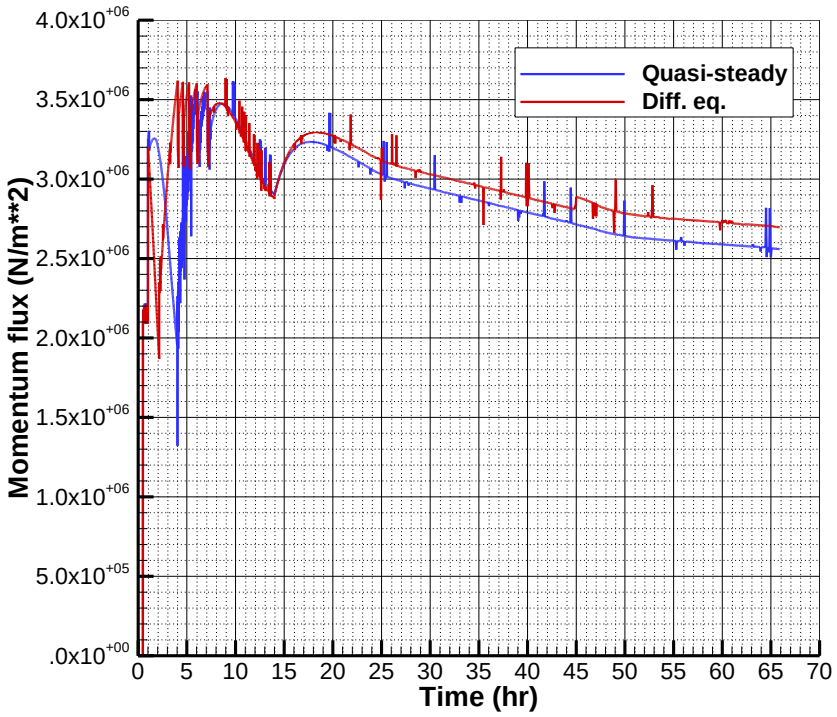

Figure 2.7. Momentum flux through nozzles for MELCOR test models

In conjunction with decreasing decay heat, a few hours of SRV cycling and RCIC operation causes the steam generation rate in the RPV to decrease enough for pressure to drop below the setpoint near 8 hours. RPV pressure continues to decrease until the CST-WW switchover. The sudden injection of hotter water from the wetwell (+100 K relative to the CST) drives an increase in steam generation rate in the RPV at 14 hours. With less subcooling of the injected water, less energy is required to bring the water to the saturation temperature and more energy is used for steam generation that drives the increase in RPV pressure. Afterwards, the higher RPV pressure increases the steam content of the two-phase mixture at the nozzles (Figure 2.5), thereby accelerating the RCIC (Figure 2.6 and Figure 2.7), and suppressing further pressure rise. The acceleration of the RCIC injects more water into the RPV, which subsequently repeats the feedback process of higher liquid content, degraded momentum flux, reduced RCIC speed, and hence reduced injection into the RPV; the system essentially returns to the state it was in before the CST-WW switchover. This is a vital demonstration of reasonable system feedback between the RPV and RCIC. The Fukushima data reveals a comparable trend but the switch in pump suction may have occurred earlier at Unit 2.

2.4 Preliminary Conclusions for System-level Model Development

In conjunction with a literature review of RCIC turbine design, a key conclusion is established that the simplicity and pure-impulse design of the turbine facilitates computational modeling using simplified (lumped-parameter) momentum methods. Preliminary calculations have been performed that show promising initial results. The calculations demonstrate that the RCIC models have the capability to predict feedback between the RPV and RCIC for beyond design basis events without operator action. The results provide physical evidence that the RCIC may

operate in a self-regulated regime for many hours, and this assertion agrees with the current state-of-knowledge for Fukushima Unit 2.

The initial results are encouraging but leave room for future development and improvement. The accuracy of a lump-parameter model is inherently dependent on the proper definition and quantification of several model parameters that require experimental derivation or computational models with higher spatial fidelity. Therefore, CFD models are developed and applied to the Terry turbine; these analyses are described in Section 3. The results from Section 2.3 also suggest that the numerical coupling between the RCS and RCIC has room for improvement. These results used a simple (explicit) coupling scheme between the models, since the RCIC equations are merely input into the MELCOR model via control functions.

Further system modeling efforts will investigate enhanced numerical implementations for coupling the Terry turbine relationships to the thermal-hydraulic code. This will improve stability and precision (not necessarily accuracy) of the model. The modeling of the RCIC pump will also be improved through the use of homologous curves. Expanded system-level analyses using MELCOR and RELAP are discussed in Section 4.

2.5 Section 2 References

[2.1] Nuclear Regulatory Commission, "Boiling Water Reactor (BWR) Systems," available at http://www.nrc.gov/reading-rm/basic-ref/teachers/03.pdf.

[2.2] General Electric, "General Electric Systems Technology Manual, Chapter 2.7, Reactor Core Isolation Cooling System," available at: http://pbadupws.nrc.gov/docs/ML1125/ML11258A311.pdf.

[2.3] A. Jude, *The Theory of the Steam Turbine*, Charles Griffin & Co., LTD., London, England, 1906.

[2.4] J. A. Moyer, *Steam Turbines*, John Wiley & Sons, New York, NY, 1914.

[2.5] J. Kelso et al., "Terry Turbine Maintenance Guide, RCIC Application," EPRI Technical Report, report number 1007460, Electric Power Research Institute, Palo Alto, CA, USA (2012).

[2.6] G.A. Orrok, "Small Steam Turbines," *Transactions of the American Society of Mechanical Engineers*, Washington D.C., May 1909, Vol. 31, pp. 263-287 (1910).

[2.7] W.J.A. London, "A Commercial Analysis of the Small-turbine Situation," *Transactions of the American Society of Mechanical Engineers*, New York, December 1917, Vol. 39, pp. 263-287 (1918).

[2.8] C.W. Dyson, "Test of Terry Steam Turbine," *Journal of the American Society of Naval Engineers*, **21** (3), pp. 884-890 (1909).

[2.9] Author Unknown, "The Terry Turbine-Driven Fans," *Journal of the American Society of Naval Engineers*, **30** (3), pp. 598-599 (1918)

[2.10] I.H. Shames, *Mechanics of Fluids*, pp. 156-166, McGraw-Hill Inc., New York, NY, USA (1982).

[2.11] D.A. Mooney, *Introduction to Thermodynamics and Heat Transfer*, pp. 293-296, Prentice Hall Inc., Edgewood Cliffs, NJ, USA (1955).

[2.12] F.M. White, *Fluid Mechanics*, pp. 167-172, McGraw-Hill Inc., New York, NY, USA (2003).

[2.13] SNL, NUREG/CR-7110 Volume 1, "State-of-the-Art Reactor Consequence Analyses Project Volume 1: Peach Bottom Integrated Analysis," USNRC, Washington, DC, 2012.

3 CFD ANALYSES

CFD analyses of a Terry turbine model are performed to complement the system-level modeling using MELCOR and RELAP. These CFD simulations are focused on investigating key features of the Terry turbine that cannot be sufficiently addressed using system-level models or simple hand-calculations. Some prime examples include:

1. The thermodynamic state of the two-phase mixture exiting the turbine nozzles;

2. The velocity of the two-phase mixture exiting the nozzles and entering the buckets;

3. Bucket flow exit velocity and direction for various RCIC speeds and two-phase mixtures;

4. Effects of the reversing chambers for various RCIC speeds and two-phase mixtures exiting the nozzles (addresses whether or not the reversing chambers have a significant impact on turbine torque);

5. Flashing of a water slug exiting a nozzle, and subsequent impacts on momentum imparted on the turbine buckets;

6. The fluid drag on the spinning turbine wheel from water pooled in the turbine casing;

7. Liquid accumulation on the inlet side of the turbine casing (the steam chest), hypothetically causing a bifurcation in flow through the nozzles (i.e. a portion of the nozzles flow only steam while others are pushing mostly liquid through).

Not all of these phenomena have been examined yet using CFD. Current efforts for this report have concentrated on quantifying the two-phase mixture composition and exit velocity through the nozzles and into the buckets. However, all of the phenomena listed above could potentially have first-order impacts on the torque developed by the Terry turbine.

Thorough understanding of these processes is particularly important for precluding severe accidents, where the plant state might deviate greatly from nominal ranges. For instance, RPV pressure during the first few days of the Fukushima Daiichi Unit 2 accident exhibited dubious peaks and valleys before appearing to continuously linger below the SRV setpoint. RPV pressure influences the inlet pressure for the Terry nozzles, which subsequently affects the supersonic velocities and two-phase composition of the flow through the nozzle. The nozzle flow discharge velocity and two-phase mixture properties are the main variables that determine the momentum delivered to the turbine and thus the developed torque. The water level associated with the RPV pressure trend for Unit 2 was also ambiguous: The sparsity and measurement accuracy of this data notwithstanding, it appears the water level in the Unit 2 RPV was well above nominal. This implies some amount of two-phase steam/water was flowing directly into the turbine for an

extended period of time[6]. The displacement of steam, in conjunction with the flashing of this liquid water through the nozzles (as opposed to a focused steam jet), may severely degrade the effective momentum that drives the turbine. These off-nominal plant conditions have unanticipated consequences on Terry turbine-pump operation that needs to be understood in reasonable detail for the development of mechanistic and predictive models. CFD tools provide a readily available, reproducible, and technically rigorous approach to undertaking such complex flow problems.

The expectation is that the CFD analyses will meaningfully inform and complement the system modeling efforts. Boundary conditions for the CFD analyses are derived from available plant data and preliminary system calculations using MELCOR and RELAP. The CFD predictions will likewise inform and enhance the system-level models. In this way, CFD and system models work harmoniously to support SNL's development of a defensible RCIC model that is capable of informing (i.e. via design analysis) the experimental phase of the Terry Turbine Expanded Performance Operations Test Program.

Section 3.1 presents CFD models of a steam nozzle experiment with (reasonably) known geometry and flow characteristics. This benchmark exercise is necessary to confirm that FLUENT and SolidWorks Flow have the capability to simulate two-phase (with heat and mass transfer) and compressible flow problems. The successful completion of this exercise lends credibility to the CFD predictions for the Terry turbine problem, for which no detailed information is publically available.

Section 3.2 summarizes the development of a 3D CAD model. CAD models are essential for proper conceptualization of system-level models. For example, they provide insights into the configuration of buckets and nozzles that can fit on a turbine wheel of a given size – these quantities are 'model parameters' that are required inputs for the system-level MELCOR and RELAP models. The CAD models are also integral to the CFD analyses of RCIC using SolidWorks Flow and Fluent.

Section 3.3 discusses the results of a simple comparison study between SolidWorks Flow and FLUENT calculations. For this report, these comparisons concentrate on CFD simulations of Terry nozzles.

Section 3.4 presents key FLUENT results for subsequent implementation into the RCIC system models. Currently, these are the supersonic velocities developed by the Terry turbine nozzle as a function of nozzle inlet pressure.

The results, analyses, and discussions in this section are summaries of the CFD analyses to support the RCIC modeling efforts. The CFD model development and calculations performed so

[6] This is in contrast the Terry turbine's known ability to handle *isolated* liquid slugs that may have accumulated in the steam piping. The Fukushima scenario is conceivably the continual ingestion of two-phase liquid at variable composition and pressure over several days, and it includes a switch in pump suction from 'cold' CST water to 'hot' wetwell water.

far are extensive enough to warrant separate documentation[7]. Full accounts of the RCIC CFD work may be given in follow-on reports.

3.1 Steam Nozzle Benchmark Analysis

A simple benchmark study is first performed for a steam nozzle experiment to confirm that FLUENT and SolidWorks Flow have sufficient two-phase flow modeling capabilities. The simulation of two-phase flows with heat and mass transfer using CFD is not a trivial task, especially for three-dimensional, compressible, and turbulent flow problems. The main analytical challenge lies in the steam nozzles for a system like the Terry turbine. Saturated steam flow through a nozzle is known to be a two-phase, compressible flow problem [3.5][3.6]. Therefore, it is prudent to test the CFD codes using a test steam nozzle with defined geometry and compare the predictions against measured data.

3.1.1 Selection of Test Steam Nozzle

A nozzle experiment is chosen that is roughly comparable to the Terry turbine nozzles: The "No. 3, 1 in 6" nozzle from Reference [3.7]. Coincidently, these tests were conducted around the time the Terry turbine was invented. The inlet pressures for the test nozzle are probably much lower than the inlet pressures for the Terry turbine nozzles in RCIC applications. More contemporary test results for saturated steam flow through a nozzle are not readily available, likely owing to the fact that modern steam nozzle applications generally use superheated steam. Documentation for modern steam nozzle tests that include detailed descriptions of the nozzle geometry is particularly difficult to find. The steam nozzle tests from Reference [3.7] are deemed sufficient for a simple benchmark study in this report. Additional CFD benchmarks may be performed against actual Terry turbine nozzles pending the status of the RCIC experimental program.

The chosen test nozzle is about 4.4 cm long with a throat diameter of 0.8 cm. The throat is located 0.88 cm into the length of the nozzle (i.e. near 20% of the nozzle length). The diverging section has a 1 in 6 taper – the nozzle expands 1 unit radially for every 6 units of length. Figure 3.1 depicts the geometry of the test nozzle used in the CFD models. The dimensions of the nozzle throat and diverging section are documented in ample detail by Reference [3.7], but the nozzle inlet region is not well defined. Hence, the geometry of the nozzle inlet plenum is arbitrarily chosen to have a diameter of 2.54 cm (1 inch), and it gradually contours to the nozzle throat.

[7] Given that this report documents model development and analyses using four codes (MELCOR, RELAP, FLUENT, SOLIDWORKS), Sections 3 and 4 provide summaries of the work to keep this report a reasonable length. Otherwise, several hundred pages are necessary to fully describe all of the modeling and simulation details (e.g. inputs, model iterations, solution algorithms/settings, etc.). Separate and focused documents are more appropriate for the CFD and system analyses.

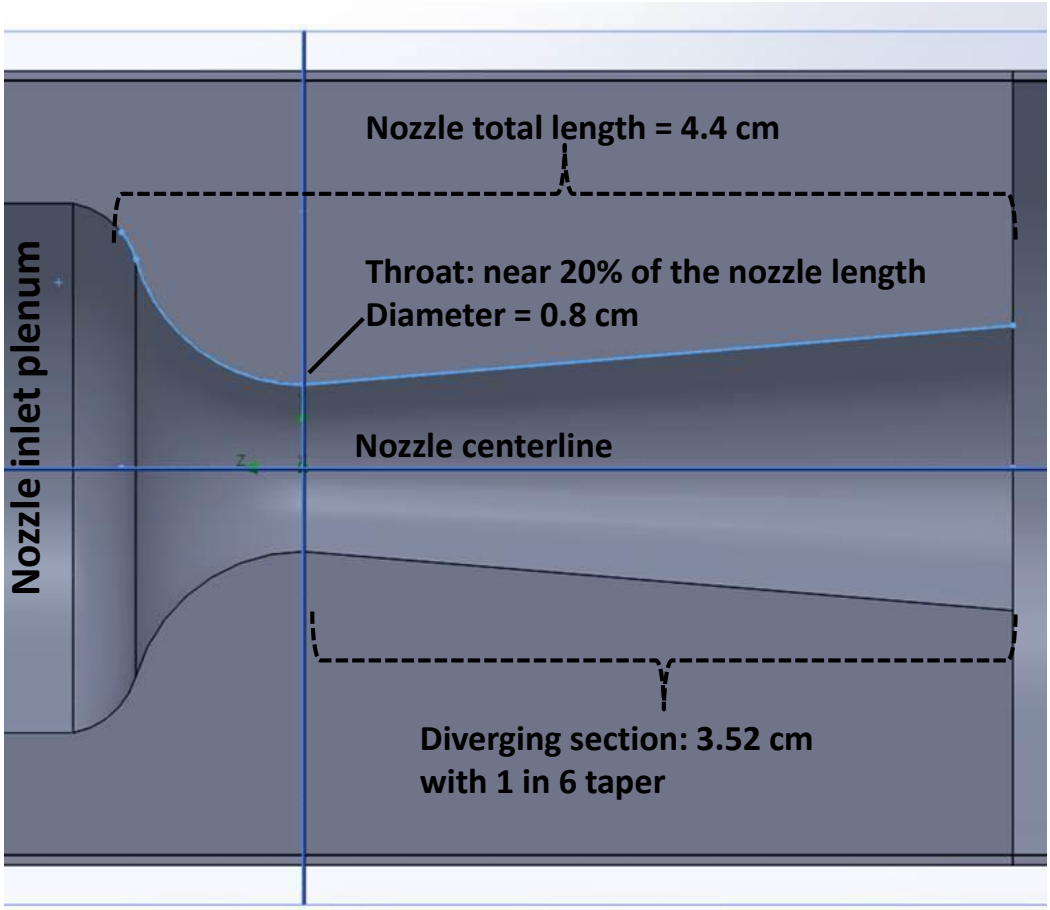

Figure 3.1. Test nozzle geometry for CFD calculations

3.1.2 SolidWorks Flow and FLUENT Models of Test Nozzle

The SolidWorks Flow and FLUENT models of the test nozzle use identical geometry inputs and boundary conditions. The full nozzle test model is depicted by Figure 3.2. The inlet surface is specified to be dry saturated steam at variable pressure (and associated saturation temperature) in accordance with the inlet pressures of the experiment, which range from 30 psig to 120 psig. The outlet surface is assumed to be dry saturated steam at atmospheric pressure. The codes may predict condensation within the domain the model, and liquid condensate may flow out the pressure outlet surfaces. However, backflow (if predicted) is dry saturated steam at atmospheric pressure.

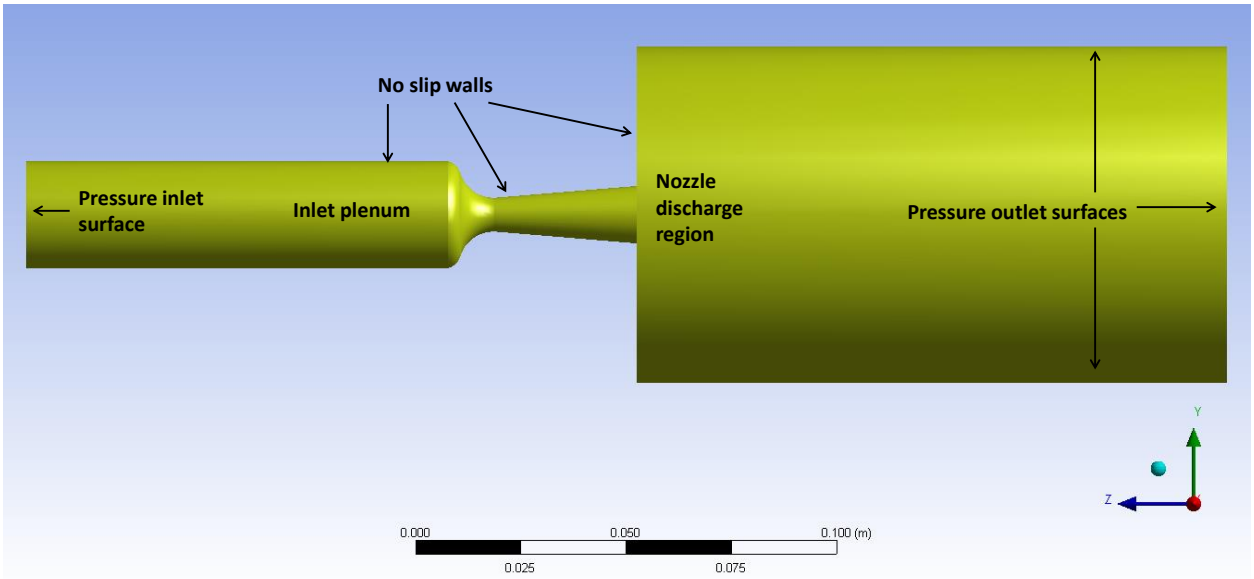

Figure 3.2. Full geometry and boundary conditions for CFD calculations of test nozzle

SolidWorks and FLUENT use different meshes for the nozzle test calculations. The codes have different physics and solution methodologies, and thus the use of distinct meshes facilitate the calculations for the purpose of a gross comparison. The FLUENT mesh is comprised of 182,000 tetrahedral cells with finer resolution at/near the nozzle, as shown by Figure 3.3. The SolidWorks Flow mesh contains a comparable number of cells, but uses cubic cells with different resolution distribution over the model–the size distribution of cells is adaptively refined by SolidWorks for each calculation. A typical SolidWorks mesh for the test nozzle is given by Figure 3.4.

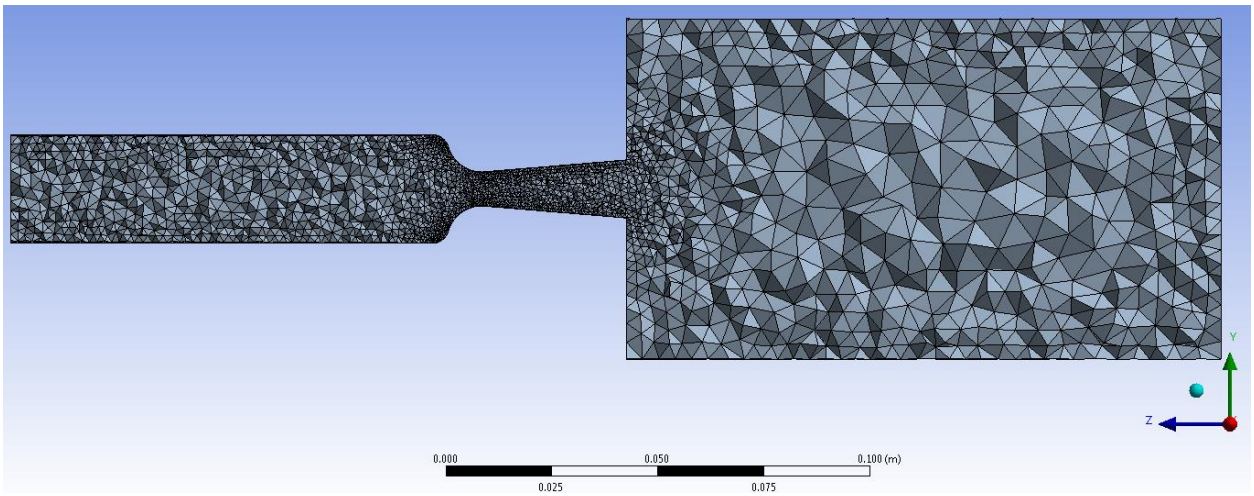

Figure 3.3. FLUENT mesh of test nozzle

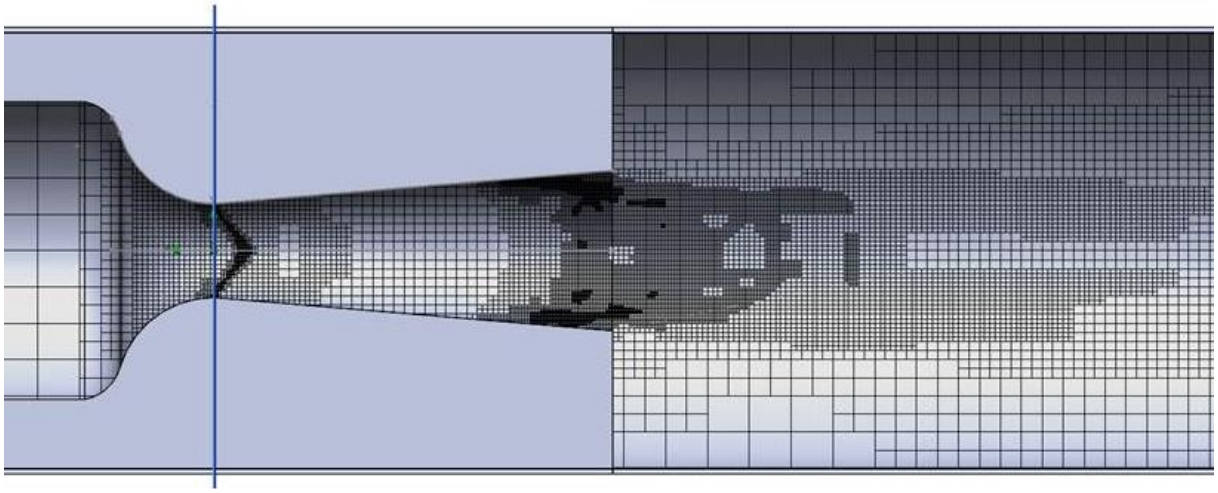

Figure 3.4. Typical SolidWorks Flow mesh of test nozzle

The FLUENT and SolidWorks Flow models of the test nozzle both use compressible, 3D, two-phase, turbulent flow solvers. Both analyses simulate turbulence: The FLUENT calculations use a k-ω turbulence model with the default parameters in the code; the SolidWorks calculations use a k-ε turbulence model with 2% turbulence intensity and 0.01 cm length scale. The wet-steam two-phase model in FLUENT is used for these calculations, which provides a dedicated treatment for water-steam mixtures where the flow is mostly steam [3.8]. The wet-steam model assumes that the secondary (liquid) phase is advected with the vapor phase, and the liquid is essentially fog or mist (sub-micron liquid particles that flow with the steam phase). This two-phase model is selected since it includes dedicated water properties internal to the code, and it can readily simulate the mass/heat transfer between the phases. There are alternative two-phase model options in FLUENT, such as Eulerian and mixture models, but the wet-steam model provided the most stable and fast-running solutions to the nozzle problem. The SolidWorks Flow calculations use a very comparable two-phase modeling option via a real gas formulation dedicated to water-steam mixtures, the details of which can be found in the SolidWorks Flow theory manual [3.9].

Wall friction is approximated in these analyses; the standard wall function models in FLUENT and SolidWorks are used. An alternative, higher fidelity approach could directly resolve the boundary layer by employing a sufficiently fine mesh near the walls, which is sometimes called inflation layer meshing. The wall function treatment should suffice for the simple benchmark study. Thermally, the walls are treated as adiabatic in these analyses.

3.1.3 CFD Results Compared to Test Data

The CFD predictions compare quite well to the nozzle test data. Figure 3.5 depicts the pressure profile along the length of the nozzle; the throat is near 0.2 normalized length. In Figure 3.5, the pressure values for both the CFD calculations and the experimental data reflect values along the wall of the nozzle. The experiment used syphons drilled into the wall of the nozzle to measure pressure, as demonstrated by Figure 3.6. The CFD-calculated pressures near and after the throat are in excellent agreement with the test data. This close agreement is impressive considering that

these are first-attempt calculations (i.e., 'blind' calculations with no tuning) and the fact that the experiment is over 100 years old. The inlet pressure trend before the throat does not have as good agreement: The CFD pressures are considerably higher than the test data. However, the inlet geometry of the test nozzle was not clearly defined in the documentation, and had to be guessed for the CFD geometry. Seeing that the pressures agree very well after the throat, which lends credibility to the CFD calculations, a reasonable deduction is the actual test nozzle had a longer inlet plenum that tapered more slowly to the throat; this would explain the lower pressures exhibited by the test data. Alternatively, the measurements before the throat might be in error, or perhaps the inlet pressures defined for each test case were not properly calibrated, given the fact that the CFD calculations actually reproduce the defined inlet pressures (120, 90, 60, 30 psig) at the entrance to the nozzle.

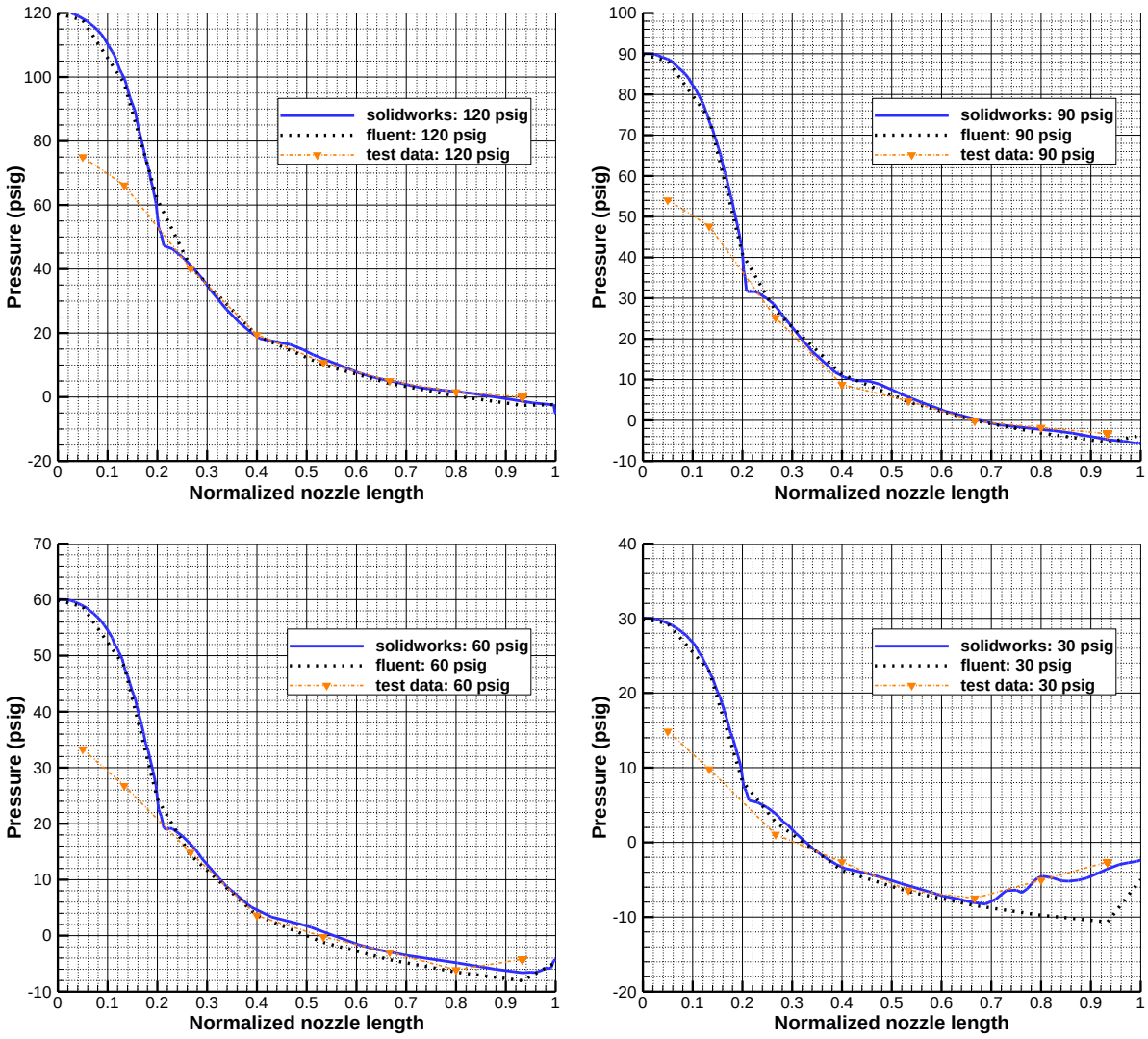

Figure 3.5. Pressure profiles for 120 psig (top-left), 90 psig (top-right), 60 psig (bottom-left) and 30 psig (bottom-right) inlet pressures

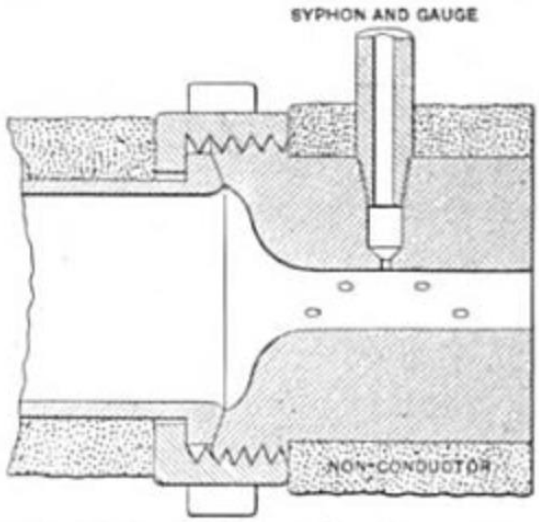

Figure 3.6. Pressure measurement method for nozzle test [3.7]

The pressure test data suggests that shocks develop in the diverging section of the nozzle for the lower inlet pressures (60 and 30 psig). The SolidWorks and FLUENT calculations corroborate this notion. For the 60 psig case, the data shows a shock developing after 80% of the nozzle length, and the CFD models predict a shock developing just after 90% of the nozzle length. For the 30 psig case, the data exhibits a shock after 70% of the nozzle length, which is predicted very well by the SolidWorks Flow calculations. The FLUENT calculation of the 30 psig case shows a shock after 90% of the nozzle length.

Shocks in the diverging section are indicative of over-expanded nozzle flow, which results from too low of pressure drop over the nozzle geometry. The fluid expands too fast through the nozzle and its pressure drops below the outlet pressure; this is evident by the vacuum pressures in the test data and the CFD predictions in Figure 3.5. To reconcile pressure with the outlet, a supersonic compression shock (an increase in pressure) must develop in the diverging section of the nozzle. Over-expanded flow is not anticipated for the Terry turbine nozzles in a BWR/PWR, given the high RPV (or steam generator) pressures for such applications. Higher inlet pressures will push shocks out the nozzle and probably result in under-expanded flow. That said, boiler pressure can vary considerably during a BDB event, and the RCIC governor valve probably has a first-order impact on the effective inlet pressure for the nozzles.

The calculated velocities for the test nozzle agree reasonably well with the test data; the calculated velocities are generally within 5-10% of the experimental values, as shown by Table 3.1. However, this comparison is complicated by the rather high measurement uncertainty in experimental velocities [3.6][3.7], particularly with respect to the available technology when these experiments were performed (around 1900). Like the pressure data, the velocity data does not extend to the very end of the nozzle exit. For simplicity, Table 3.1 compares the test data velocities against the peak CFD values at the exit plane of the nozzle. The measurement location of the test data is closer to 90% of the nozzle length, and this is most important for the 30 psig case that has a strong shock in the diverging section (hence the test velocity is much higher than the CFD values). The sonic velocity of the exhaust is about 330 m/s, as reflected by the CFD exit velocities for the 30 psig case with the shock in the diverging section.

Table 3.1. Velocities near test nozzle exit

Inlet pressure (psig)	Nozzle test data (m/s)	SolidWorks* (m/s)	FLUENT* (m/s)
120	871	926	916
90	874	917	906
60	808	896	894
30	650	332	330

* Listed CFD values are the peak velocities at the nozzle exit. The nozzle test data reflects conditions just before the exit (near 90% nozzle length).

Both CFD codes predict considerable condensation as the steam expands and exits the nozzle. Unfortunately, there is not direct test data for liquid fraction exiting the nozzle. The CFD codes calculate liquid mass fractions up to 13% for the 120 psig case, as demonstrated by Figure 3.7. Qualitatively, the prediction of condensation is well-supported by years of steam nozzle research–saturated steam (including wet steam) condenses when it undergoes sudden expansion [3.5]-[3.8]. Furthermore, examination of a Mollier chart (e.g. see Appendix D, Figure D.3 from Reference [3.11]) can provide an estimate of steam condensation for isentropic expansion. The Mollier chart is an enthalpy-entropy diagram for water-steam mixtures, and Appendix D discusses an example problem for using the chart. It suggests that the steam quality is about 90% (i.e., 10% liquid fraction) after undergoing isentropic expansion from 120 psig to atmospheric pressure. The flow is isentropic if there are no shocks inside the nozzle. Hence, the 60 psig and 30 psig cases have some non-isentropic influences that would require special consideration for hand calculations or proper usage of pre-compiled data like a Mollier chart. Modern CFD tools offer a convenient alternative for such complicated problems.

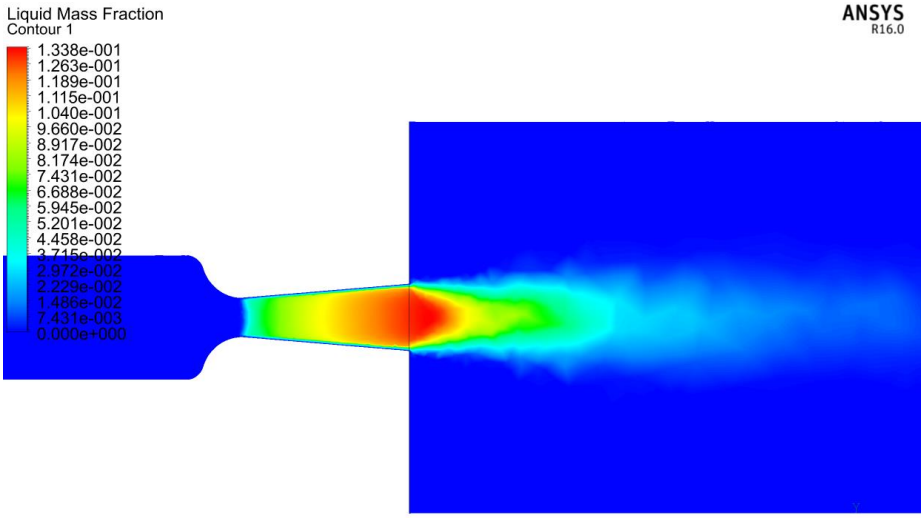

Figure 3.7. Liquid mass fraction for 120 psig FLUENT calculation of test nozzle

The primary conclusion of this simple benchmark study is that SolidWorks Flow and FLUENT have the capability to simulate two-phase steam flow through converging-diverging nozzles. Moreover, converging-diverging nozzles yield supersonic steam flow when the inlet pressure exceeds the back pressure by sufficient margin. This assertion is substantiated by the test nozzle

measurements, two independent CFD analyses (Table 3.1), and technical literature on steam nozzles ([3.5]-[3.8]). Figure 3.8 depicts a velocity contour through the mid-plane of the test nozzle for the 120 psig case, as calculated by FLUENT. Velocity magnitude is supersonic several centimeters from the nozzle exit, which is where an impulse bucket would notionally be located, and there is some evidence of shocks in the beginning of the exhaust plume. Figure 3.9 shows some low-magnitude pressure disturbances that may indicate shocks after the nozzle exit. However, the FLUENT mesh is probably too coarse to illustrate a clear diamond shock pattern. The SolidWorks calculations, which use a dynamically refined mesh, show a clearer shock patterns in the nozzle plume. SolidWorks contour plots of velocity and pressure for the 30 psig and 120 psig cases are shown by Figure 3.10, Figure 3.11, Figure 3.12, and Figure 3.13. The 30 psig results clearly demonstrate over-expanded flow, with resultant flow separation from the nozzle wall and diamond shock patterns downstream of the nozzle discharge.

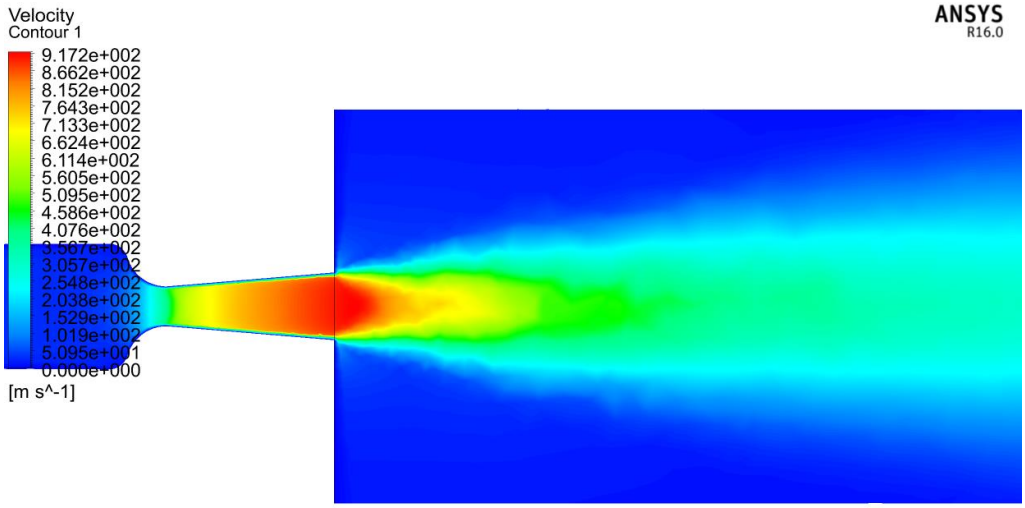

Figure 3.8. Velocity for 120 psig FLUENT calculation of test nozzle

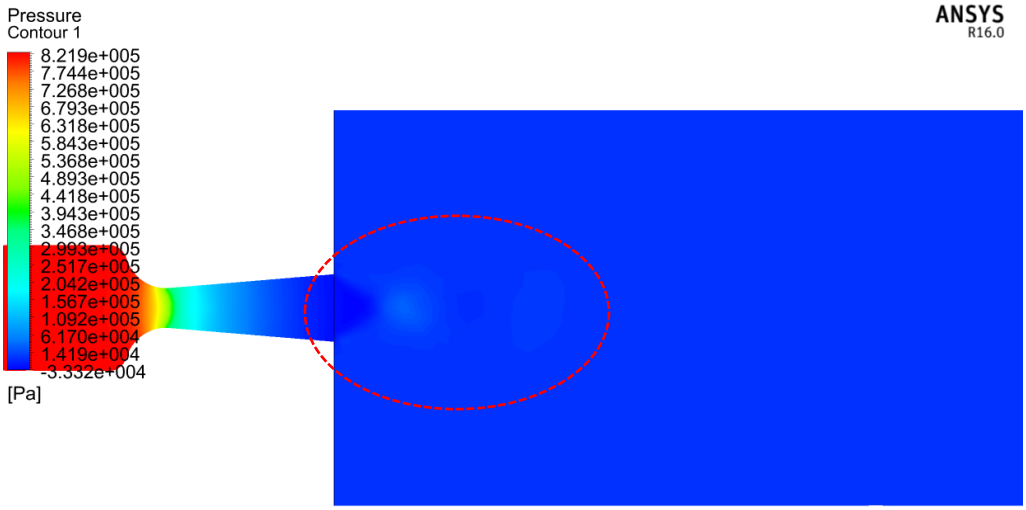

Figure 3.9. Pressure for 120 psig FLUENT calculation of test nozzle

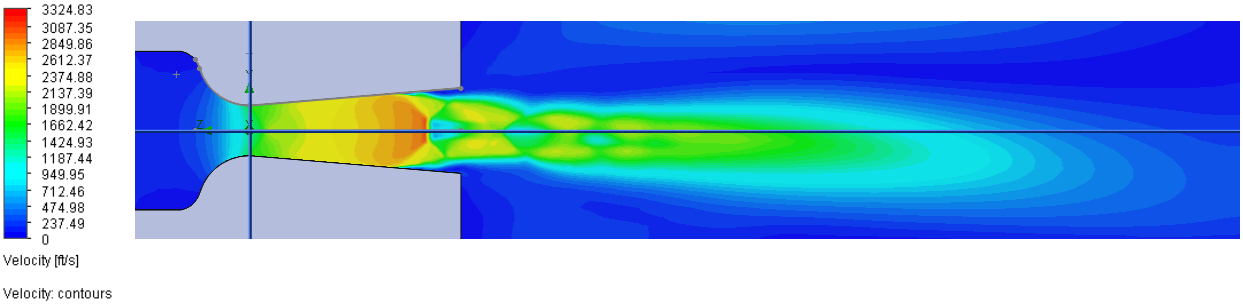

Figure 3.10. Velocity for 30 psig SolidWorks calculation of test nozzle

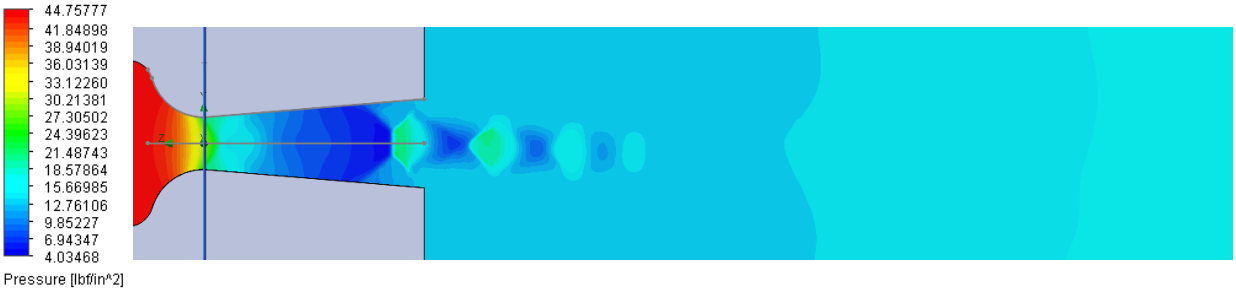

Figure 3.11. Pressure for 30 psig SolidWorks calculation of test nozzle

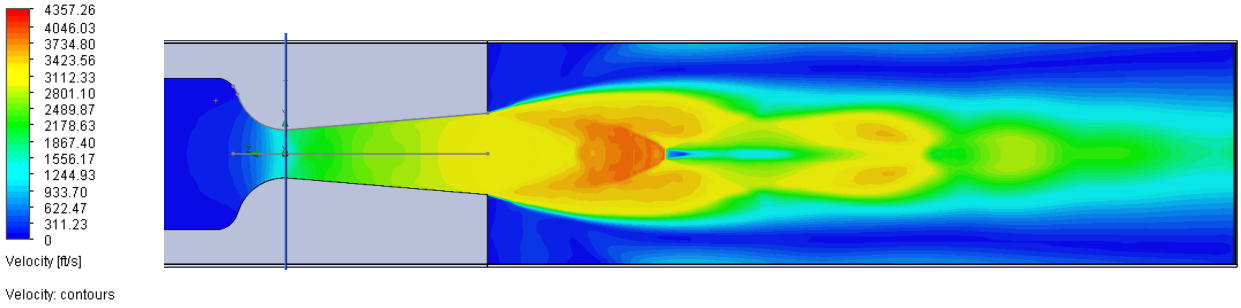

Figure 3.12. Velocity for 120 psig SolidWorks calculation of test nozzle

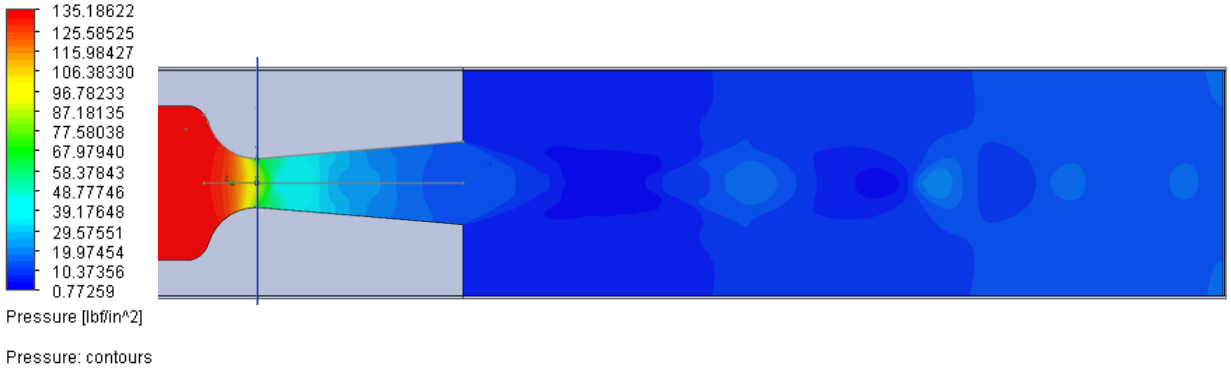

Figure 3.13. Pressure for 120 psig SolidWorks calculation of test nozzle

3.2 Terry Turbine CAD Model

The Terry turbine wheel in all U.S. RCIC applications is a 24" diameter (61 cm) wheel. However, the number and orientation (i.e. nozzle-bucket angle) of the buckets are not specified in available literature. The number of nozzles (and associated reversing chamber sets) is also not precisely stated. Because each nozzle only interacts with a portion of the turbine wheel at any given time, the number of nozzles is probably a more important quantity than the total number of buckets on the wheel (i.e., GS-1 Terry turbines have five steam nozzles, while GS-2 Terry turbines have ten steam nozzles, and both are used in RCIC systems). Such design characteristics are currently unknown and treated as model parameters until more plant information is made available.

3D geometry analysis using CAD tools such as SolidWorks provides a conceptual framework for assessing some of the unknown turbine properties. For example, SolidWorks analysis of the Terry turbine suggests that the bucket angle, relative to the horizontal bucket velocity vector, is probably around 30^o to 45^o, as shown in Figure 3.14 and Figure 3.15, respectively. A shallower bucket angle much less than 30^o would probably result in an excessively thin wall between the buckets; it is known that the buckets are hydraulically isolated from one another (i.e. flow cannot pass through the bucket walls). Therefore, a minimum amount of wall material is necessary to handle the mechanical stresses from the impinging high-velocity steam, while simultaneously rotating near 4500 rpm. The 45^o configuration is probably the maximum value for the nozzle-bucket angle – the CAD model shown by Figure 3.15 exhibits sufficient wall thickness and any further increase in the bucket angle would have deleterious effects on the moment arm of the jet impulse. Lower bucket angles increase the moment arm of the steam jet and thus should drive high turbine torques. As another sanity check, Figure 3.14 and Figure 3.15 look comparable to the Terry depictions from historical literature (see Figure 2.2).

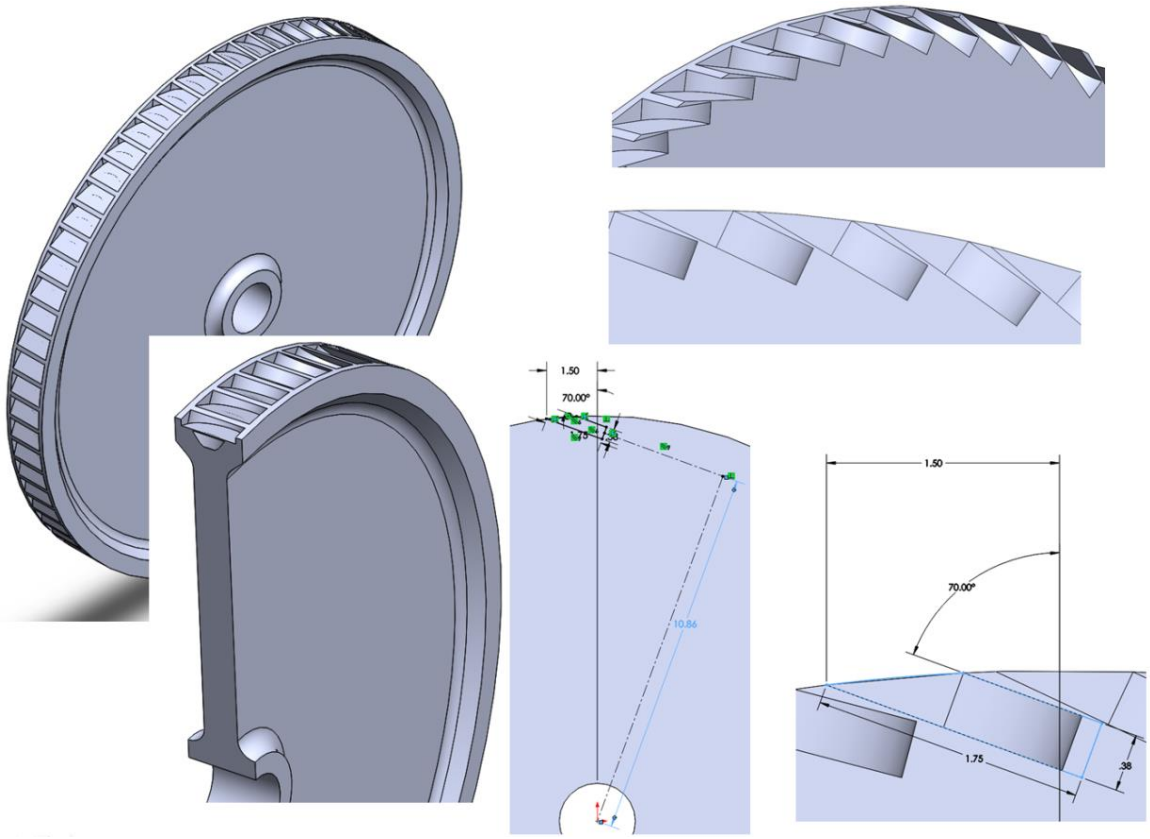

Figure 3.14. Terry CAD model with 30^{o} bucket angle (relative to bucket velocity vector)

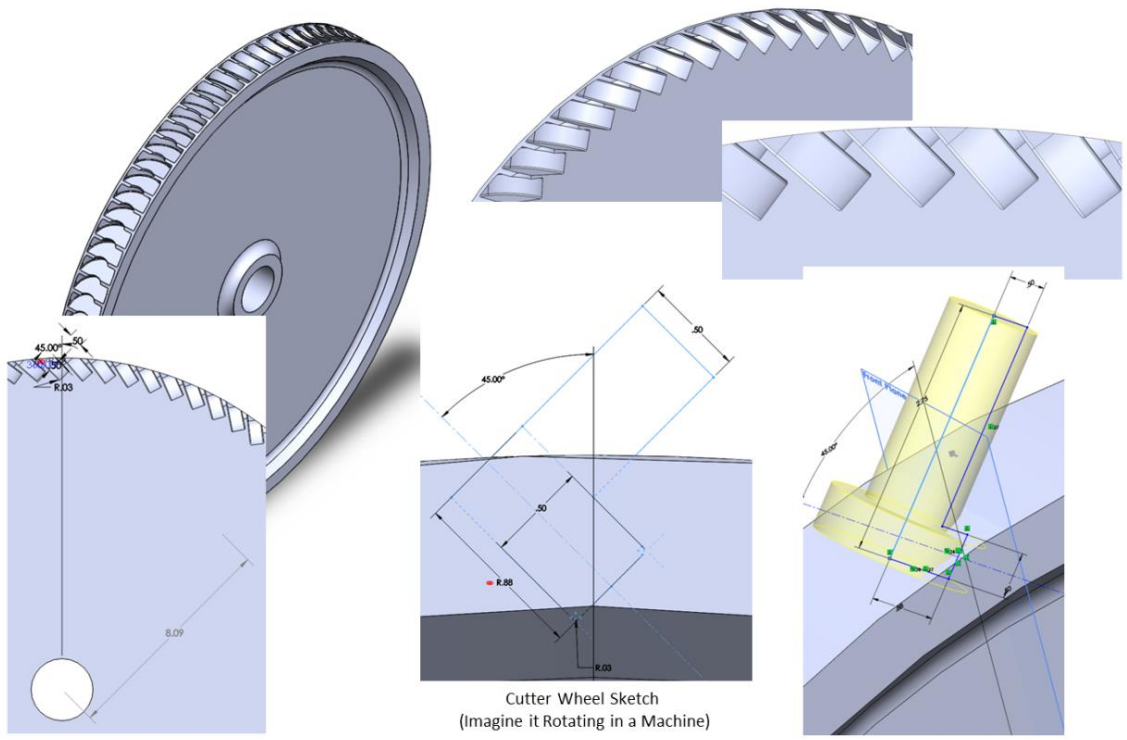

Figure 3.15. Terry CAD model with 45^{o} bucket angle (relative to bucket velocity vector)

Figure 3.16 illustrates the dimensions of the Terry turbine nozzle. The full CAD model includes 3D representations of the nozzles, reversing chamber sets, and casing for the Terry turbine, as shown in Figure 3.17. The nozzles have a circular throat (diameter assumed near 0.56 cm) but transition to a square diverging (exit) section, which has a side length of 0.64 cm. The Terry turbine nozzle is inferred to be about 1.7 cm in length. Table 3.2 provides a summary of dimensions and other important characteristics of the Terry turbine model. Exterior views of the CAD model are provided by Figure 3.18. The CAD model is generated using very limited data for dimensions of the system. References [3.1] through [3.4] provide some coarse estimate. The exact dimensions of features of the Terry CAD model will undoubtedly need continuous modification and refinement as more valid information is made available. As such, a comprehensive description of every dimension and geometric feature of the CAD model is not given in this report.

Table 3.2. Key dimensions and quantities for Terry turbine model

Model variable	Quantity
Turbine wheel diameter	61 cm (24 inches)
Turbine wheel and bucket width	7 cm
Number of nozzles and reversing chamber sets	5
Number of reversing chambers per nozzle set	4
Number of buckets on wheel	84
Nozzle length	1.7 cm
Nozzle circular throat diameter	0.56 cm
Nozzle square exit side length	0.64 cm
Distance from nozzle exit to bucket entrance	≈1.5 cm

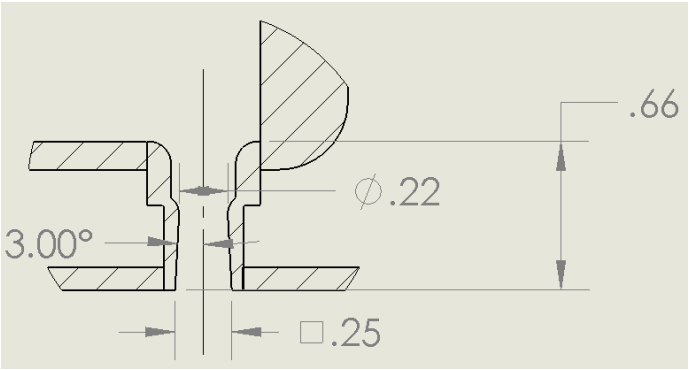

Figure 3.16. Terry nozzle dimensions in inches

The CAD model also provides the ability to estimate the number of nozzle/reversing chamber sets that can fit around the 24" Terry wheel. It is found that up to 10 (possibly more) nozzle sets could easily fit around the turbine, which agrees well with available literature (e.g. [3.1][3.2]) that typically suggests 5 to 10 nozzles. More nozzles yield a higher effective choked flow area, thereby increasing the total mass flow rate and momentum rate (i.e. $\dot{m}v$) to the turbine buckets. The resultant turbine torque may be nearly linear with respect to the number of nozzles. The final

CAD model used for the CFD analyses in Section 3.3 and Section 3.4 use a Terry CAD model with five nozzles, and the buckets are assumed to have a 45^{o} orientation with the nozzle.

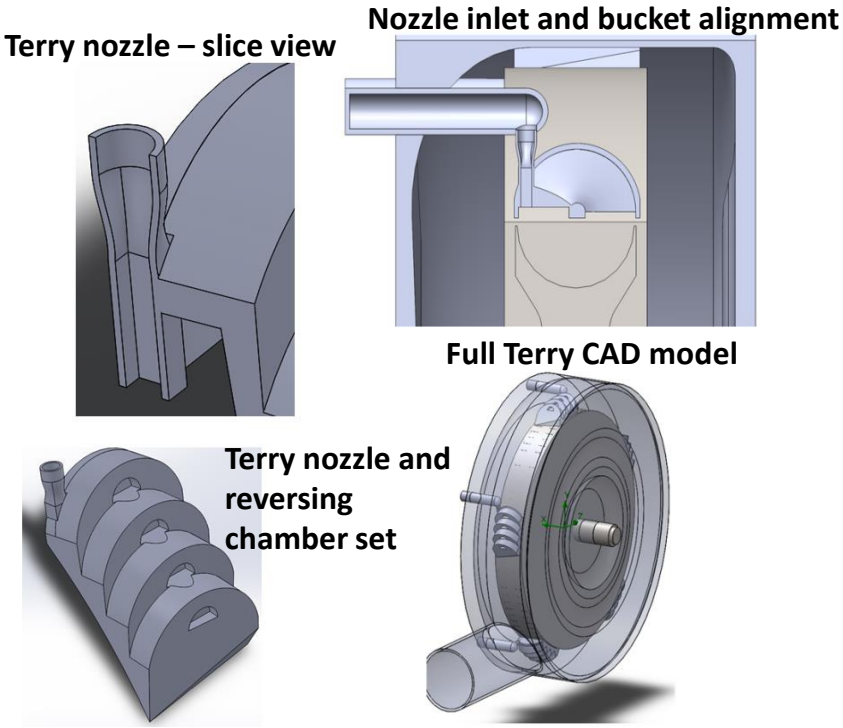

Figure 3.17. CAD depictions of Terry nozzle, reversing chambers, and bucket orientation

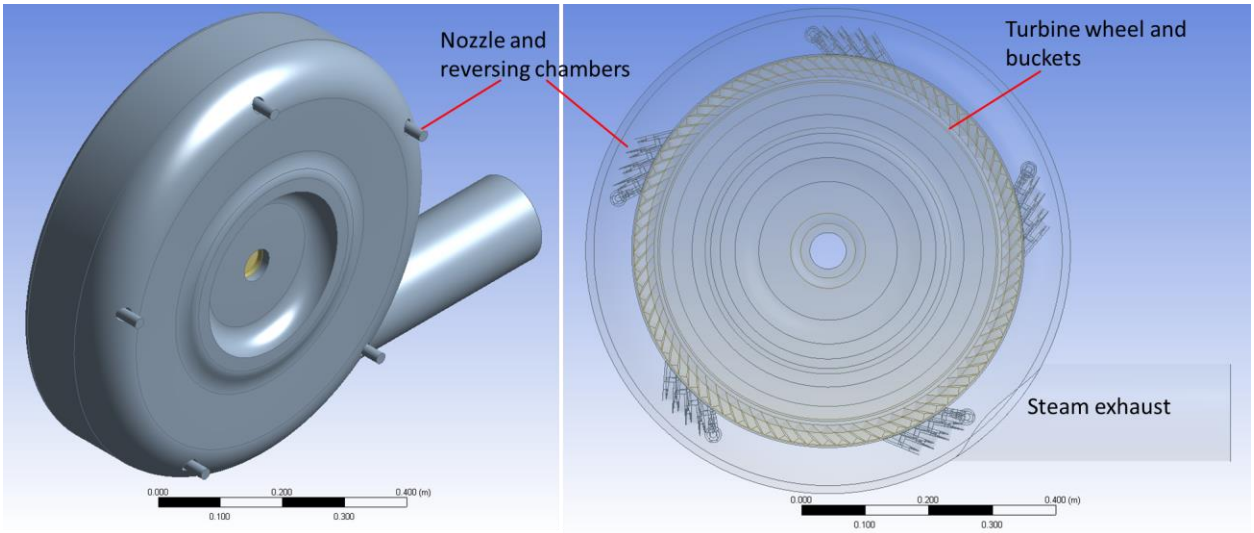

Figure 3.18. Full 3D CAD model of Terry turbine

3.3 CFD Analyses of Terry Nozzle

CFD analyses using FLUENT and SolidWorks Flow are compared for the preliminary model of the Terry turbine nozzle. It is reiterated that geometry of the nozzle is inferred using very limited public information – the geometry will likely require refinement when more representative information is made available.

3.3.1 Terry Model Parameters for CFD Calculations

The model parameters for the Terry CFD analyses are comparable to those used in the test nozzle benchmark study presented in Section 3.1, but applied to the Terry turbine nozzle geometry. Table 3.3 provides a summary of these parameters. The SolidWorks Flow calculations examine the nozzle discharging to an empty reservoir that has outlet boundary conditions with pressures and temperatures that reflect the RCIC turbine exhaust. The FLUENT calculations examine a wedge of the full Terry turbine geometry, and hence it also models a set of reversing chambers and 11 turbine buckets. These features are included in the FLUENT model in order to expedite other calculations such as bucket inlet and outlet velocities that will provide important inputs for the system models. Since the buckets and reversing chambers have no meaningful influence on the flow through the nozzle, their addition in the FLUENT model does not prevent a comparison with the SolidWorks nozzle-only model. Nozzle flow characteristics are compared between the two codes in Section 3.3.2 and Section 3.3.3.

Table 3.3. Model parameters for Terry CFD analyses

Model variable	SolidWorks	FLUENT
Two-phase formulation	Real gas water/steam	Wet steam
Turbulence model	k-ε	k-ω
Turbulent intensity	2%	3%
Turbulence length scale	0.01 cm	NA
Turbulent viscosity ratio	NA	6
Mesh type	Cubic	Tetrahedral
Number of cells	~1 million*	1,006,868
Minimum cell orthogonality**	NA	0.2
Maximum cell skewness**	NA	0.85
Inlet boundary condition	Pressure specified	Pressure specified
Outlet boundary condition	Pressure specified	Pressure specified

* The SolidWorks mesh is dynamically refined for each calculation, but it generally yields a mesh of about 1 million cells.

** Cell orthogonality and skewness important indicators of mesh quality for the FLUENT mesh, but they are not applicable to the cubic SolidWorks mesh. Generally, orthogonality greater than 0.2 and skewness less than 0.95 reflect a good quality mesh.

The FLUENT model used for assessment of the Terry nozzle is shown by Figure 3.19. Mesh size and CPU time is reduced by modeling a wedge of the turbine. The mesh is depicted in Figure 3.20. The interior of the turbine, which includes the wheel and buckets, is in a separate domain from the nozzles, reversing chambers, and turbine casing wall. This will enable future calculations of moving reference frames to simulate turbine rotation. The angular speed of the turbine likely has important effects on the bucket exit velocity and the efficacy of the reversing

chambers, but it does not have immediate impacts on the nozzle flow. System feedback on the nozzle flow is a delayed influence; the nozzle flow drives the turbine-pump, which eventually changes the thermal-hydraulic conditions in the core and RPV via pump injection into the feedwater lines. This will have subsequent effects on the pressure and two-phase mixture that enters the nozzles. The system models permit mechanistic simulations of gross system feedback. For the purposes of a quasi-steady or short transient CFD calculation, the turbine behavior causes no immediate changes on the nozzle flow behavior.

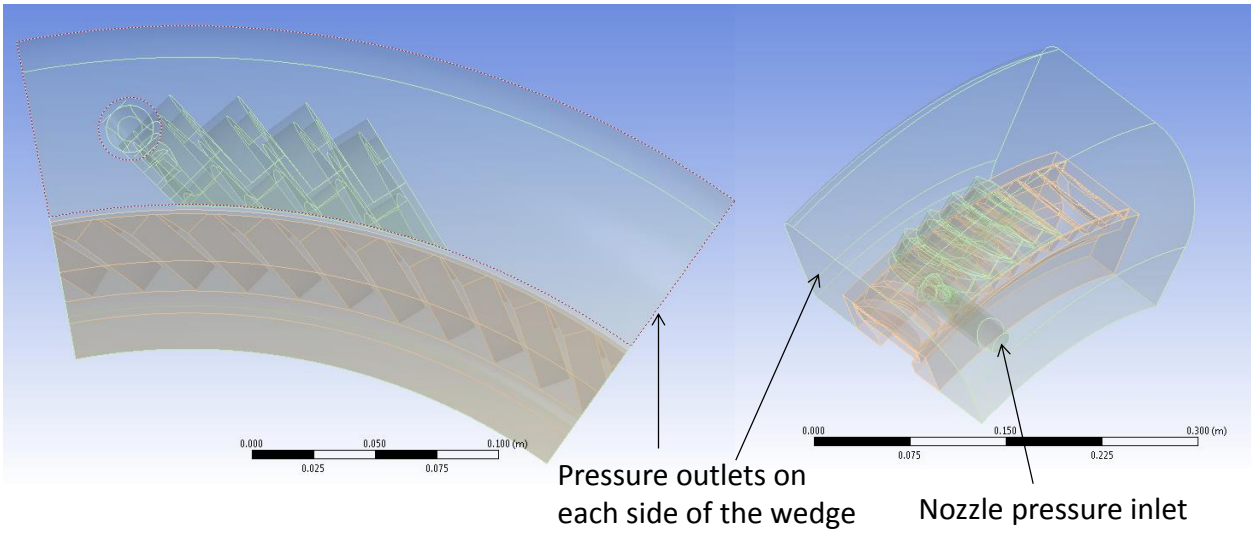

Figure 3.19. Wedge of Terry turbine used in FLUENT assessments of nozzle flow

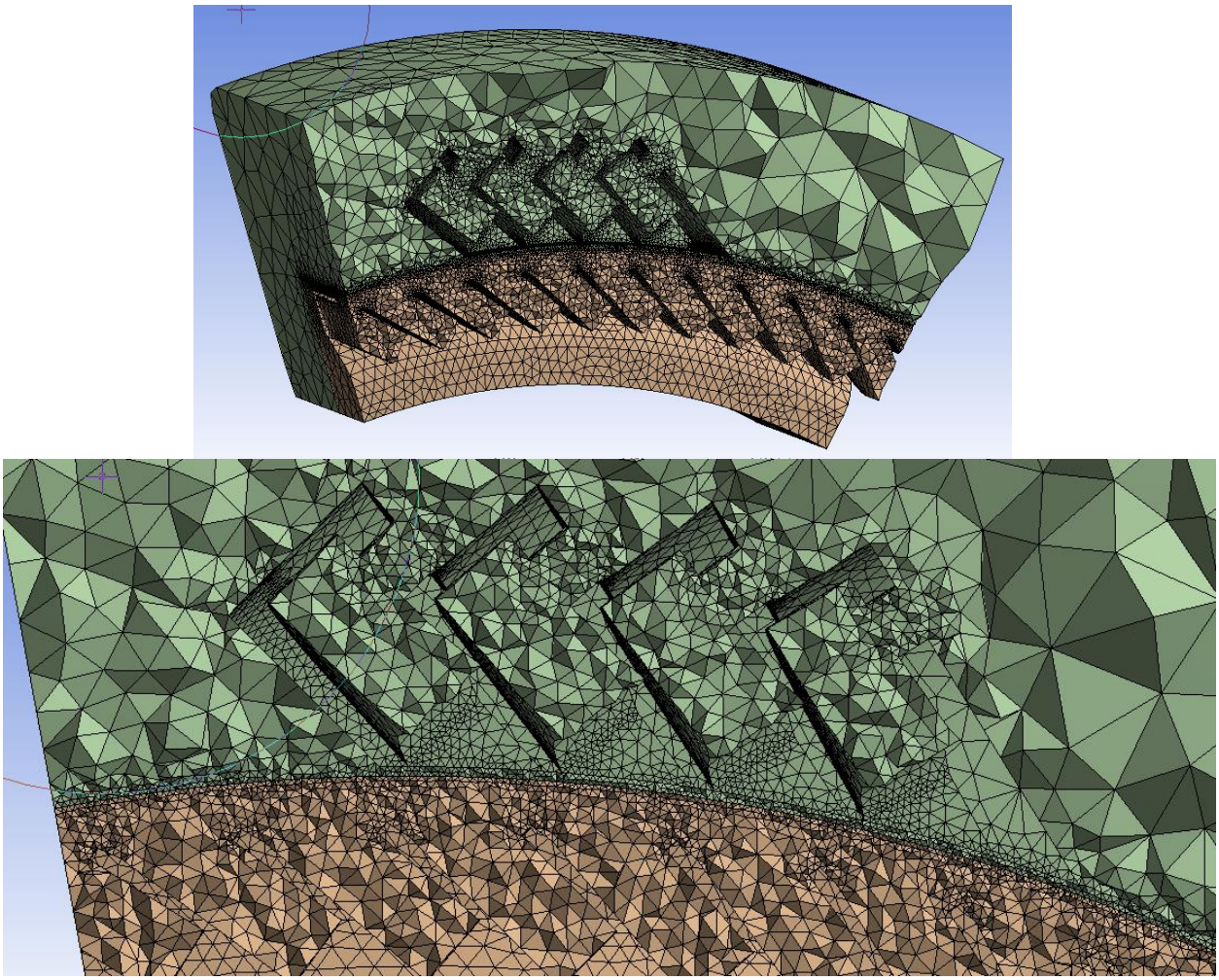

Figure 3.20. FLUENT mesh of wedge model for Terry turbine

3.3.2 Mass Flow Rate and Solution Convergence

The predicted mass flow rates for the nozzle as a function of inlet pressure are shown by Figure 3.21. The mass flow rates calculated by the CFD codes are less than 1% different at each inlet pressure. The CFD predictions are also very comparable to a hand calculation for choked flow of steam through an orifice with area of about 0.25 cm^2 (i.e. the nozzle throat area). Simple formulas for choked flow are readily accessible from most introductory fluid textbooks, and even relationships for ideal gases yield good estimates for saturated steam, which is not an ideal gas. The blue curve depicted in Figure 3.21 is derived using formulas from Reference [3.5], where the isentropic expansion coefficient is assumed to have a constant value of 1.1.

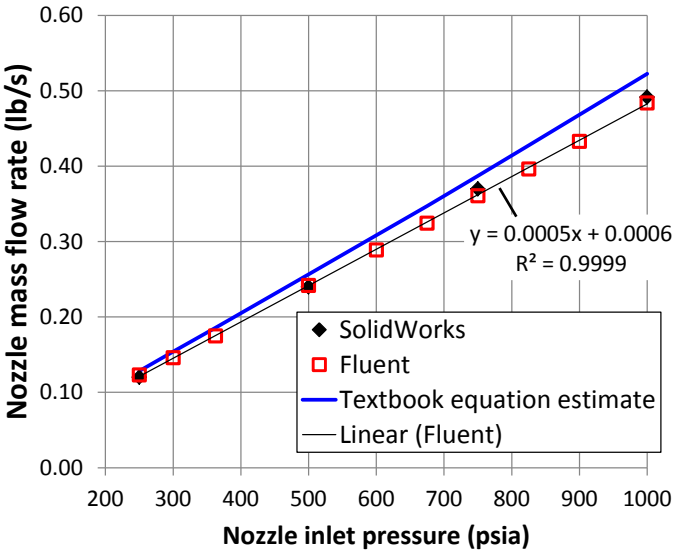

Figure 3.21. Choked mass flow rate for preliminary model of Terry nozzle

Given pressure inlet and outlet boundary conditions, the accurate prediction of choked mass flow rate is encouraging and is the first step in validating other predictions by the codes. The critical flow rate should nearly be a linear function of inlet pressure, and have no dependence on outlet pressure if it is less than the critical pressure. The critical pressure for steam can be estimated using Equation 3.1.

$$\frac{P_{crit}}{P_{in}} = \left(\frac{2}{k+1}\right)^{\frac{k}{k-1}} \tag{3.1}$$

In Equation 3.1, P_{in} is the nozzle inlet pressure, P_{crit} is the critical throat pressure, and k is the isentropic coefficient. k is not a strong function of steam pressure, but depends more on the thermo-physical state of the steam. For superheated steam, a value of 1.3 might be appropriate; a value of 1.135 may be used for dry saturated steam; and wet steam may have a k value closer to 1.1. The k value for saturated wet steam mixtures can be estimated using the parametric relationship given by Equation 3.2 [3.6][3.12], where x is the steam quality.

$$k = 1.035 + 0.1x \tag{3.2}$$

The critical pressure for dry saturated steam (k≈1.135) is usually close to 0.58 P_{in}, since Equation 3.1 is not a strong function of k, and k itself does not vary too much for saturated steam mixtures [3.5][3.6]. The Terry turbine nozzles should always exhibit choked flow, judging by the large pressure drop from the RCIC steam inlet (possibly near RPV pressures, i.e. 1000 psi) to RCIC exhaust, which should be near the containment/wetwell pressure (20-50 psi).

The CFD-predicted mass flow rates for each inlet pressure are checked against different outlet pressures, and the converged choked flow rates exhibit essentially no change, as expected (less than 0.5%, which is within the first-order resolution of the solver methods used in the analyses). The difference between calculated flow rates for the inlet and outlet is also an important indicator

of solution convergence. Each CFD calculation exhibits inlet and outlet flow rates within 1% of each other, which is sufficient for these analyses. Solution convergence is also dependent on the mass flow rates achieving quasi-steady levels for at least 2000 iterations.

Solver residuals are closely inspected for each CFD calculation to confirm reasonable solution convergence. Most residuals decrease by over three orders of magnitude for each calculation and remain reasonably steady after several thousand iterations; some of the velocity residuals (namely y and z velocity) only decrease by one or two orders of magnitude, but they flat-line for thousands of iterations. Calculations with higher pressure drop over the nozzle naturally require more iterations to converge properly. Each CFD calculation is executed in steady-state mode for 5,000 to 10,000 iterations.

Convergence is facilitated in the FLUENT analyses by using previous solutions (typically with lower pressure drops) as initial conditions. For instance, the 250 psia inlet case with a 44 psia outlet is first converged using an initial guesses for pressure, velocity, and temperature throughout of the model domain. Convergence is first attained with the wet steam model off (i.e. no condensation); after reasonable mass flow rates and residuals are reached, the wet steam model is activated and the calculation proceeds for a few thousand more iterations to reach final convergence. The converged solution for 250 psia inlet pressure is then used to provide initial conditions for the next calculation at 500 psia (and outlet pressure still at 44 psia).

Example residuals for the 250 psia FLUENT calculation are shown in Figure 3.22. The wet steam model is activated after 2000 iterations, as evident by the ‘wsb’ and ‘wsn’ residual curves starting from a value of 1.0 and dropping three orders of magnitude after about 1000 iterations; other residuals such as energy, continuity, and turbulence (k, omega) are perturbed by the initiation of the wet steam model and require some time to re-converge. This calculation is allowed to proceed to 5000 total iterations to ensure that the residuals remain steady or continue decreasing monotonically.

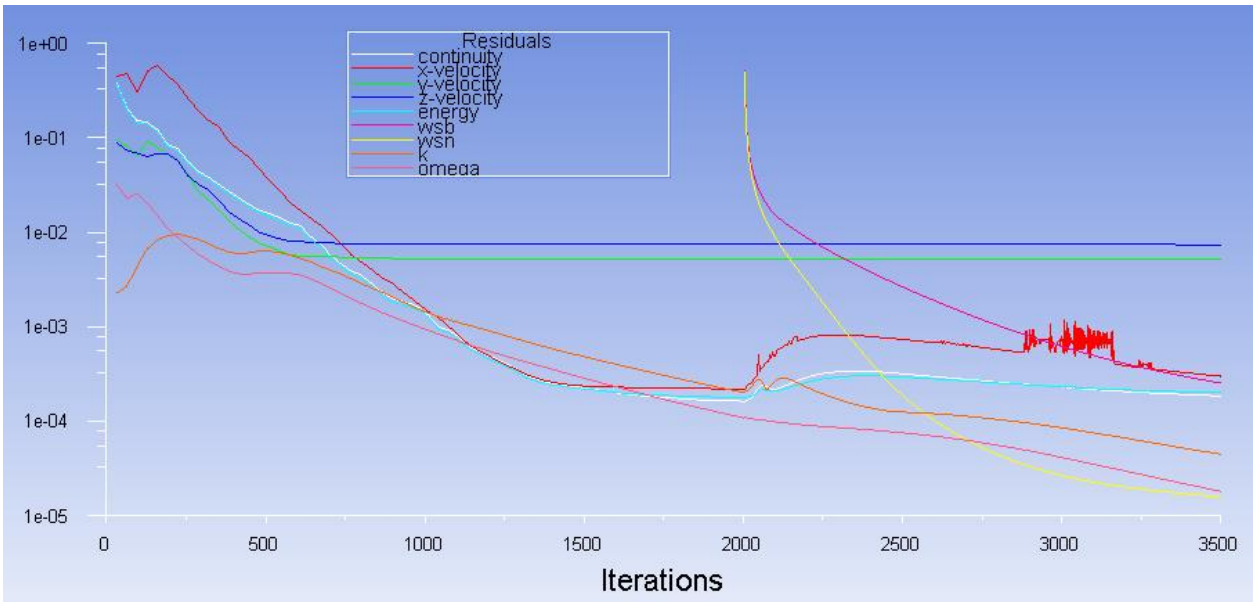

Figure 3.22. Sample FLUENT residuals with wet-steam model activated at 2000 iterations

3.3.3 General CFD Deductions from FLUENT and SolidWorks Flow

Both CFD codes predict supersonic flows exiting the nozzle for inlet pressures ranging from 250 psia to 1000 psia. Velocities calculated using SolidWorks Flow are shown in Figure 3.23; velocity magnitudes in this figure are normalized to the sonic velocity that is generally near 300 to 350 m/s depending on the thermo-physical properties of the fluid. SolidWorks predicts peak Mach numbers around 2 to 3. Dark blue contours denote subsonic flow; light blue contours denote near sonic velocity magnitude; and green, yellow, orange, and red contours denote supersonic velocities. Although the Terry impulse buckets are not included in these SolidWorks calculations, they would be very near the regions of peak velocity magnitude. The Terry buckets are less than 1 nozzle length from the exit of the diverging section (about 1.5 cm away from the nozzle exit). The FLUENT calculations, which include the turbine buckets and reversing chambers, predict very similar velocity magnitudes as shown by Figure 3.24.

SolidWorks and FLUENT predict features of under-expanded flow. In the SolidWorks calculations, this is evident by the flaring of the jet plume and rather strong shocks downstream of the nozzle exhaust. The shocks generally occur past 1 nozzle length downstream. There are no clear shocks that degrade velocity in the jet exhaust for the FLUENT calculations, but then again the exhaust region is obstructed by the turbine buckets. However, several calculations from both codes show a very sudden velocity increase immediately outside the nozzle, which is indicative of a supersonic expansion process to reconcile the steam pressure with the outlet pressure when the flow is under-expanded (i.e. the nozzle is not expanding the steam fast enough). The CFD analyses confirm that the steam will completely expand before it reaches the turbine, even if the nozzle flow is under-expanded, as exemplified by Figure 3.25 (for SolidWorks) and Figure 3.26 (for FLUENT). This holds true for even larger pressure drops over the nozzle, such as 1100 psia to 28 psia. Figure 3.27 shows that the steam pressure will immediately reach the outlet pressure just outside the nozzle exit; static pressure is invariant long before the steam reaches the buckets. The fluid velocity for this case (Figure 3.28) depicts under-expanded flow conditions.

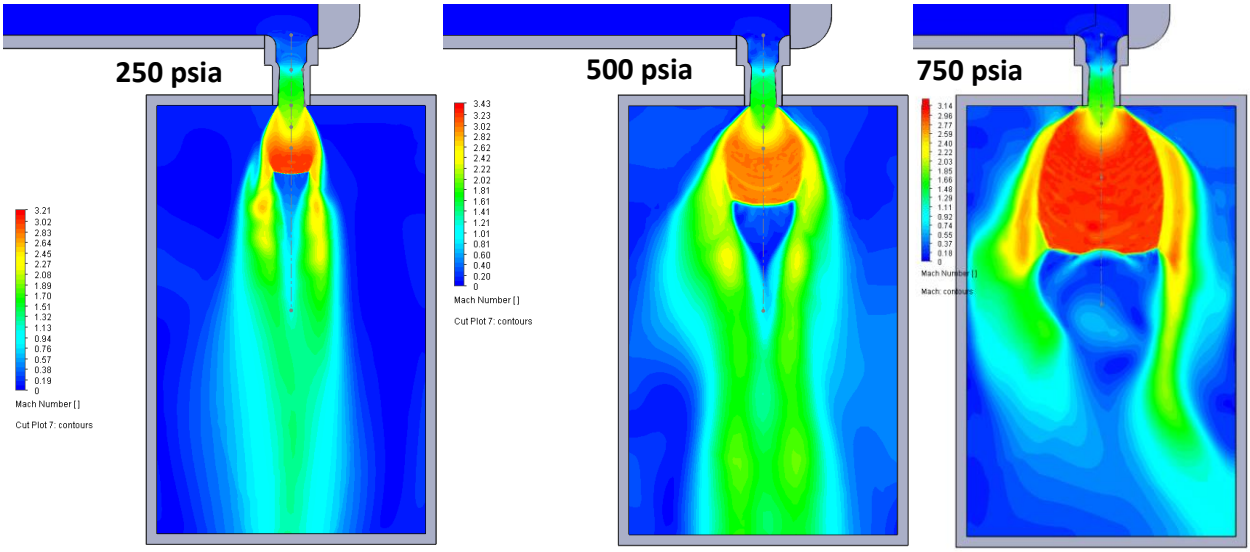

Figure 3.23. SolidWorks velocities for Terry nozzle: 250, 500, and 750 psia inlets with 15 psia outlet pressure

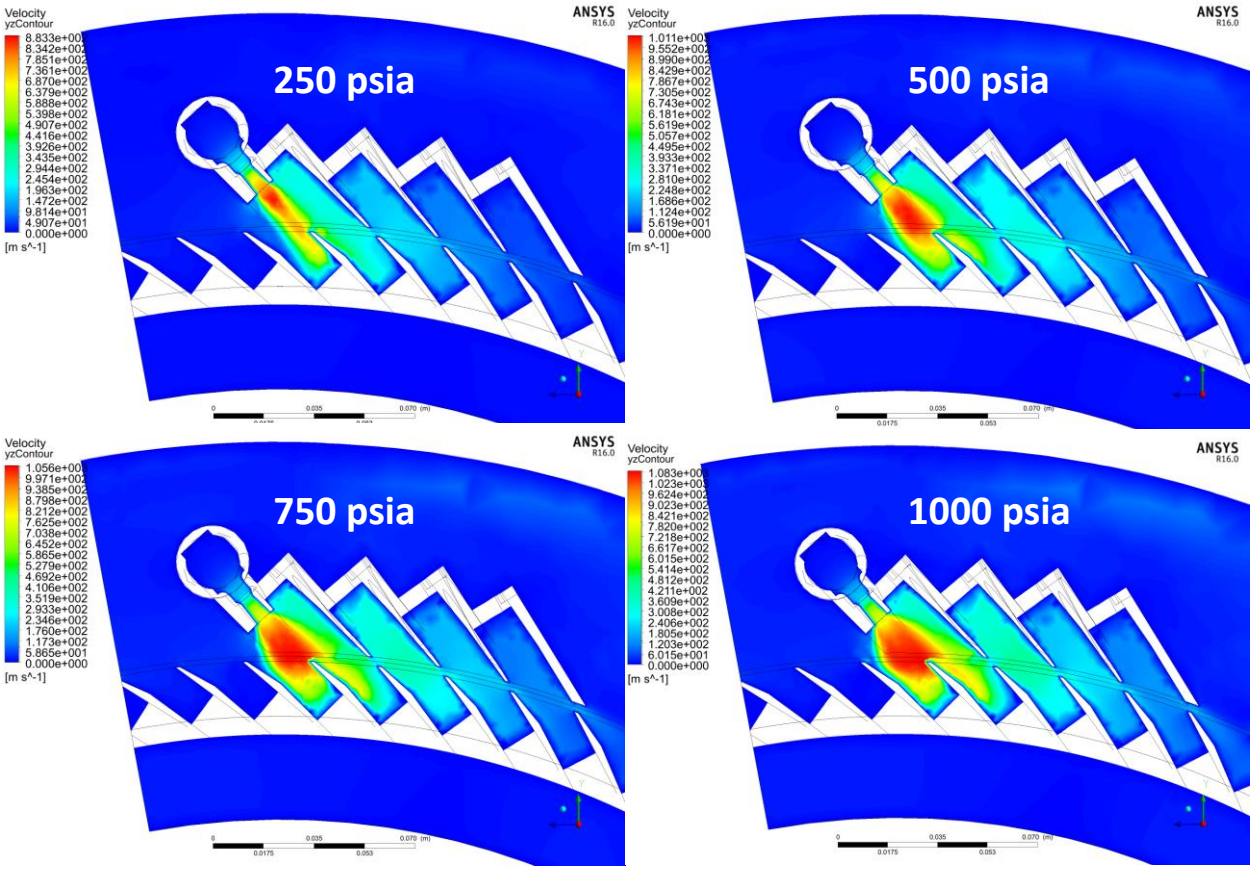

Figure 3.24. FLUENT velocities for Terry nozzle: 250, 500, 750, and 1000 psia inlets with 28 psia outlet pressure

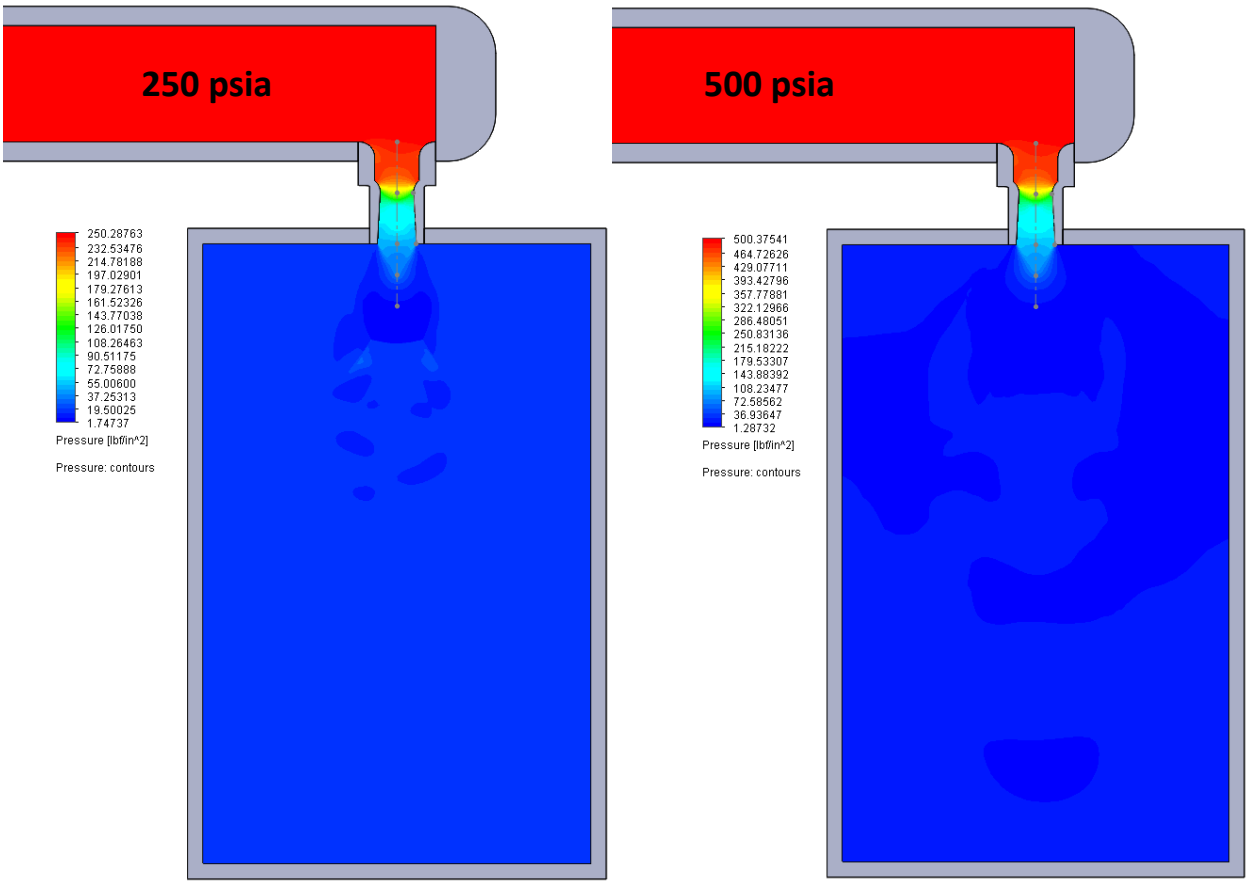

Figure 3.25. SolidWorks pressures for Terry nozzle

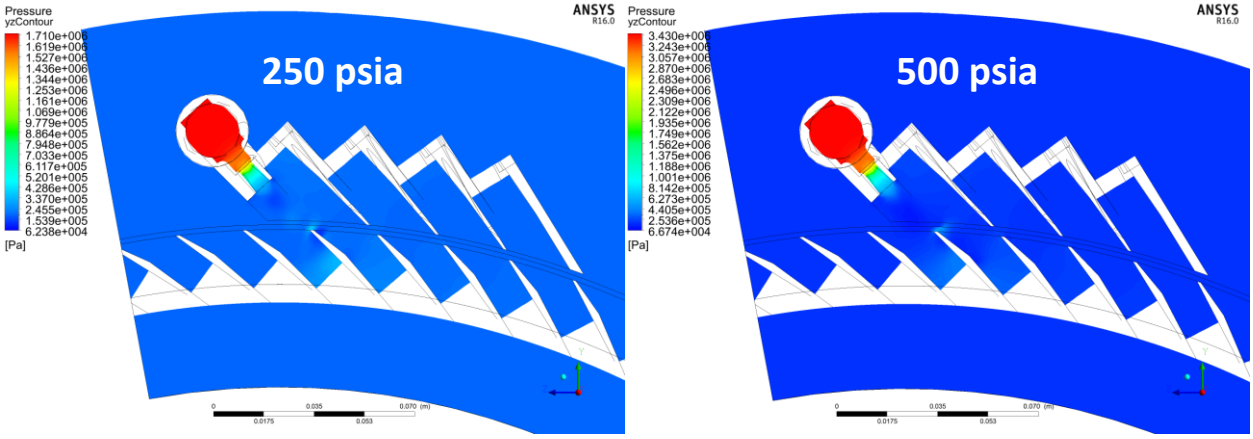

Figure 3.26. FLUENT pressures for Terry nozzle

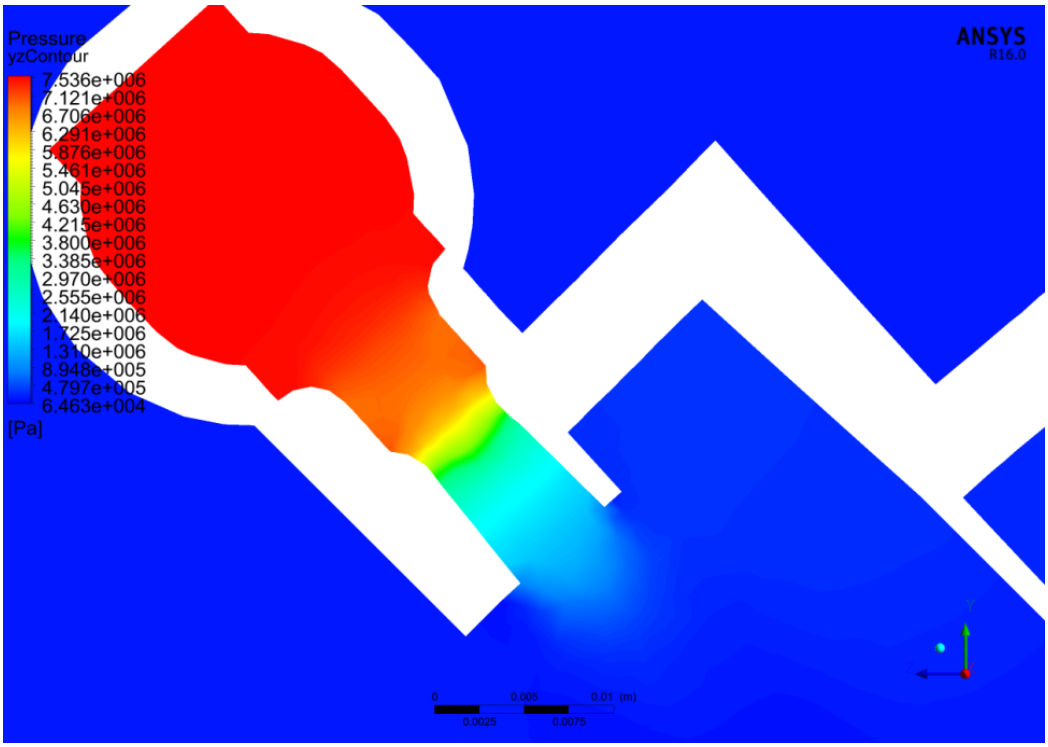

Figure 3.27. FLUENT pressure for Terry nozzle pressure drop from 1100 psia to 28 psia

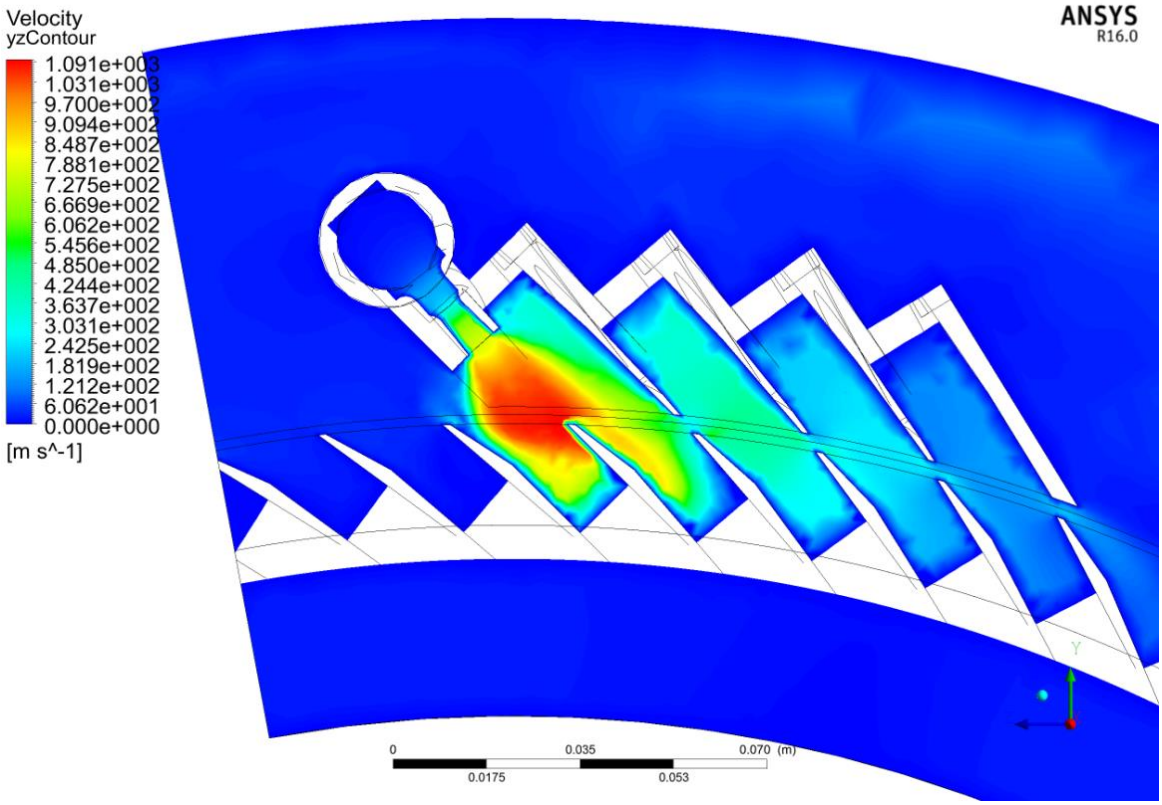

Figure 3.28. FLUENT velocity for Terry nozzle pressure drop from 1100 psia to 28 psia

3.4 FLUENT Calculations for System Model Support

This section documents FLUENT analyses that yield meaningful information for the system models. The Terry turbine governing equations in Section 2 have dependencies on the rate of momentum for each phase flowing through the nozzles, which is given by $\dot{m}v\ (= \text{Area} * \rho v^2)$. The mass flow rate is accurately determined by two-phase critical flow models in MELCOR and RELAP, but the codes cannot predict the supersonic velocities developed by the nozzles. Therefore, the system code must be informed by more focused CFD analyses. There are several ways to go about this, such as:

1. Developing a sub-model for the system analysis, based on an abstraction of the full pertinent physics, that can calculate the nozzle velocities based on other plant-level predictions (e.g. pressures, two-phase mixture contents, etc.). The sub-model could be implemented into the source codes or more simply through user-calculations (i.e., MELCOR control functions and RELAP control variables),

2. Table lookup of CFD results as a function of various plant variables, or

3. Analytic formula fit of CFD results as a function of various plant variables.

The third option is used here for the initial application of the CFD insights into the system models. Analytical functions permit continuous relationships between the supersonic velocity and the plant variables, in contrast to table lookups that generally use linear interpolation and may exhibit discontinuities. Analytical fitting is also a much more expedient method than developing a nozzle sub-model for the system analyses.

Inlet and outlet surfaces are defined for the Terry buckets in order to extract the most representative values from the velocity field calculated using FLUENT. The Terry turbine momentum equation requires velocity magnitudes that reflect the flow into the control volume of the bucket, which is not equivalent to peak velocity or the velocity at the exit plane of the nozzle. Figure 3.29 shows the definition of the bucket inlet and outlet surfaces. Velocity magnitudes for the system model are integrated (averaged) over these surfaces. All CFD calculations of the Terry model in this report are steady state and the turbine is stationary. This represents the turbine at startup or low speed. Relative movement between the nozzle and buckets should not drastically affect the bucket inlet flow, but it will probably have an influence on the bucket outflow; this will be examined in future CFD analyses.

The nozzle-bucket alignment is intended to approximately simulate the average flow behavior of a moving turbine. The bucket thickness is comparable to the jet width, so most of the time the flow is split between two adjacent buckets. The FLUENTS model assumes a split of about 25/75 flow between two buckets, as shown in Figure 3.29.

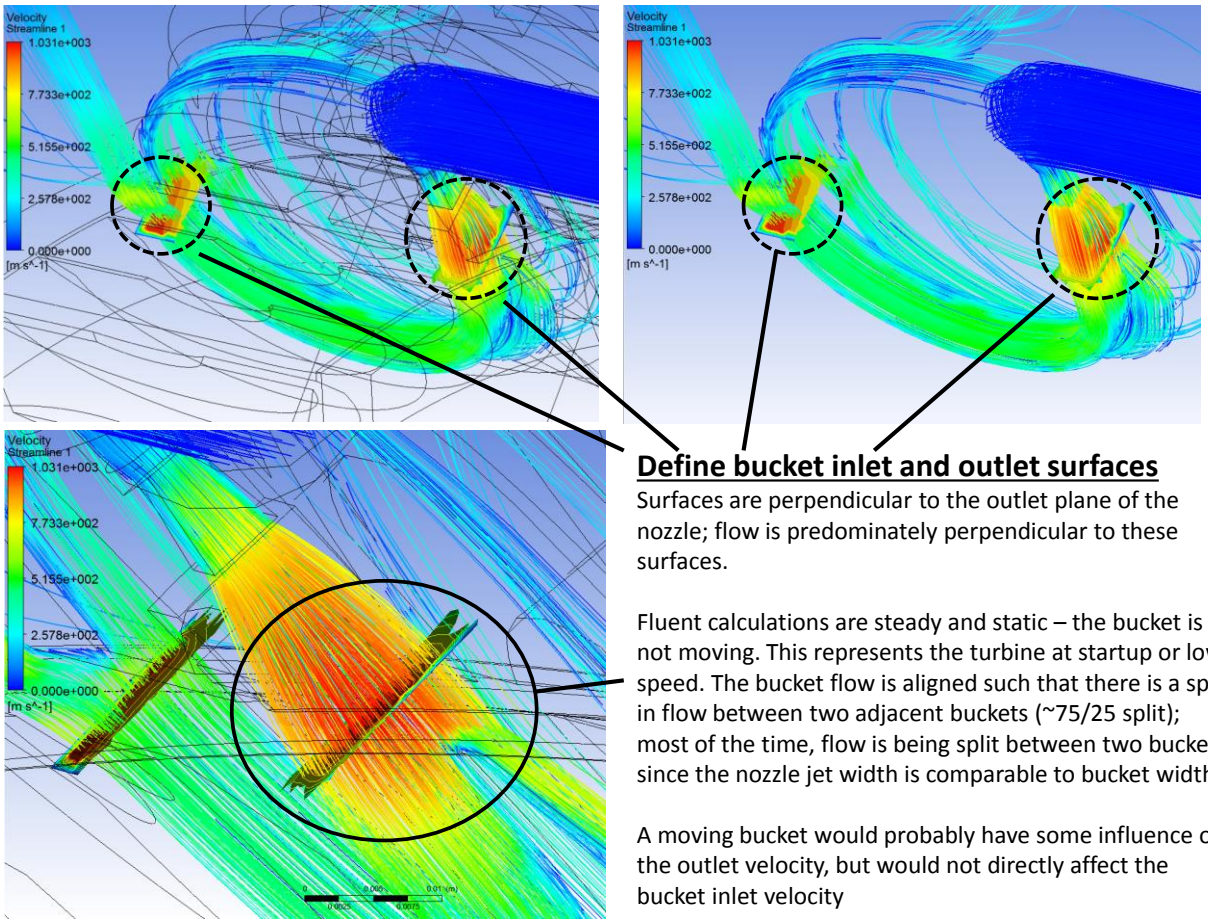

Figure 3.29. Definition of bucket inlet and outlet surfaces

3.4.1 Analytic Fitting of CFD Results for System Implementation

FLUENT calculations are executed for the reduced Terry model (Figure 3.19) for 11 inlet pressures and 2 outlet pressures. Pertinent results from these analyses are listed in Table 3.4. Logarithmic fits to the bucket inlet and outlet velocities as a function of nozzle pressure ratio (P_{in}/P_{out}) are shown by Figure 3.30 and Figure 3.31, respectively. Larger pressure drops yield higher velocities. Higher inlet pressure obviously increases the density and available enthalpy of the inlet fluid, which allows for more expansion of the fluid through the nozzle and greater kinetic energy generation. The independent influence of the outlet velocity is slightly counterintuitive, given that outlet pressure cannot affect the mass flow rate due to choked flow. Nevertheless, FLUENT consistently predicts that lower outlet pressure can increase the nozzle and bucket velocities without changing the flow rate through the nozzle. This is clearly demonstrated by Figure 3.32 and Figure 3.33. Some qualitative explanations of this behavior are:

1. Lower outlet pressure leads to more steam expansion and lower density; hence total mass flow rate remains unchanged, density decreases, and velocity increases;

2. Lower outlet pressure decreases the saturation enthalpy of the steam outflow, thereby increasing the enthalpy drop over the nozzle and increasing kinetic energy generation;

3. Lower outlet pressure yields more condensation that significantly decreases the effective mixture enthalpy of the nozzle outlet flow as discussed further in Appendix D.

Table 3.4. Summary of FLUENT results for bucket inlet and outlet velocities

Inlet Pressure (psia)	Outlet Pressure (psia)	Pressure drop (psia)	Pressure drop ratio	Avg. inlet velocity (m/s)	Avg. outlet velocity (m/s)	Avg. ratio
250	43.51	206.49	5.75	518.11	275.72	0.532
300	43.51	256.49	6.89	542.00	303.31	0.560
363	43.51	319.49	8.34	557.21	334.58	0.600
500	43.51	456.49	11.49	620.57	405.11	0.653
600	43.51	556.49	13.79	662.91	441.01	0.665
675	43.51	631.49	15.51	714.94	461.84	0.646
750	43.51	706.49	17.24	758.26	485.07	0.640
825	43.51	781.49	18.96	761.62	494.25	0.649
900	43.51	856.49	20.68	791.85	509.73	0.644
1000	43.51	956.49	22.98	826.54	522.50	0.632
1100	43.51	1056.49	25.28	850.89	548.54	0.645
250	28.00	222.00	8.93	586.09	343.62	0.586
300	28.00	272.00	10.71	627.33	379.38	0.605
363	28.00	335.00	12.96	678.33	421.37	0.621
500	28.00	472.00	17.86	768.06	478.32	0.623
600	28.00	572.00	21.43	799.76	500.03	0.625
675	28.00	647.00	24.11	839.86	517.88	0.617
750	28.00	722.00	26.79	868.83	538.02	0.619
825	28.00	797.00	29.46	891.66	559.27	0.627
900	28.00	872.00	32.14	909.87	583.49	0.641
1000	28.00	972.00	35.71	929.84	592.95	0.638
1100	28.00	1072.00	39.29	943.61	602.07	0.638

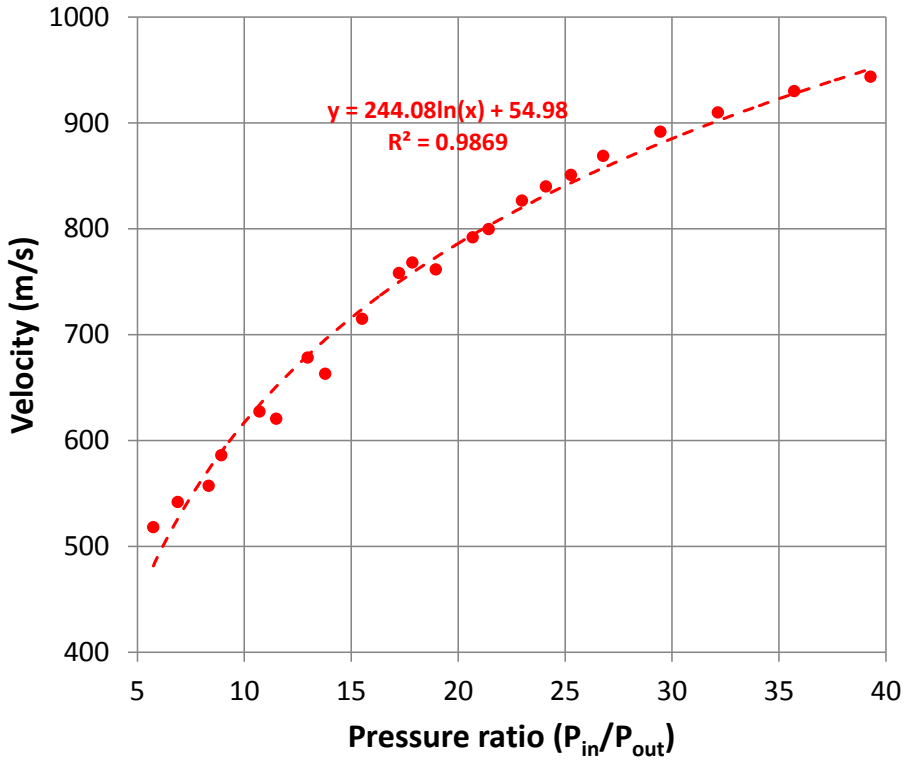

Figure 3.30. Bucket inlet velocity as a function of nozzle pressure ratio

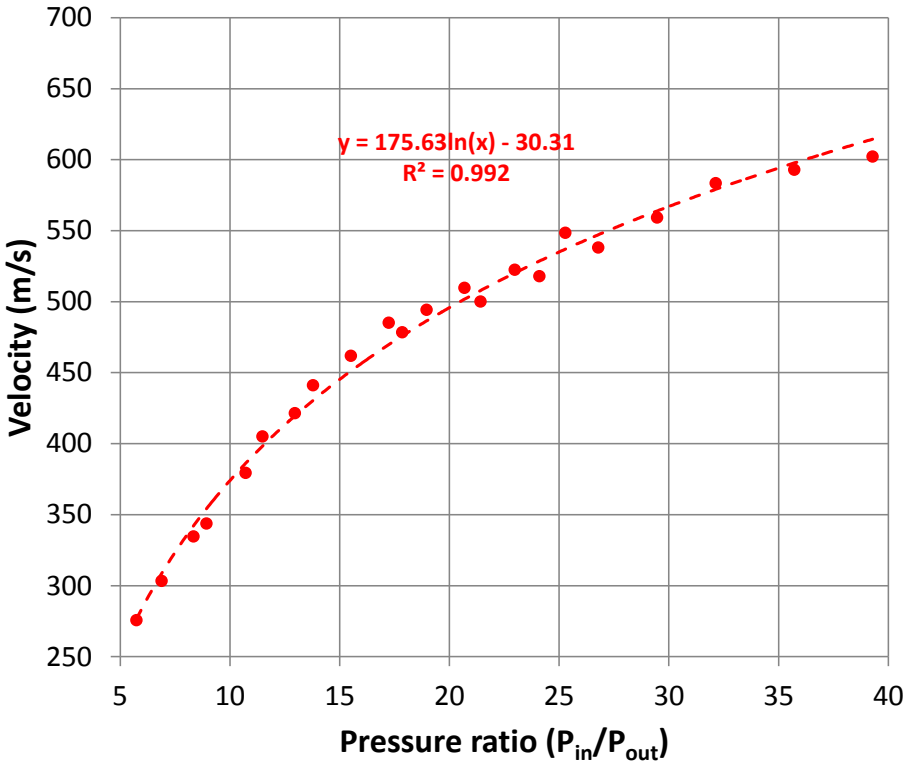

Figure 3.31. Bucket outlet velocity as a function of nozzle pressure ratio

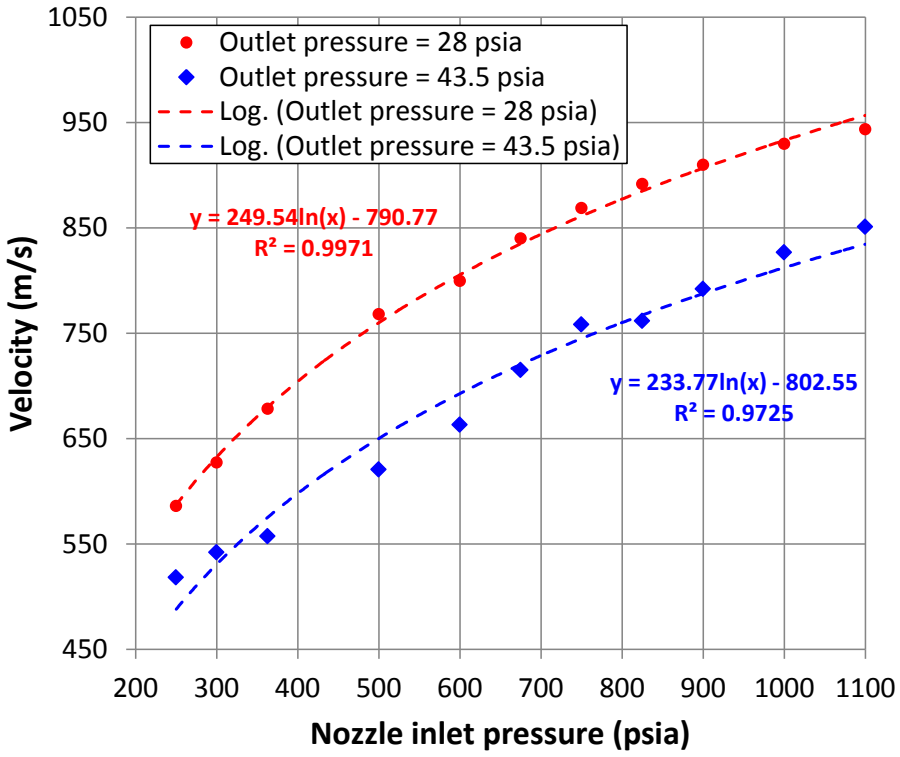

Figure 3.32. Bucket inlet velocity as a function of pressures

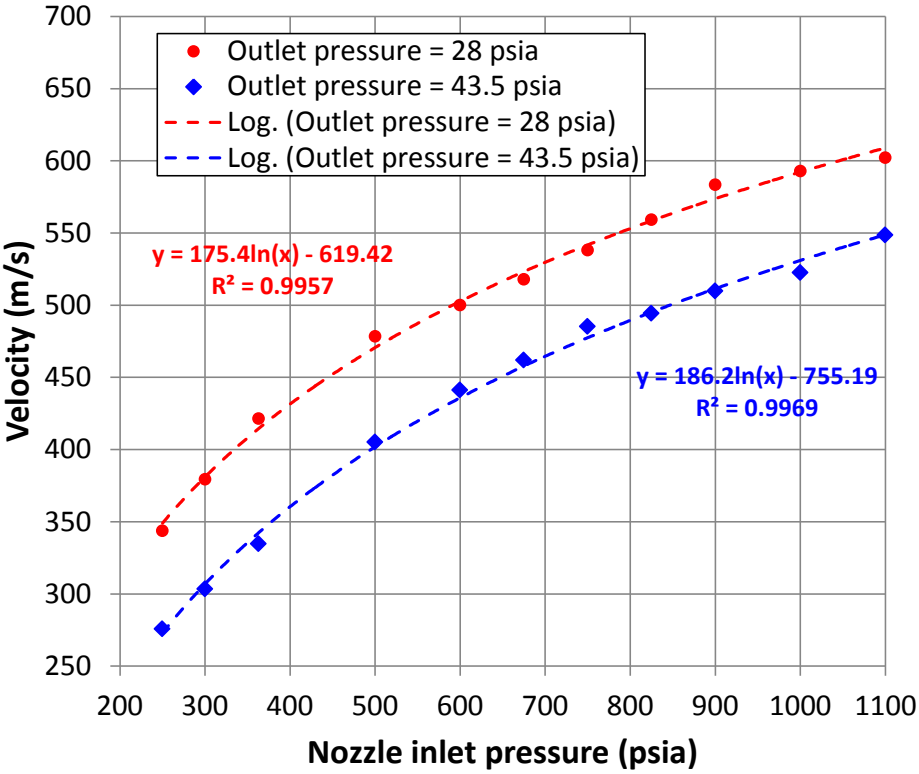

Figure 3.33. Bucket outlet velocity as a function of pressures

3.4.2 Bucket Flow and Qualitative Reversing Chamber Examination

Flow contours through the nozzle mid-plane of are presented to illustrate the effects that inlet and outlet pressures have on the developed velocity field and liquid fraction through the turbine. Figure 3.34 through Figure 3.41 show contours of velocity magnitude for inlet pressures of 250, 500, 750, and 1100 psia; each inlet pressure case is shown with two outlet pressures of 44 and 28 psia. The FLUENT analyses show a monotonic trend between the nozzle pressure drop and the velocity magnitude exiting the nozzle and entering the bucket. Higher inlet pressure and lower outlet pressure may independently influence the velocity field; for example, Figure 3.35 shows that the 250 psia inlet case with 28 psia outlet pressure yields higher velocities than the same case with 44 psia outlet pressure (Figure 3.34). Figure 3.36 through Figure 3.41 show that this trend exists for the higher inlet pressure cases too.

Inlet pressures above 350 psia start to feature under-expanded nozzle flow, especially with lower outlet pressure. Thus, further expansion and acceleration of the steam may occur immediately outside the nozzle exit as the result of a supersonic expansion process that is necessary to reconcile the fluid pressure with the outlet pressure. Once inlet pressure exceeds 500-600 psia, the nozzle flow always appears under-expanded and further steam acceleration (i.e. due to high inlet or lower outlet pressures) manifests just outside the nozzle exit. However, it is reiterated that the steam has fully expanded before it reaches the turbine or the buckets.

A larger pressure drop also generates more liquid condensation through the nozzle (Figure 3.42). This agrees qualitatively with a Mollier chart analysis, as discussed more in Appendix D. Increased liquid formation might have a direct role in generating more kinetic energy since the condensation decreases the effective specific enthalpy of the mixture outflow. The specific enthalpy of saturated liquid is considerably lower than that of saturated steam, particularly at low pressure.

The contour plots of velocity magnitude suggest that the steam makes at least one or two reversing actions through the reversing chambers. Higher pressure drops (with high velocities) appear to make more usage of the reversing chambers. Velocity streamlines support this assertion, as shown by Figure 3.43 (250 psia inlet) and Figure 3.44 (1000 psia inlet). The case with 250 psia inlet only displays one meaningful reversing action. In contrast, the 1000 psia inlet case exhibits two or three reversing actions. It is noted that about 50% of the flow exiting the first bucket appears to miss the reversing chambers entirely, and this might be the result of the nozzle-bucket alignment used in the current FLUENT model (i.e. the nozzle jet is split between two adjacent buckets, see Figure 3.29).

Initial CFD estimates of torque imparted on the turbine range from 78 Nm for 250 psia inlet pressure and 210 Nm for 1000 psia. Of course, this represents the torque associated with one nozzle and reversing chamber set since the FLUENT model only considers a wedge of the full Terry geometry (Figure 3.19). Rated torque values for various BWR RCIC systems, which probably have 5 to 10 nozzles, are typically listed near 285 Nm for low pressure (near 150 psia) and 730 Nm for high pressure (1000 psia and above). Assuming 5 nozzles, the FLUENT calculations yield torque values of 390 Nm to 1050 Nm. The initial estimates appear grossly

reasonable but deserve further analysis. In particular, CFD analyses with turbine rotation should yield more representative estimates of turbine torque.

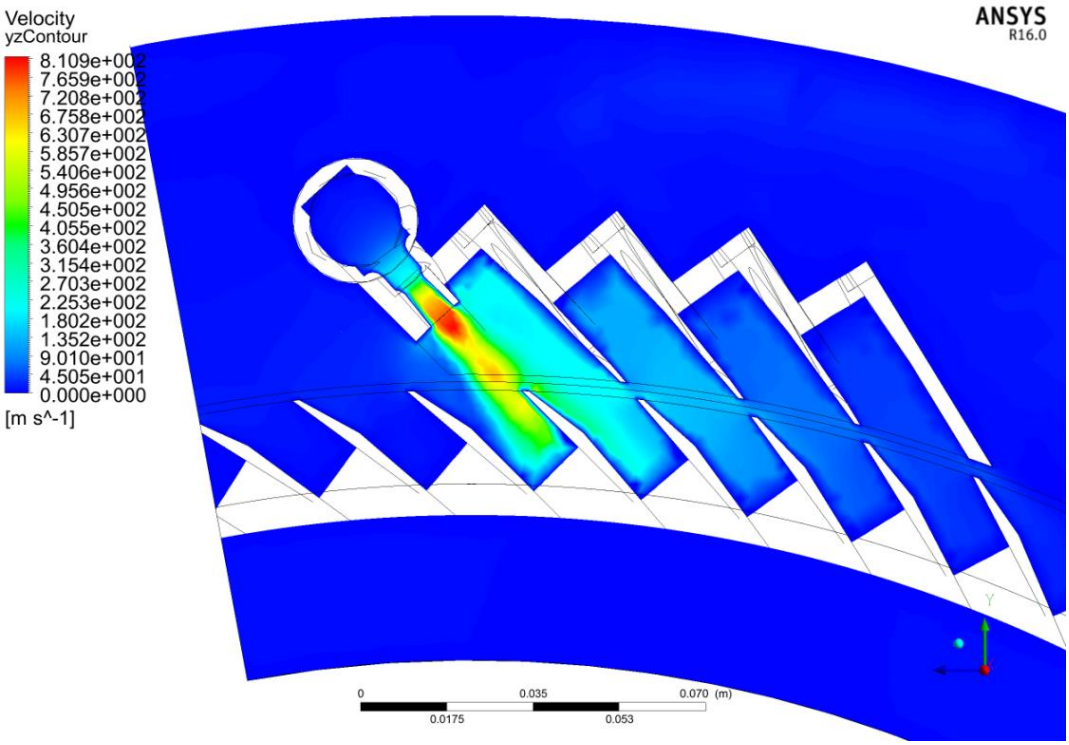

Figure 3.34. Velocity field for 250 psia to 44 psia pressure drop

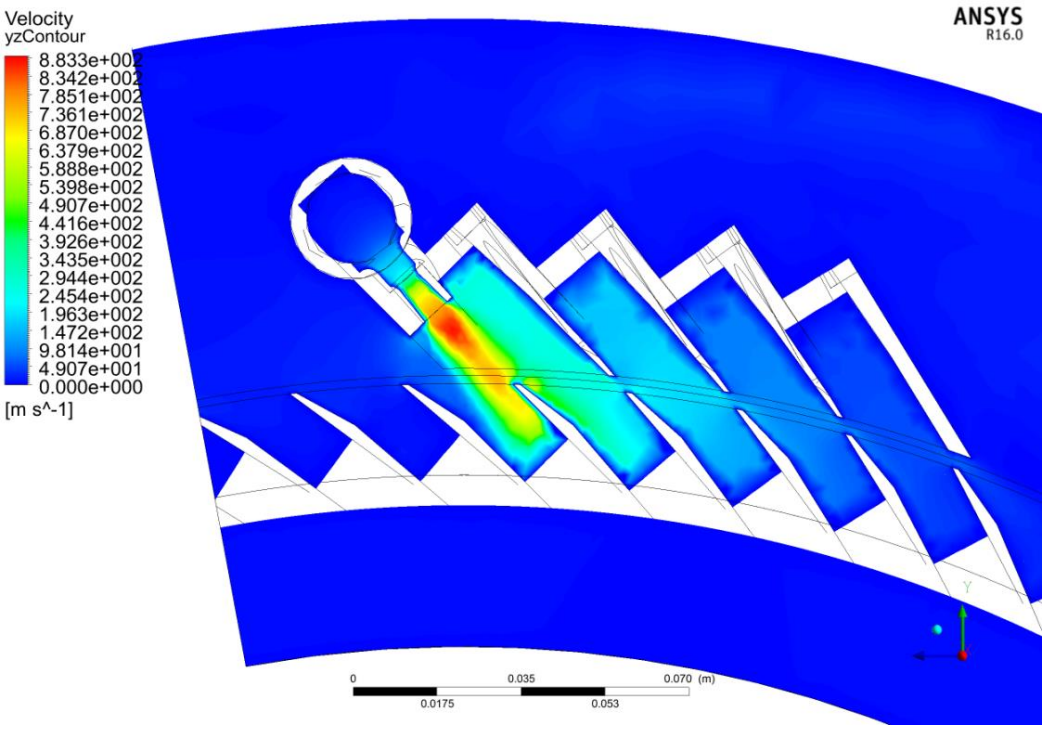

Figure 3.35. Velocity field for 250 psia to 28 psia pressure drop

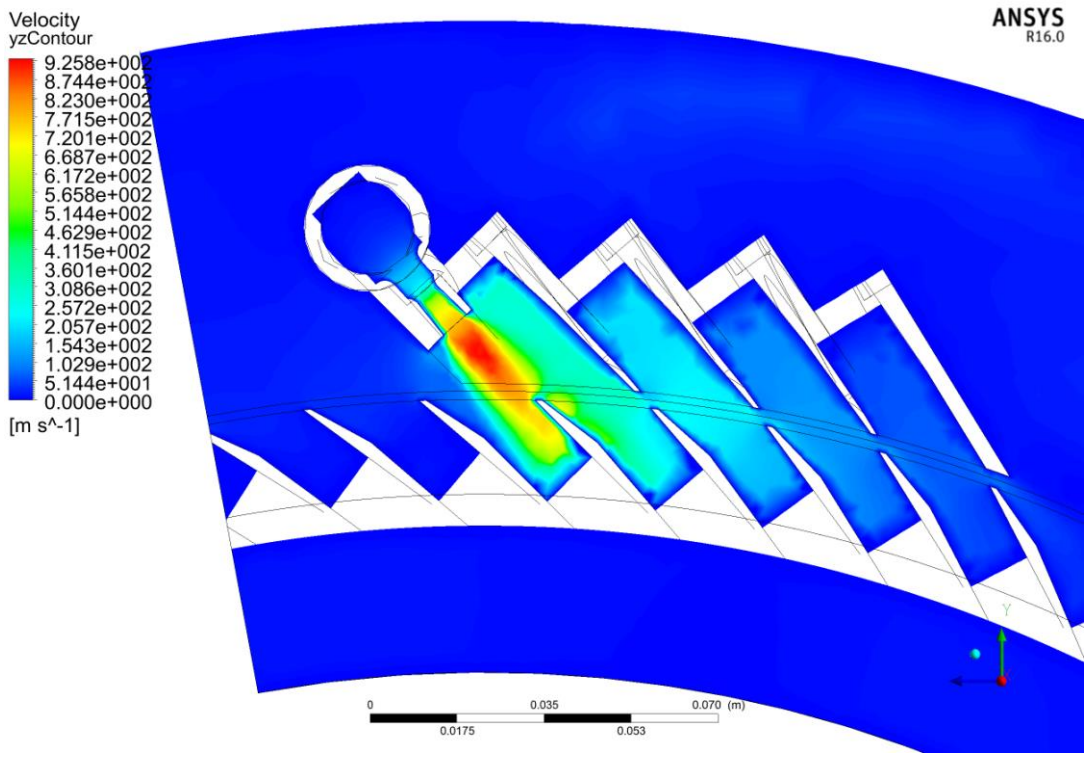

Figure 3.36. Velocity field for 500 psia to 44 psia pressure drop

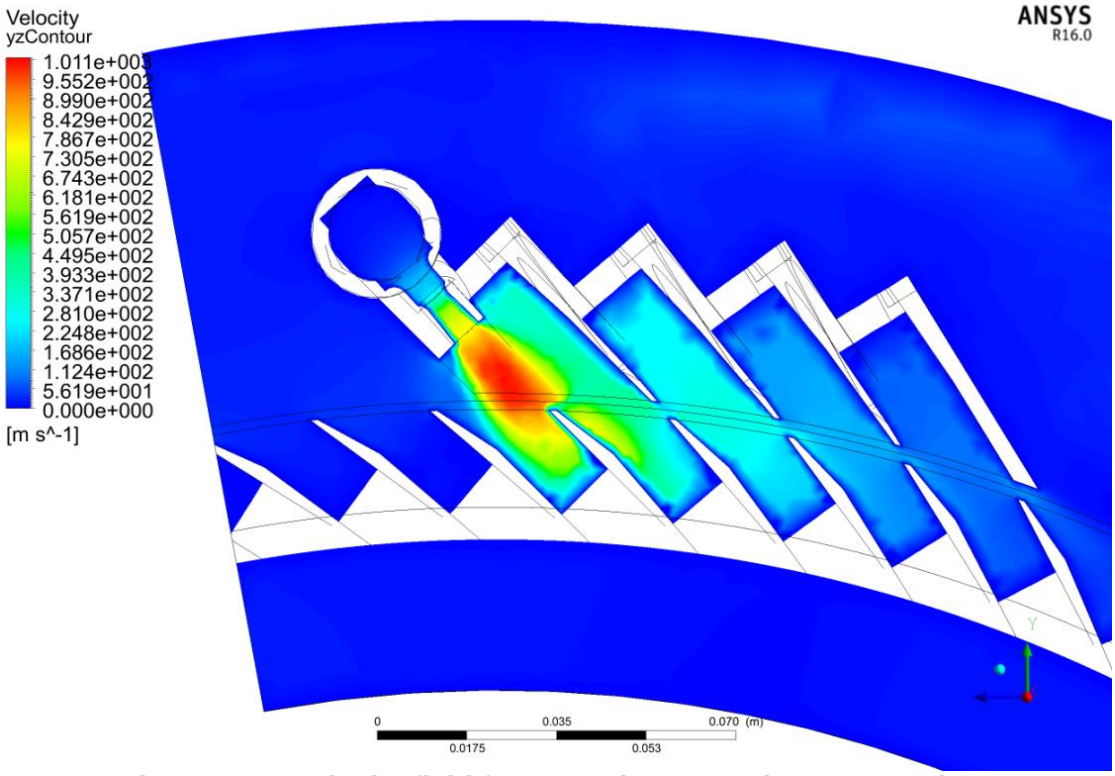

Figure 3.37. Velocity field for 500 psia to 28 psia pressure drop

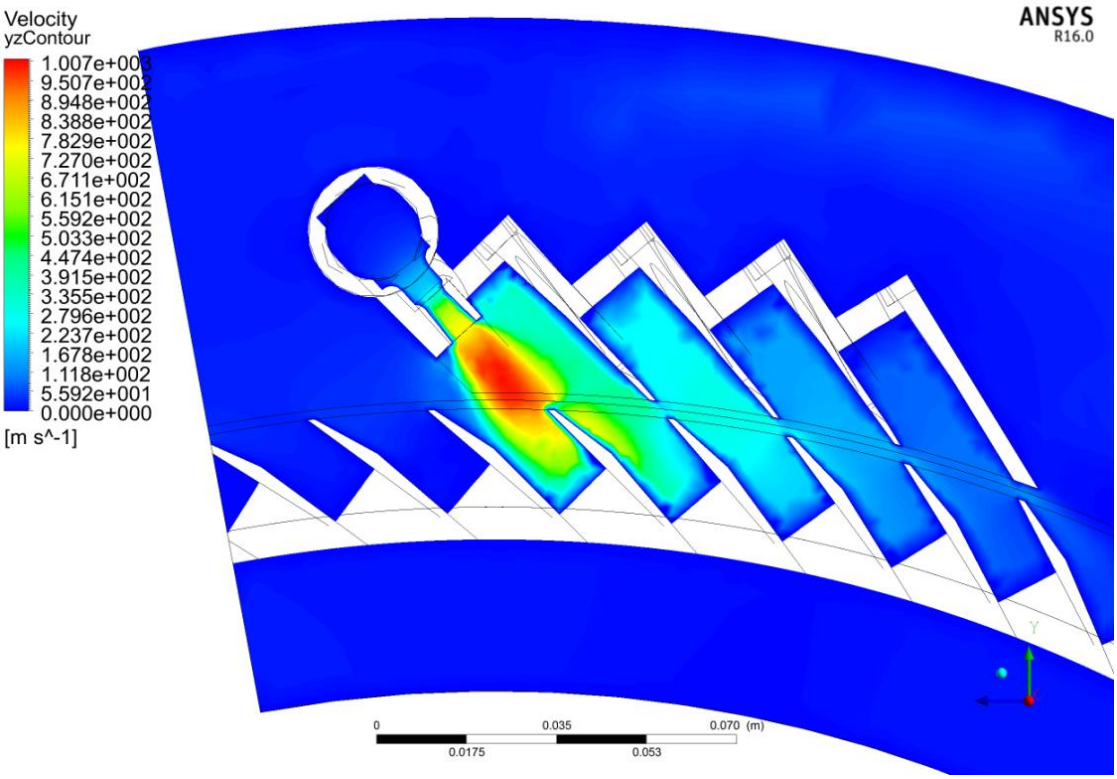

Figure 3.38. Velocity field for 750 psia to 44 psia pressure drop

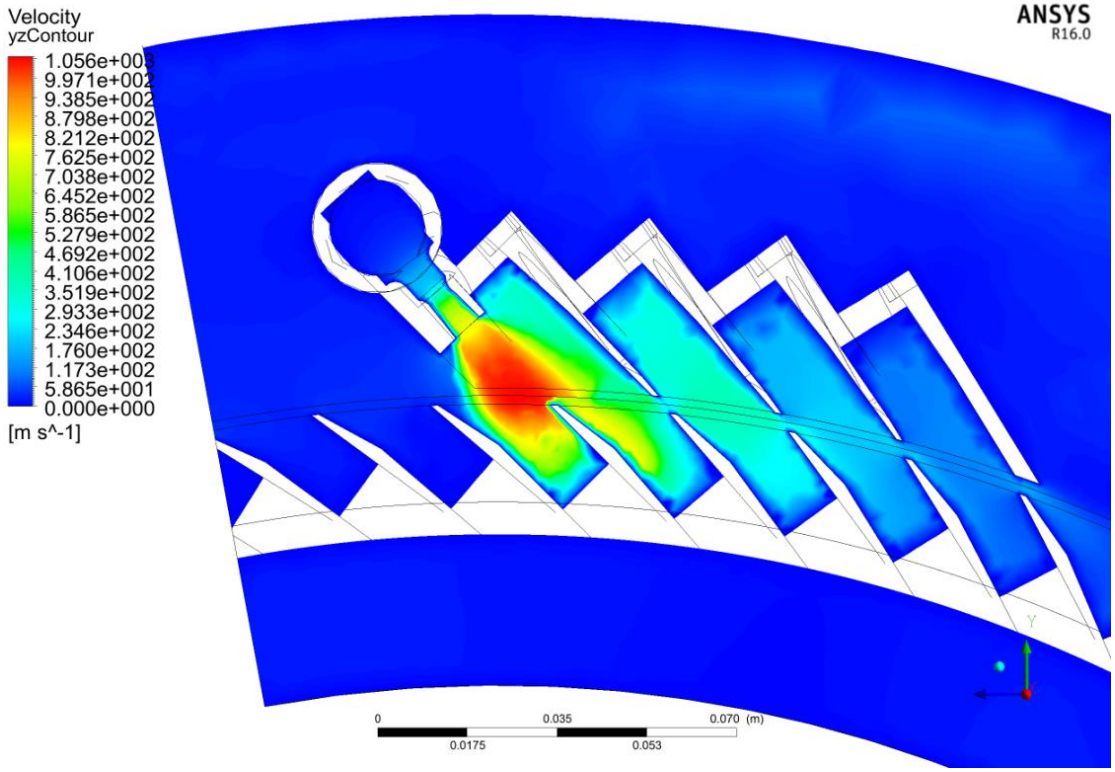

Figure 3.39. Velocity field for 750 psia to 28 psia pressure drop

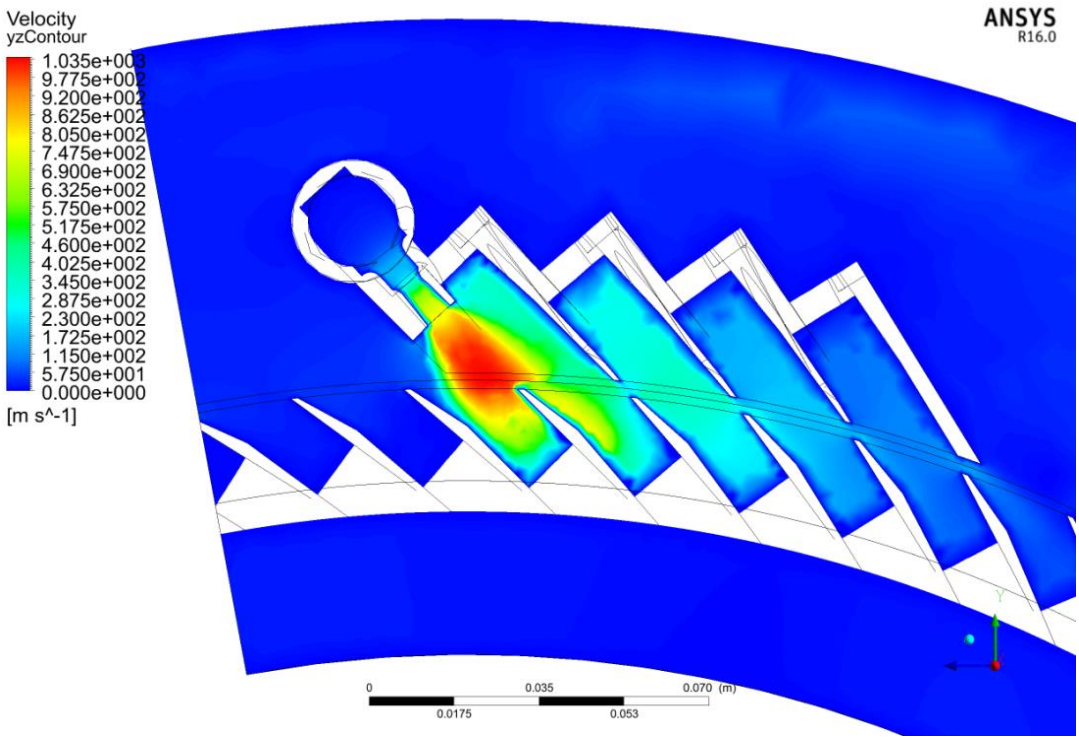

Figure 3.40. Velocity field for 1000 psia to 44 psia pressure drop

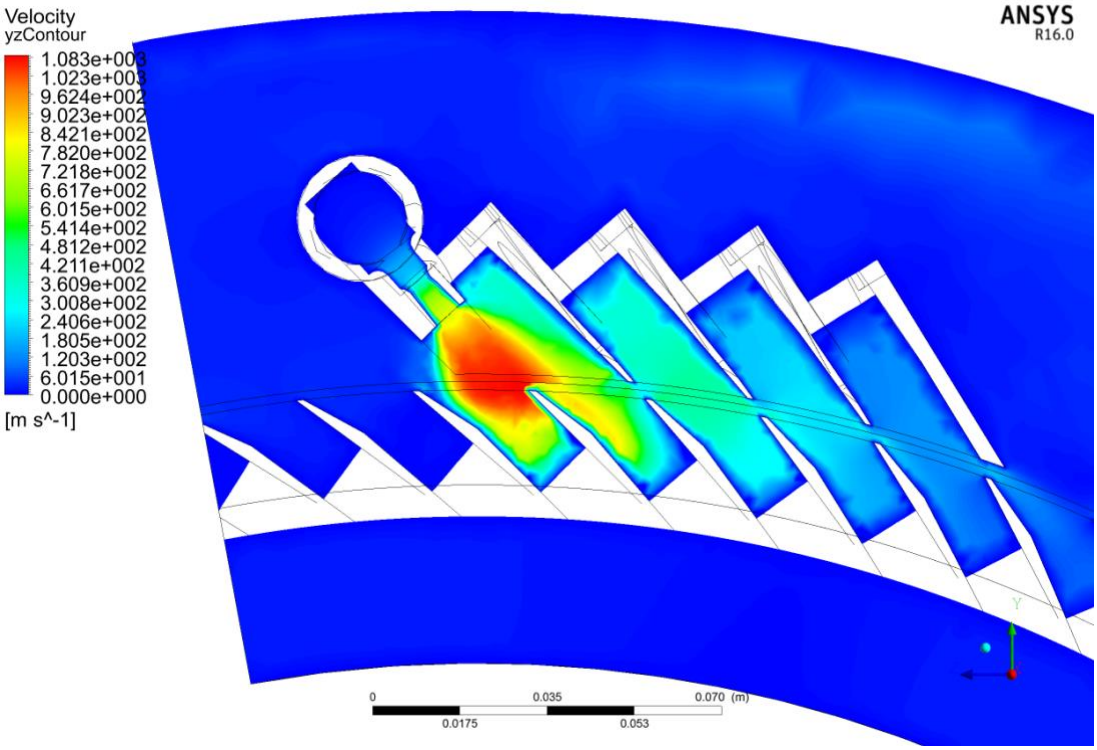

Figure 3.41. Velocity field for 1000 psia to 28 psia pressure drop

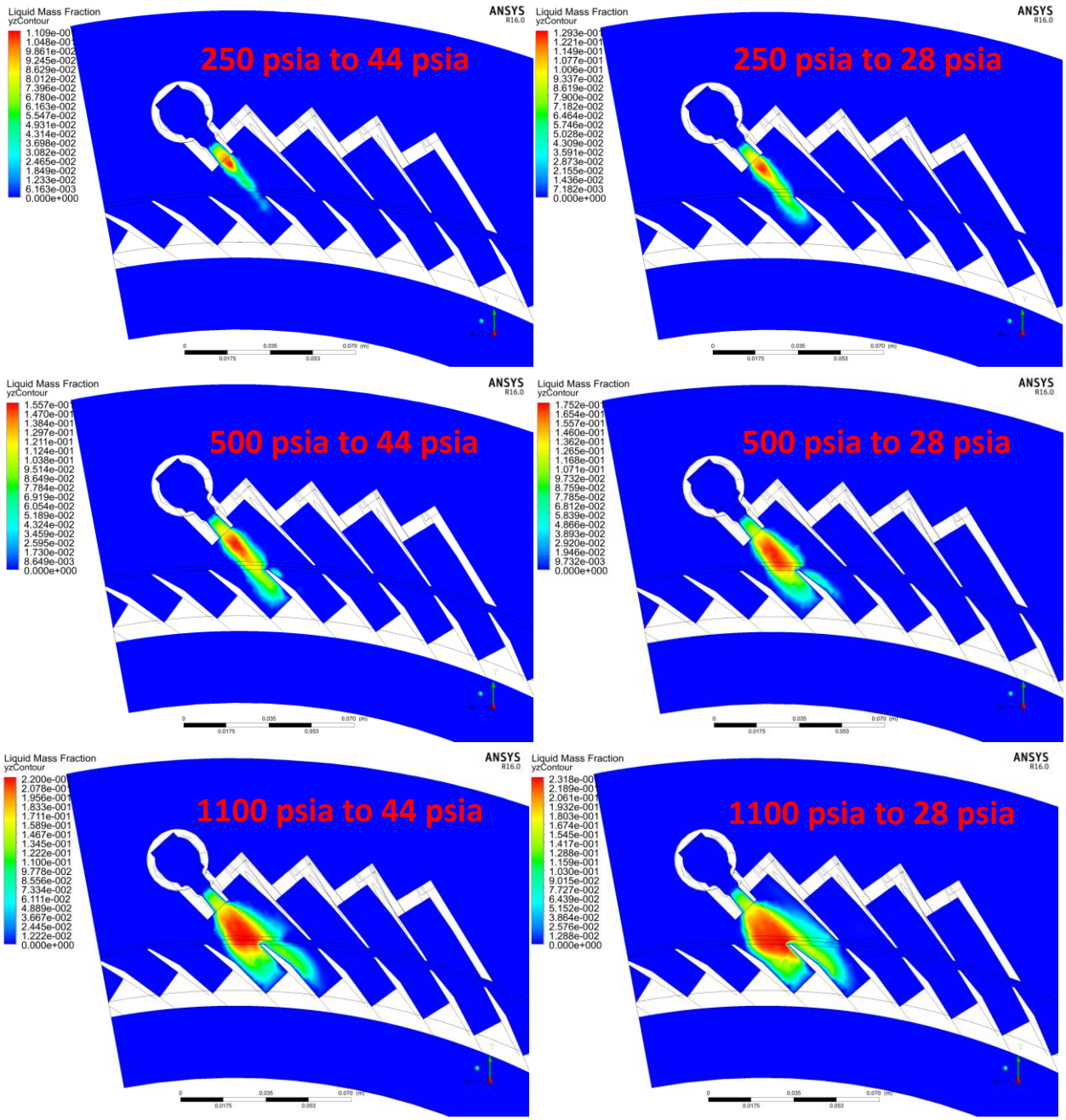

Figure 3.42. Calculated liquid condensation through nozzle for several inlet and outlet pressures

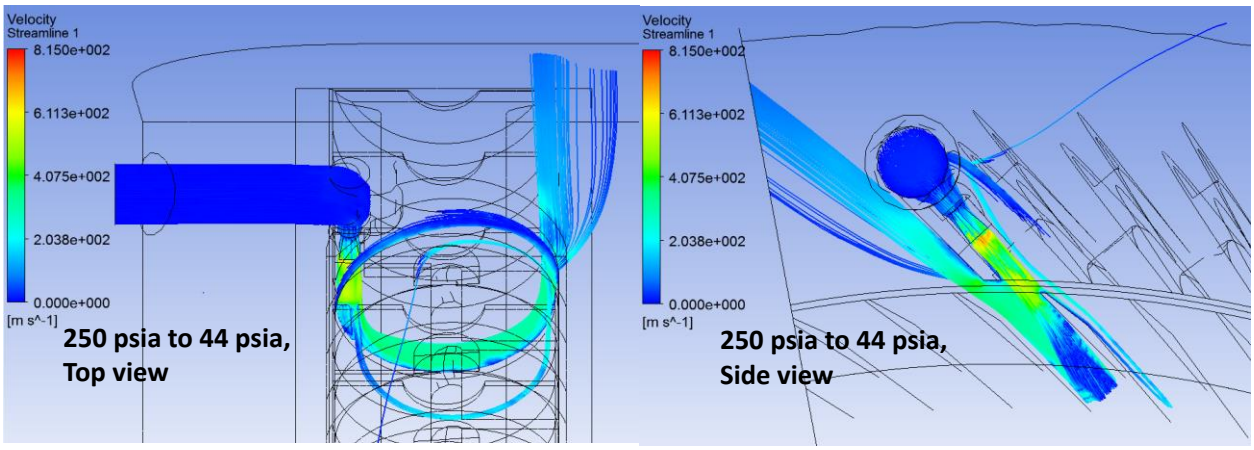

Figure 3.43. Velocity streamlines for 250 psia to 44 psia case

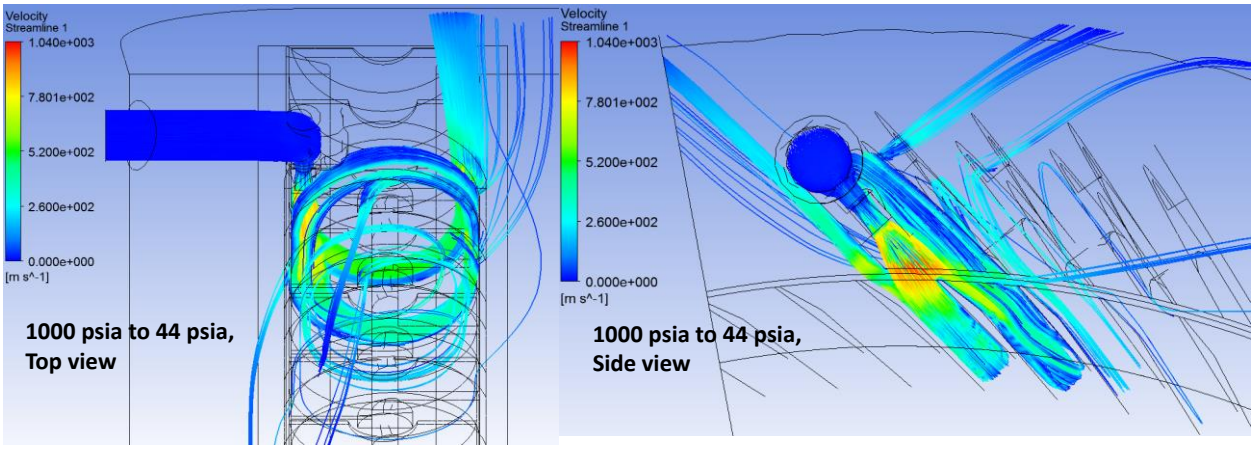

Figure 3.44. Velocity streamlines for 1000 psia to 44 psia case

3.5 Further CFD Analyses

Substantial CFD model development and analysis has been accomplished to support the development and improvement of system-level RCIC models. The CFD problems completed so far are the 'low-hanging fruit;' they have focused on the necessary first steps such as proper geometry creation, and the simulation of fundamental system behavior. Nozzle flow of dry saturated steam at various pressures has been studied in detail, and these analyses have produced several essential inputs that will improve the primary system modeling efforts. Nonetheless, there are several additional CFD analyses that will also improve the system model. CFD analysis of liquid flashing through the nozzles is probably the most important for understanding RCIC performance during BDB scenarios.

3.5.1 Liquid Slug Flashing Simulation

The behavior of liquid flowing through the Terry turbine nozzles and its subsequent impact on torque developed by the turbine is crucial for reliable RCIC functioning during a BDB event. Flashing is believed to degrade the effective momentum flux delivered to the turbine buckets, thereby slowing down the RCIC and decreasing pump flow to the RPV; water level in the RPV

subsequently decreases and the liquid content entering the turbine decreases, and thus the RCIC then accelerates and refills the RPV. This is one potential explanation of uninhibited RCIC operation with high RPV water level. While the details are not yet fully understood, it is a reasonable feedback mechanism that allows the RCIC to operate in a self-regulated mode for a long period of time.

Flow simulations with high liquid content through the nozzles/turbine were not attempted with FLUENT or SolidWorks. The two-phase models used in this work are geared towards dry and wet steam analysis, and are not capable of assessing two-phase problems with high liquid content. Both FLUENT and SolidWorks suggest that these two-phase treatments should be limited to problems where the liquid mass fraction remains below 20%. Above 20% mass fraction, the wet steam approximation (i.e. liquid particles advected in steam) starts to become invalid. There are other two-phase modeling options in FLUENT and SolidWorks that might be capable of considering a nozzle with a mostly-liquid inlet and a two-phase outlet following the flashing process. However, the wet steam models are found to facilitate convergence for the initial assessments; this enables initial simulations of the Terry turbine under normal (or near normal) conditions, which is a necessary first step for informing the system-level RCIC models.

The CFD calculations in this report only examined dry steam inlets for the Terry nozzle, but wet steam ingress should be qualitatively similar [3.10]. The vapor phase behaves as it normally would (i.e. just like if it were dry steam) by expanding, condensing, and accelerating through the nozzle. The liquid phase would either be entrained in the steam flow as droplets or form a film that flows along the nozzle walls [3.10]. Depending on the size of the liquid droplets, some liquid may flash through the nozzle. Sufficiently small liquid can avoid flashing if the liquid temperature decreases just as quickly as the pressure through the expansion. In contrast, larger liquid droplets may cavitate (flash) if the interior liquid temperature does not decrease as fast as the pressure of the fluid [3.6]. For wet steam comprised of fog (micron-sized liquid droplets), liquid flashing is generally limited to the largest of liquid droplets that form a small fraction of the two-phase mixture, and most of the liquid in the mixture simply drops in temperature and remains liquid through the expansion. Therefore, wet steam flow through the nozzle will likely yield even wetter steam at the nozzle exit, and even with some limited flashing, a wet steam inlet should produce sufficient momentum to drive the turbine.

The complication remains that the quality and flow regime at the RCIC inlet are currently unknown, and could potentially be variable throughout a BDB event like the Fukushima Daiichi Unit 2 extended RCIC operations. The quality and flow regime of the two-phase mixture likely have a significant influence on the nozzle flow and consequently turbine-pump performance. For example, stratified flow with 90% quality probably behaves very differently than 90% quality fog/mist flow (i.e. wet steam): The liquid droplets in the wet steam may not undergo much flashing (given the above discussion on liquid droplet size and flashing), and thus the liquid in the wet steam mixture might not degrade turbine torque very much. In contrast, the stratified flow would lead to considerable flashing through one or several nozzles, which degrades the turbine. Stratified flow may also bifurcate in the steam chest (i.e., the nozzle inlet casing); pure steam (or wet steam) may flow through the upper nozzles, while liquid water flashes through the lower nozzles.

CFD simulations of liquid flashing through the Terry turbine should enable better predictive analysis of RCIC performance for severe accidents. Without CFD insights, the liquid degradation on the turbine drive momentum can still be inferred parametrically using the system model and the limited Fukushima plant data. That said, corroborative CFD analyses will increase the technical confidence in the system model and improve its capabilities as an experimental design tool.

3.5.2 Additional Scenarios and CFD Sensitivities

Besides liquid flashing, several additional CFD calculations could provide important information for system-level models. The effects of the reversing chambers at variable conditions warrant more CFD analyses. The angular speed of the turbine will affect the bucket exit flow and the efficacy of the reversing chambers, both of which have impacts on the turbine torque.

The CFD analyses in this report implemented several approximations to facilitate an initial examination of the Terry turbine. The accuracy and precision of the RCIC models (both CFD and system-level) will require continual improvement in order to meaningfully support strategies in transitioning from RCIC to Phase 2 FLEX equipment, and expanded Terry turbine operation experimental design. This might require quantification of modeling and numerical sensitivities in the CFD calculations, such as:

- CFD mesh sensitivity: Base FLUENT calculations used a reasonable (1 million cell) mesh with good quality for one nozzle, one reversing chamber set, and 11 buckets.

- FLUENT solver settings: Base FLUENT calculations used first-order discretization options to facilitate convergence. Further analyses should investigate higher-order solution methods.

- Approximations of wet steam model: Higher pressure drops leads to higher condensation outside the nozzle; inlet pressures near 1000 psi exhibit condensation near the advised limit of 0.2 mass fraction. The FLUENT wet steam model can go higher, but the predictions might require validation using more versatile two-phase models.

3.6 Section 3 References

[3.1] J. Kelso et al., "Terry Turbine Maintenance Guide, RCIC Application," EPRI Technical Report, report number 1007460, Electric Power Research Institute, Palo Alto, CA, USA (2012).

[3.2] G.A. Orrok, "Small Steam Turbines," *Transactions of the American Society of Mechanical Engineers*, Washington D.C., May 1909, Vol. 31, pp. 263-287 (1910).

[3.3] W.J.A. London, "A Commercial Analysis of the Small-turbine Situation," *Transactions of the American Society of Mechanical Engineers*, New York, December 1917, Vol. 39, pp. 263-287 (1918).

[3.4] C.W. Dyson, "Test of Terry Steam Turbine," *Journal of the American Society of Naval Engineers*, **21** (3), pp. 884-890 (1909).

[3.5] J. A. Moyer, *Steam Turbines*, John Wiley & Sons, New York, NY (1914).

[3.6] M.J. Moore and C.H. Sieverding, *Two-Phase Steam Flow in Turbines and Separators*, Hemisphere Publishing Corporation, Washington, D.C. (1976).

[3.7] L.G. French, *Steam Turbines: Practice, and Theory*, Hill Publishing, New York, NY, 1907. See discussion on Strickland L. Kneass nozzle experiments on pages 221-228.

[3.8] Ansys, Inc., "ANSYS FLUENT User's Guide," Version 16.2, July, 2015, Canonsburg, PA, http://www.ansys.com.

[3.9] Dassault Systems, "Technical Reference: SolidWorks Flow 2014," http://www.solidworks.com/sw/products/simulation/flow-simulation.htm (2014).

[3.10] A. Amini and I. Owen, "The use of critical flow venturi nozzles with saturated wet steam," *Flow Measurement and Instrumentations*, **6** (1), pp. 41-47 (1995).

[3.11] http://www.engineeringtoolbox.com/mollier-diagram-water-d_308.html

[3.12] G. Zeuner, "Technical Thermodynamics," Vol. 2, 83.

4 EXPANDED SYSTEM-LEVEL MODELING

The promising results from the system-level model development in Section 2 have established the basis of a momentum-based, lumped parameter description of the Terry turbine for severe accident simulations. In conjunction with CFD results on Terry turbine nozzle behavior from Section 3, the next steps in system-level modeling are:

1. Improve pump modeling through the use of homologous curves;

2. Create a RELAP and MELCOR system model of the RCIC system, using the governing equations derived in Section 2; and

3. Integrate CFD insights on supersonic flow through the Terry turbine nozzles by implementing velocities curves into MELCOR and RELAP models for the RCIC system.

These system model enhancements are further discussed within this section, in addition to updated test calculations. The calculations yield new insights on the potential for a turbine overspeed trip following the loss of power. Although uncertainties still exist concerning the design of the governor valve at Fukushima Daiichi Unit 2, it is possible that the governor valve may sufficiently open after power is lost to consequently trip the RCIC pump due to excessive momentum flux and overspeed. The updated models and calculations have expanded capability to examine such scenarios.

4.1 Homologous Pump Modeling

Centrifugal pump modeling capabilities employing homologous pump curves were recently added to MELCOR as a proof-of-concept in support of the RCIC modeling efforts. Two sets of built-in curves using a generic algorithm were included; similarly as in RELAP, representative of Westinghouse and Bingham-brand pumps, allowing the use of homologous definitions without a comprehensive knowledge of pump characteristics. The user can adjust (i.e., scale) the built-in curves by specifying problem-dependent design numbers such as rated pump speed, rated head, and rated torque. Given sufficient pump information, the user may also uniquely specify homologous curves. The pump source terms require an implicit or semi-implicit solution for stability given the large (relative to the courant condition) time steps necessary for efficient severe accident simulations. MELCOR originally represented pumps as an explicit pressure (ΔP) term in its momentum/velocity equation.

Taking advantage of the centrifugal pump modeling features, homologous head and torque curves have been constructed from representative RCIC pump data and defined in the simplistic Unit 2 MELCOR test model described in Section 2.3. Important in considering the simplistic model is to realize that it was designed to support key happenings and trends associated with the Unit 2 accident but that it is not a full representation of the reactor system. Exercising the new pump modeling features increases the realism of the model but the model remains simplistic. Including the homologous curves has placed the responsibility of calculating RCIC pump dynamics on the system-level code, such as MAAP or MELCOR, rather than on the user. In the case of MELOCR, the user, through control functions, remains responsible for calculating the shaft torque developed by the RCIC turbine, but the pump response and speed response of the

RCIC system as a whole becomes system-level model's responsibility. Noteworthy with respect to the homologous curves constructed for use in this RCIC modeling effort is that the generic algorithms are not MELCOR-specific; they could be utilized just as well in RELAP, TRACE and MAAP calculations.

Exercising the simplistic MELCOR Fukushima Unit 2 model with the new centrifugal pump modeling features is generally furthering the RCIC modeling effort. Certain modeling considerations are being reviewed in light of recent model responses (see Section 4.3.2). Enhancements that could benefit the early quasi-steady modeling have presented themselves; such as a speed predictor/corrector based on pump head and flow rather than solely head, and are allowing the modeling to predict over-speed given full steam to the RCIC turbine which is expected. Recent realizations about the accident are being investigated such as the operators having throttled RCIC before the loss of DC power by recirculating a portion of RCIC pump flow to the CST. These investigations challenge the RCIC modeling and so contribute to the modeling effort.

The CAD and CFD accomplishments described in Section 3 of this report have critically informed the latest system-level model solution (i.e., the homologous-curve solution) with respect to:

1. The approach angle of a steam jet to the RCIC turbine wheel.

2. The Mach number of a steam jet entering a bucket on a turbine wheel (~3 at reactor operating pressures).

3. The Mach number of a steam jet leaving a bucket on a turbine wheel (~2 at reactor operating pressures).

Additional information needs in the ongoing RCIC modeling work include:

1. The number and size of the steam nozzles consistent with the performance information of a particular RCIC turbine (e.g., a GS-1 model Terry turbine has five steam nozzles while a GS-2 model Terry turbine has ten steam nozzles).

2. The flow characteristics of a RCIC turbine governor valve and the minimum flow area of a fully open governor valve.

3. The state of the CST recirculation valve(s) in the Fukushima Daiichi Unit 2 accident after switchover of RCIC suction to the wetwell (e.g., were the valves closed at switchover?).

The system-level model RCIC solution utilizing the new homologous pump features are intended to be the solution carried forward in future RCIC modeling work. The solution is expected to add needed realism to Fukushima Unit 2 accident simulations and will inform the design of full-scale testing configurations.

4.2 RELAP Model of RCIC

A RELAP model of the RCIC system is created using an existing BWR RELAP model as a template. The BWR RELAP model used in this report was originally developed by Idaho National Laboratory (INL). Most of the thermal-hydraulic inputs for the core, RPV, and RCS are left unchanged for the RCIC analyses. Nonetheless, considerable input revisions and additions are still necessary to simulate the thermal-hydraulic components of the RCIC system. Control variable inputs (the analog of MELCOR control functions) are required to implement the Terry turbine relationships.

4.2.1 RCS Nodalization

The RELAP model has a reasonably detailed nodalization of the primary RCS. This includes nodalization of the steam line that leads to the RCIC steam piping. Figure 4.1 depicts the original nodalization of the BWR RELAP model. The original HPCI/RCIC connections are removed for the implementation of the new RCIC hydraulic elements and associated control variables.

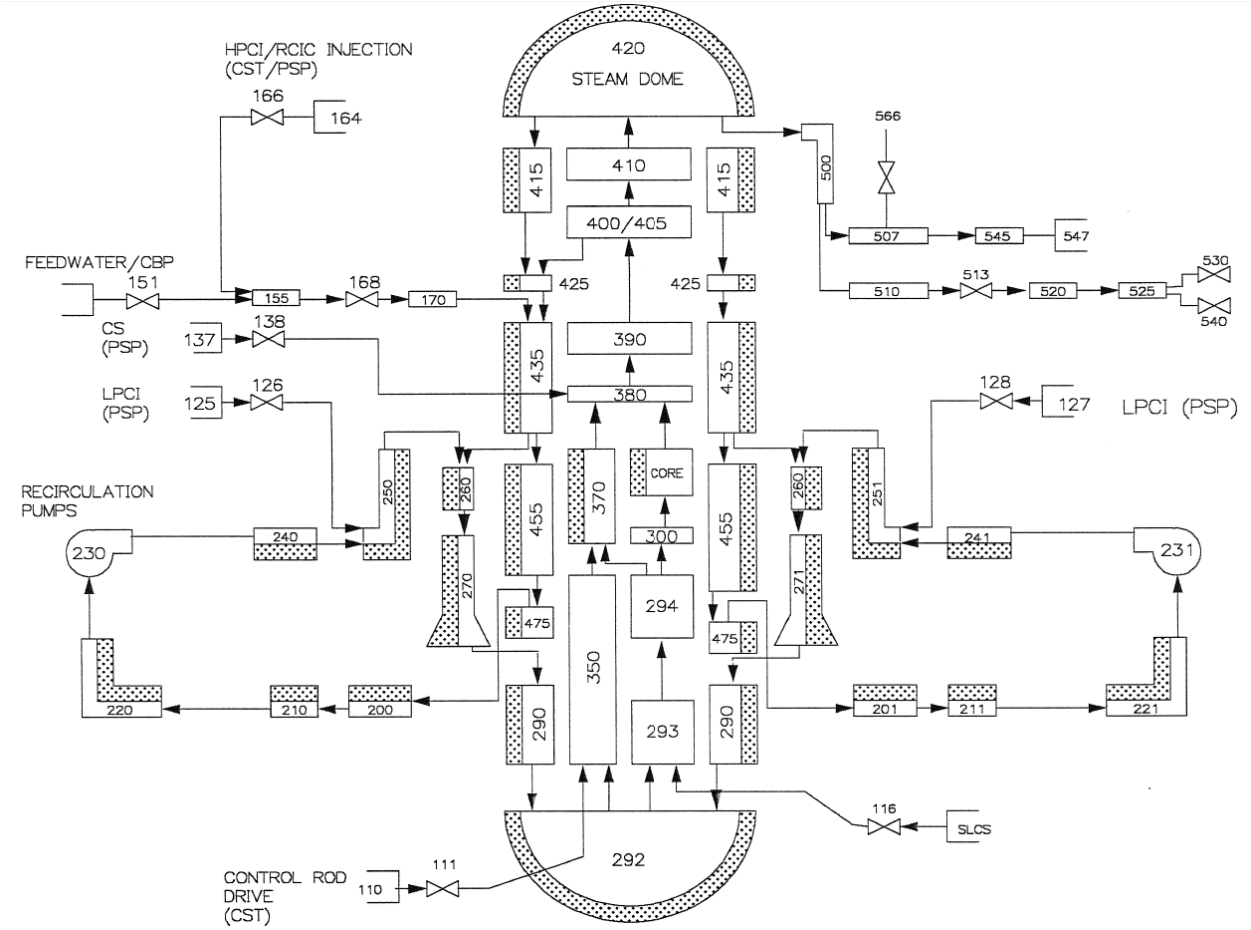

Figure 4.1. Original nodalization of BWR RELAP model[8]

[8] Figure courtesy of Idaho National Laboratory.

4.2.2 Inputs for RCIC and Associated Piping

Figure 4.2 provides an illustration and summary of the steam piping nodalization for the RCIC. The RCIC piping, which is considerably smaller than the MSL (i.e., 0.22 ft vs. 1 ft inside diameter), taps off the MSL after it descends about 50 ft from the MSL-RPV interface elevation, but before it runs horizontal in the lower drywell-to-containment penetration. The SRV piping is near the RCIC-MSL steam piping interface. The RCIC steam piping is assumed to be 190 ft long, including a 60 ft decrease in elevation. The RCIC piping length and diameter are reasonable, but approximate values that are inferred from limited information (e.g., References [4.1] and [4.2]); most geometry data and pump ratings (see Table 4.1) are derived from information made available under the OECD-NEA's Benchmark Study of the Accident at the Fukushima Daiichi Nuclear Power Station (BSAF) project [4.3]. There are three main valves leading to the Terry turbine: the steam inlet valve, turbine stop valve (i.e. trip/throttle valve), and the RCIC governor valve [4.3][4.4]. Only the governor valve is currently represented in the RELAP model. The Terry turbine is a user-specified volume (i.e. a RELAP time-dependent volume component) which can reflect the pressure and temperature of the wetwell. RCIC discharge to the containment is currently not modeled directly; the Fukushima Daiichi Unit 2 containment data is used as a boundary condition.

Table 4.1. Input values for RELAP test calculations

Input variable	Value
Turbine radius	12 inches
Nozzle inlet/outlet angle	32-45^{o}
Nozzle total choked flow area	0.006 ft^2
RCIC steam chest volume	1.5 ft^3
Terry turbine design torque	500-540 ft lb
Turbine moment of inertia	237 lb ft^2
RCIC pump moment of inertia	10 lb ft^2
Rated RCIC speed	4287 rpm
Rated pump head	2531 ft
Rated pump torque	331 ft lb
RCIC pump injection flow area	0.18 ft^2
RCIC pump minimum flow bypass area	0.002 ft^2
RCIC steam piping flow area	0.038 ft^2
RCIC governor valve flow area	0.034 ft^2
CST-WW suction switch	14 hours
CST temperature	70 ^{o}F
WW pool temperature at suction switch	235 ^{o}F
RELAP homologous pump curve set	Bingham
Time of governor valve opening	200 sec
Governor valve maximum open fraction	1.0

The nodalization of the RCIC pump and injection piping is depicted in Figure 4.3. Pump suction piping is assumed to be 150 ft of piping with an internal diameter of 0.48 ft. The CST and wetwell water reservoirs are represented by the same time-dependent volume; the pump suction switch (assumed at 14 hours) is treated as a change in pressure and temperature in the time-

dependent reservoir volume. The RCIC injection piping is assumed to be 150 ft of piping (I.D. = 0.48 ft) that includes a 50 ft increase in elevation. The injection piping connects to the feedwater (FW) volumes shown in Figure 4.1. Check valves prevent back flow through the injection piping and water reservoir; this prevents thermal-hydraulic convergence errors if RELAP predicts RPV pressures that momentarily exceed the dynamic pump head. High RPV pressure may also preclude pump injection into the FW lines, and hence a minimum flow bypass line is necessary in the RCIC thermal-hydraulic nodalization. Otherwise, RELAP will predict a rapid increase in liquid temperature, which leads to boiling in the pump component/piping and subsequent thermal-hydraulic errors. The minimum flow line leads back to the water reservoir, which represents the CST or wetwell depending on the simulation time. The minimum flow line is small enough (0.002 ft^2, see Table 4.1) to have a trivial influence on the pump's nominal flow rate to the RPV, but large enough to ensure that the pump is always able to move water even if the RPV pressure is relatively high. This increases the realism and stability of the RELAP model with the RCIC components.

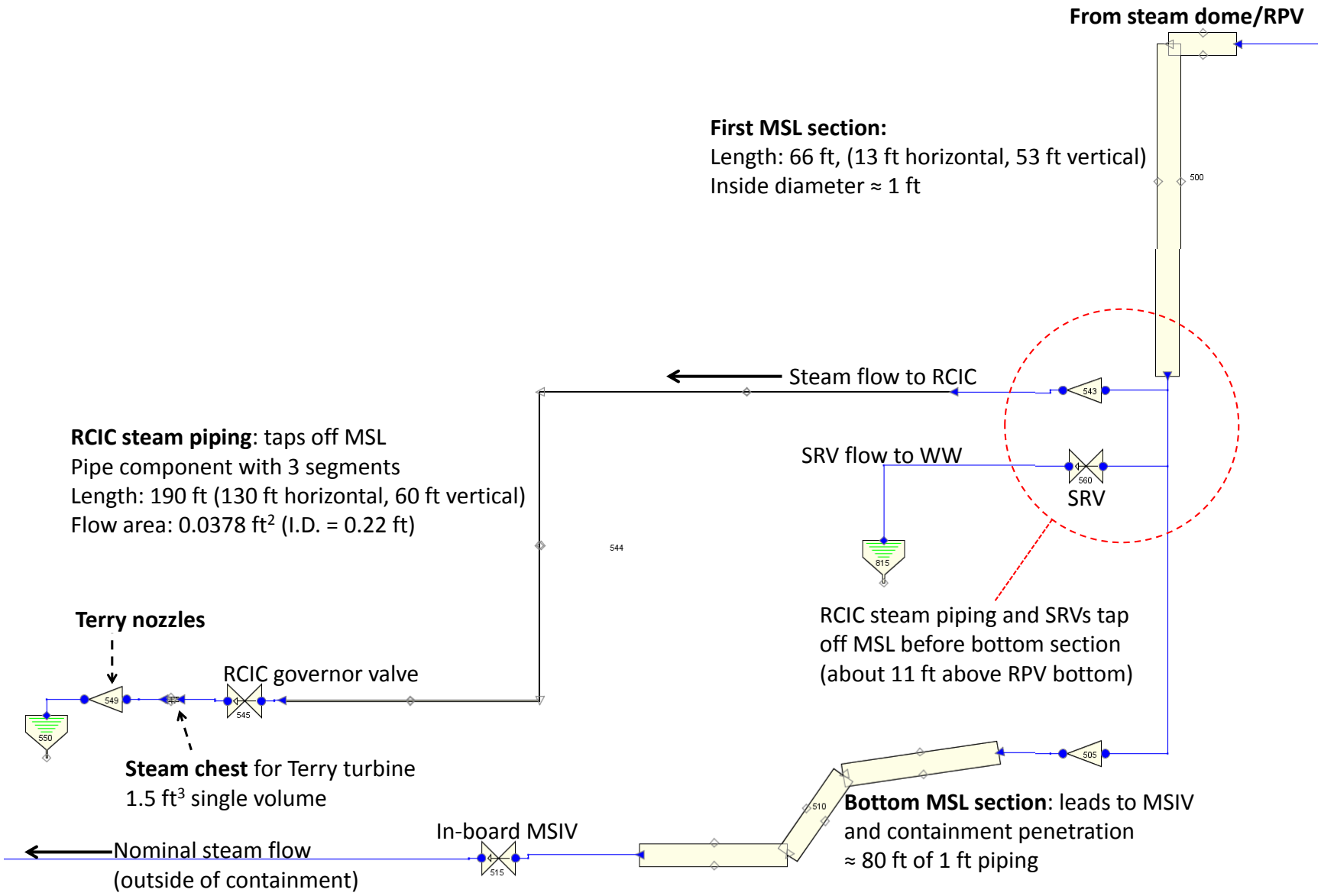

Figure 4.2. RELAP nodalization of steam piping to RCIC

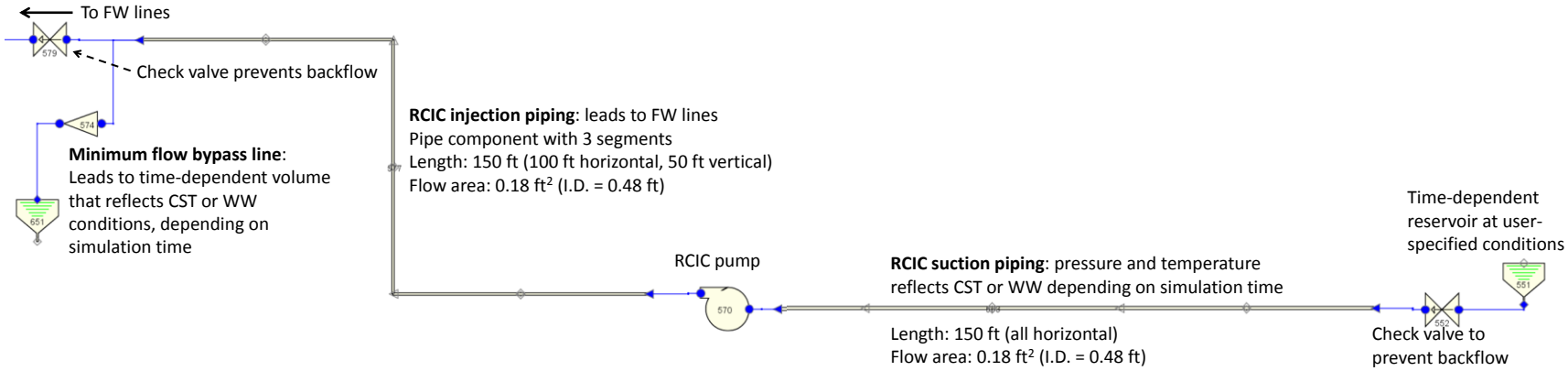

Figure 4.3. RELAP nodalization of RCIC injection components

The Terry turbine relationships from Section 2 are incorporated into the RELAP model via control variables. RELAP has the internal ability to advance equations of motion for rotational components coupled by a common shaft. This essentially amounts to solving the cross product of Newton's Second Law (i.e., $\sum I \frac{d\omega}{dt} = \sum M$) for the turbine and pump. It is preferable to have the thermal-hydraulic code perform as much of the calculus as possible, instead of solving a differential equation in the control system (i.e. user side-calculations). Therefore, the quasi-steady torque expression derived for the Terry turbine (Equation 4.1) is evaluated via control system inputs:

$$T_{Terry} = 2r(\dot{m}_v V_v + \dot{m}_l V_l)cos\beta - r^2\omega(\dot{m}_v + \dot{m}_l)(1 + cos\beta) \quad (4.1)$$

The turbine drive torque is linked to a RELAP shaft component, which is subsequently connected to a pump component. The pump component uses pre-existing homologous curves for a Bingham pump, since sufficient RCIC-specific pump information is currently unavailable, and the pump is scaled to the representative design values for a Fukushima Unit 2-sized (~2000 MW_{th}) RCIC system (see Table 4.1). The drive torque given by Equation 4.1 represents the torque generated by the Terry turbine (excluding friction losses that RELAP can estimate via the shaft component), and is not necessarily the torque developed by the RCIC pump. The pump efficiency is treated by the RELAP pump component and its associated homologous curves. This decreases the pump torque relative to the driving turbine torque. Eventually, homologous curves that closely represent a specific RCIC system will be developed and implemented into this system model.

To calculate the jet momentum rate for each phase in Equation 4.1, RELAP calculates the mass flow rate through its two-phase choked flow models, and the velocity is provided by analytic fits of the FLUENT results. Logarithmic fits on the bucket velocities, as a function of pressure drop ratio over the nozzles, are implemented into the RELAP model through control variables. The FLUENT calculations and the analytic fits are discussed in Section 3.4.1. RELAP calculates the pressure in the steam chest volume just before the nozzles (Figure 4.2); it could also dynamically calculate the containment pressure that directly influences the turbine discharge pressure, but turbine pressure is currently treated as a boundary condition that reflects the wetwell pressure data from Fukushima unit 2. Control variables then examine the ratio of steam chest pressure to the turbine exhaust pressure to determine the current bucket velocity values.

Conceptually, the RELAP test model is similar to the original MELCOR test model from Section 2. A system-level thermal-hydraulic code simulates the RPV and RCS response, and separate formulations treat the response of the turbine. However, the RELAP model now considers the MSLs and the RCIC steam piping in further detail, including changes in elevation. The RELAP model also has a reasonably detailed nodalization of the core and RPV, as shown by Figure 4.1. Most importantly, RELAP now simulates the pump dynamics through the use of scaled homologous pump curves, where before the pump was treated more simply via a user-derived head term. Hence, a pump component in the RELAP model is connected to a shaft component that is driven by the Terry torque relationship given by Equation 4.1. Figure 4.4 provides a simplified illustration of the key physics components in the RELAP model. It is largely comparable to the model from Section 2 (see Figure 2.3). In the RELAP model, the nozzles are effectively modeled in two parts: RELAP determines the mass flow rate through the

nozzles using its two-phase choked flow models (this is flow behavior up to the throat of the nozzles), and the supersonic velocities that develop in the diverging section are informed by the FLUENT calculations which are discussed in Section 3. The critical velocities (including the rates of change) predicted by RELAP's choked flow model are not applicable to the diverging section of the nozzle.

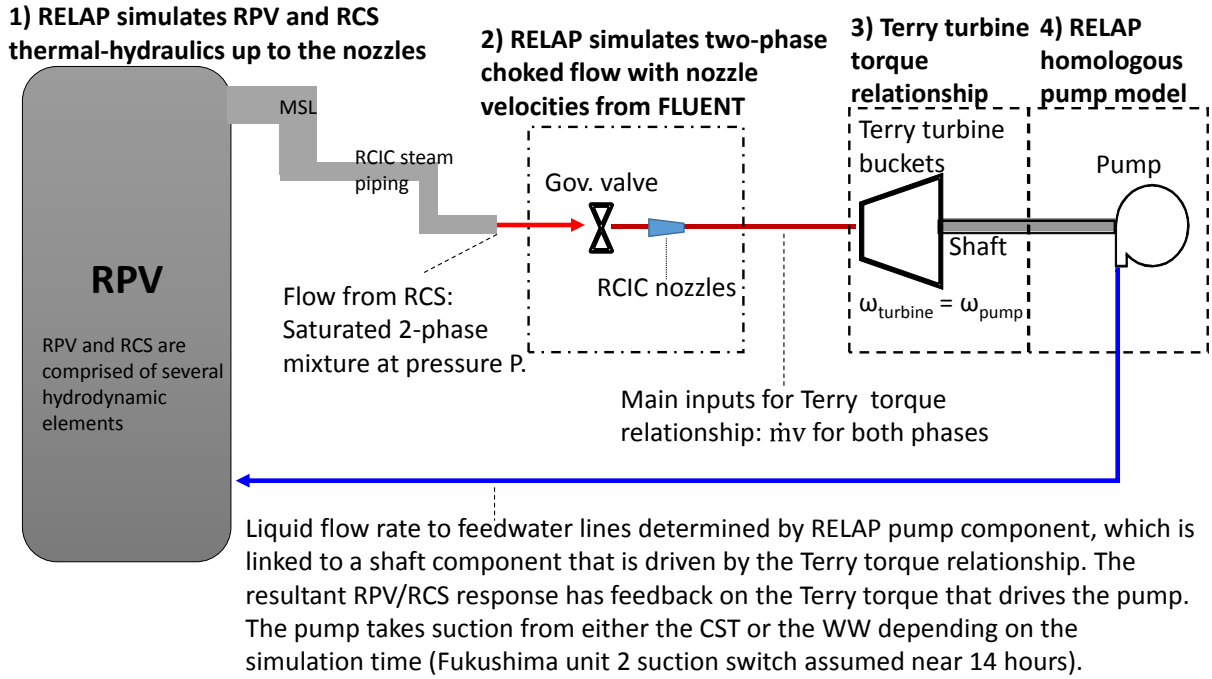

Figure 4.4. RELAP calculations of RPV pressure compared to Fukushima data

The RELAP model implements a degradation multiplier on the liquid momentum rate in Equation 4.1 ($\dot{m}_l V_l$) that is derived parametrically by running several hundred RELAP calculations with different multipliers. A *reasonable*, *preliminary* value for the liquid degradation multiplier is then selected by juxtaposing the RELAP calculations against plant data for Fukushima Unit 2. The assessment is not quantitatively rigorous, particularly since the RELAP model does not closely reflect Unit 2. A degradation multiplier of about 0.13 is found to produce decent pressure trends relative to the Fukushima data. A much higher value leads to excessive momentum delivered to the turbine following RPV overfilling (i.e. the RCIC pump runs faster and faster with no negative feedback). A much lower value leads to RCIC stopping completely with any liquid flowing through the nozzles (even ~1% liquid mass fraction), which seems unreasonable considering the Terry turbine has a known ability to work through isolated slugs of liquid water [4.4]. Ultimately, the liquid degradation multiplier may be corroborated by CFD calculations or experimental analysis.

4.3 System Model Results

This section provides the updated system-level calculations performed with homologous pump models coupled to the Terry turbine relationships developed in Section 2. Higher-fidelity pump representations in the RCIC modeling framework enables the investigation of RCIC overspeed,

which is of fundamental significance for the system during uncontrolled beyond design basis events. The updated system-level calculations in this section also incorporate the CFD results for supersonic nozzle velocities.

4.3.1 RELAP Calculations

Figure 4.5 shows RPV pressure for three RELAP calculations. The calculations are examined against Unit 2 plant data from the accident. The comparison is qualitative since the RELAP model does not closely represent Fukushima Unit 2. The three RELAP calculations have a few differences, as listed in

Table 4.2, in order to assess the simulation space of the RELAP model with the Terry turbine relationships.

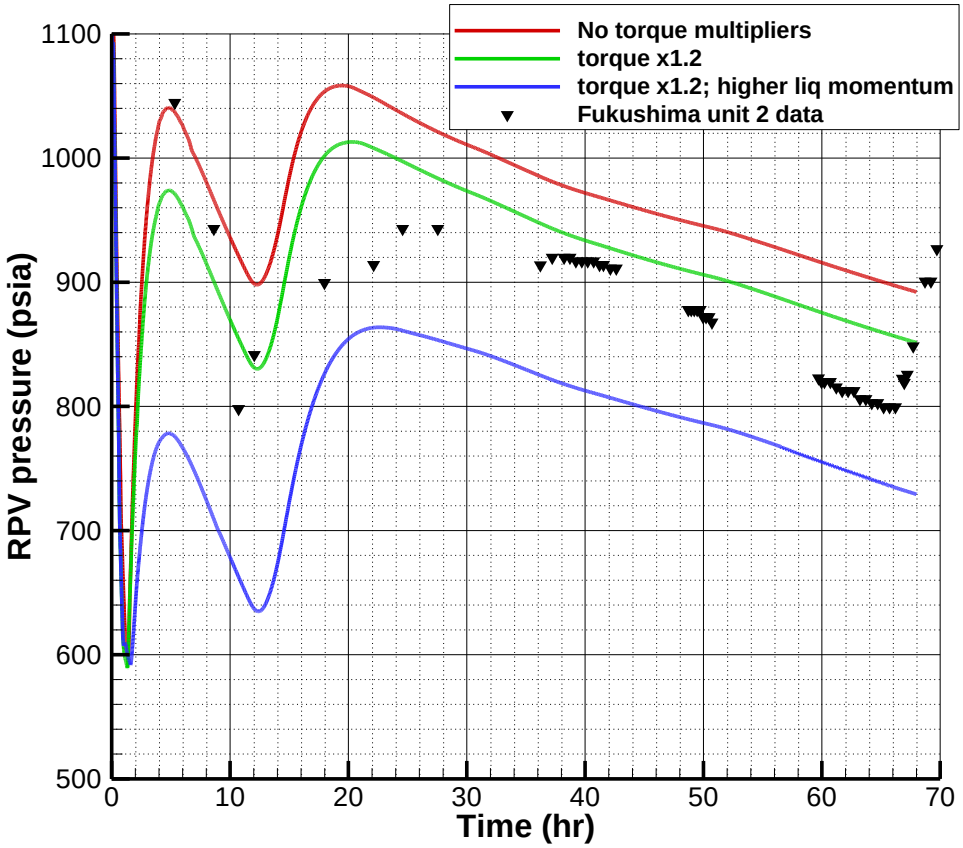

Figure 4.5. RELAP calculations of RPV pressure compared to Fukushima data

Table 4.2. Key parameters for RCIC in RELAP test model

	Red curve	Green curve	Blue curve
Liquid degradation multiplier	0.13	0.13	0.17
Terry torque multiplier	1.0	1.2	1.2
Shaft friction coefficient	0.35 lb-ft-s	0.35 lb-ft-s	0.35 lb-ft-s

The green and blue curves shown in Figure 4.5 prescribe a small multiplier on the Terry torque relationship from Equation 4.1 in order to approximately consider the influence of the reversing chambers. As discussed in Section 2, the reversing chambers are known to have little influence at high speeds, but they might be more important at low speed such as during startup or during degraded two-phase operation. Nonetheless, a constant multiplier of 1.2 is a reasonable value to assess the impact of slightly increased drive torque due to the reversing chambers. The blue curve also has a slightly higher multiplier for the liquid momentum. Thus, this calculation takes more credit for liquid momentum flux through the nozzles. All three calculations use the same friction coefficient on the shaft component; this parameter is listed since it was found to have a strong influence on the resultant turbine-pump performance.

Many of the pressure features in Figure 4.5 are very similar to those from the MELCOR preliminary test calculations discussed in Section 2. The RCIC is started at 200 sec in the RELAP calculations by gradually opening the governor valve, and it is assumed to open fully after an additional 100 seconds. This causes RCIC to rapidly accelerate (Figure 4.6), and RPV pressure drops to 600 psia before the vessel floods (i.e. liquid water reaches the MSL elevation and flows to the Terry turbine) due to excessive RCIC injection. The full opening of the governor valve is predicted to drive RCIC speeds that exceed the design speed by a factor of two, as shown by Figure 4.6. Such an overspeed would mechanically trip the turbine, since the inertial trip is typically around 115-120% [4.4] of the design speed (4287 rpm assumed here), but the turbine is allowed to proceed past the trip setpoint for the purposes of these test calculations. The prediction of overspeed following the full opening of the governor valve at high RPV pressure is in agreement with literature on RCIC operation and maintenance [4.4] and the current state-of-knowledge for Fukushima Unit 2 [4.2].

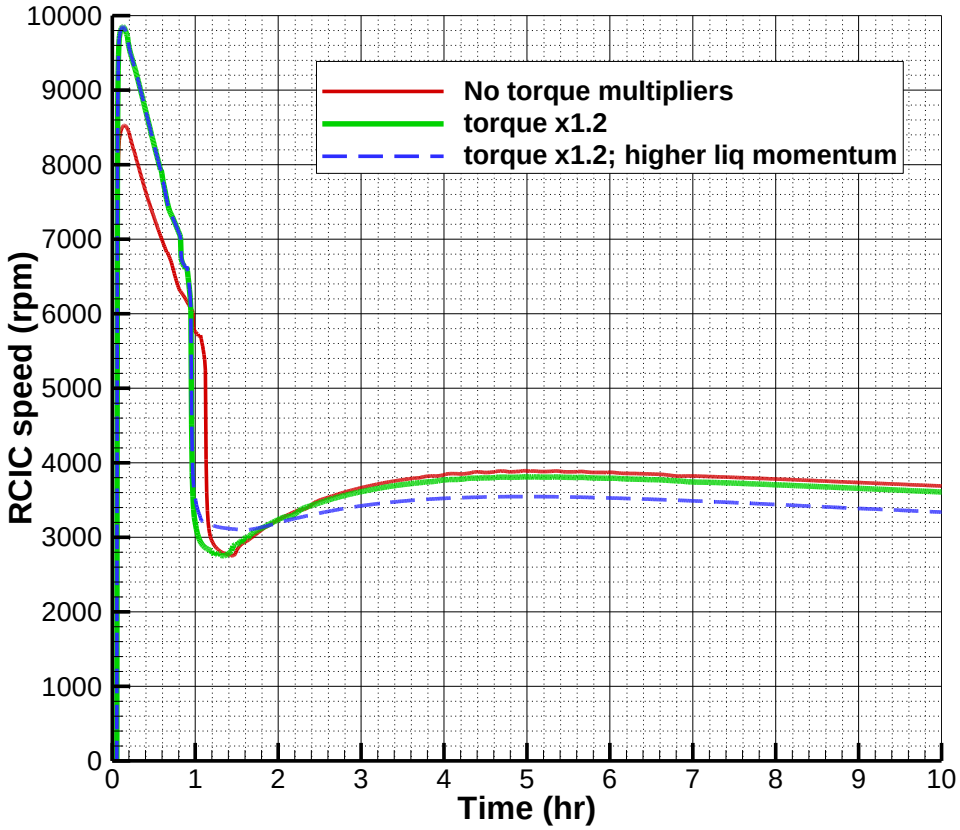

Figure 4.6. RELAP RCIC speed, 1-10 hours

The water ingestion decreases the Terry turbine torque and slows the RCIC (Figure 4.6 and Figure 4.7), and thus RPV pressure quickly increases (Figure 4.5) and nearly reaches the SRV setpoint around 5 hours. Over the long term, the RCIC operates at 75% to 90% of its design speed, as shown in Figure 4.7. After 5 hours, continual RCIC injection, two-phase turbine draw, and decreasing decay heat results in RPV pressure slowly decreasing until the RCIC pump switches suction from the CST (70^{o} F water) to the wetwell (assumed to be 235^{o} F), which drives another increase in RPV pressure. With less subcooling of the injection water, less energy is required to bring the water to saturation temperature, and hence more decay heat is available for boiling. This increases the steam generation rate in the RPV from 14 to 20 hours. The higher RPV pressure increases the Terry drive torque (Figure 4.8) via higher choked mass flow rate and higher bucket inlet velocity (i.e. higher nozzle pressure drop generates higher velocity), and this accelerates the RCIC from 14 to 20 hours. Increased RCIC speed and pump injection into the RPV (Figure 4.9) inhibits further RPV pressure rise, and RPV pressure turns over after 20 hours and decreases slowly and monotonically until the end of the simulation at 68 hours.

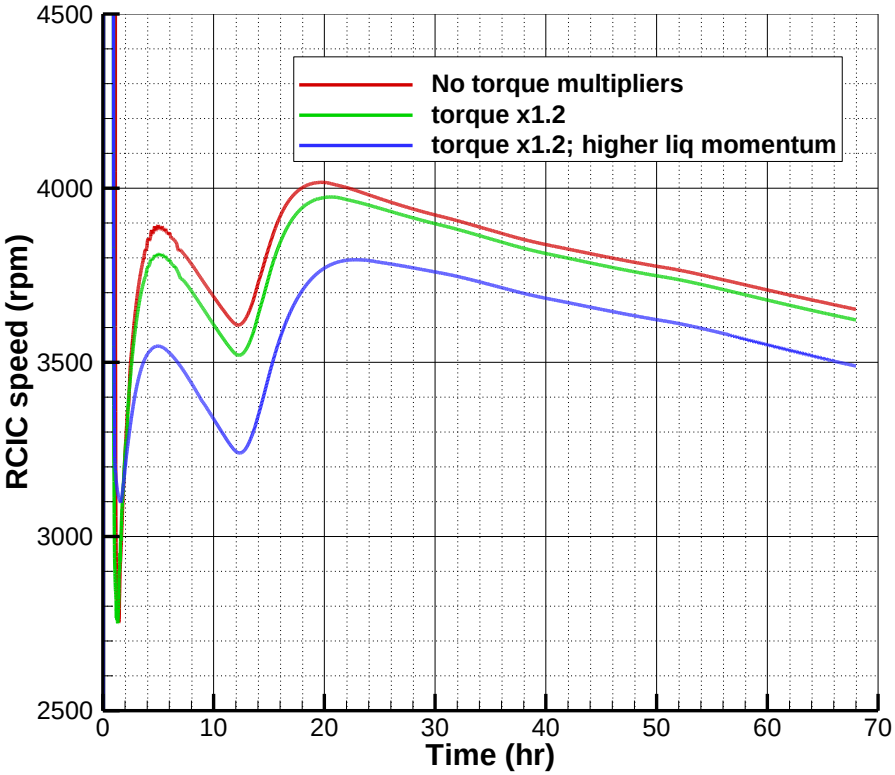

Figure 4.7. Long-term RELAP RCIC speed

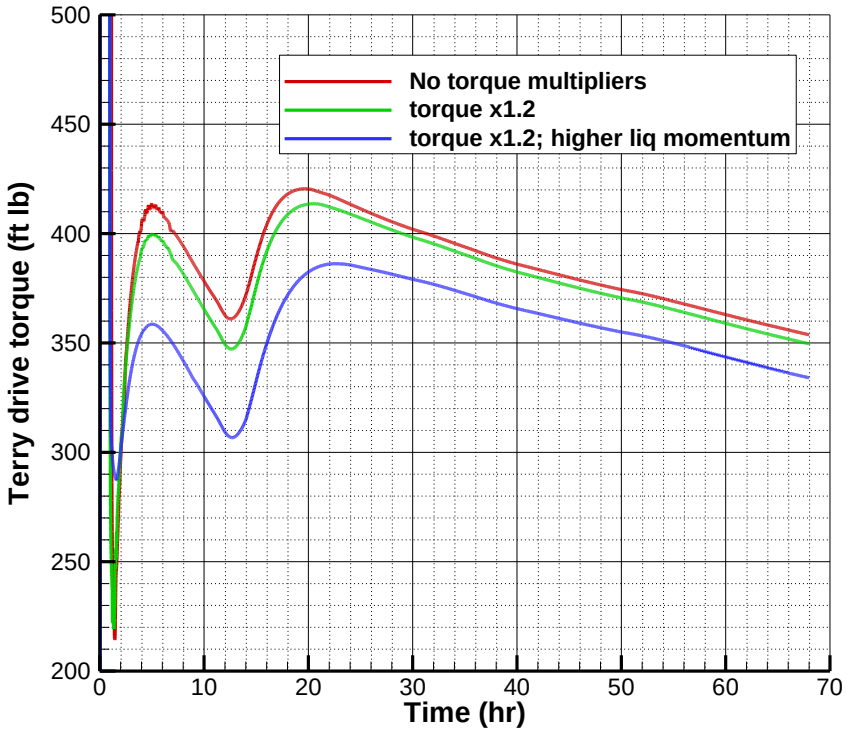

Figure 4.8. Terry turbine drive torque in RELAP calculations

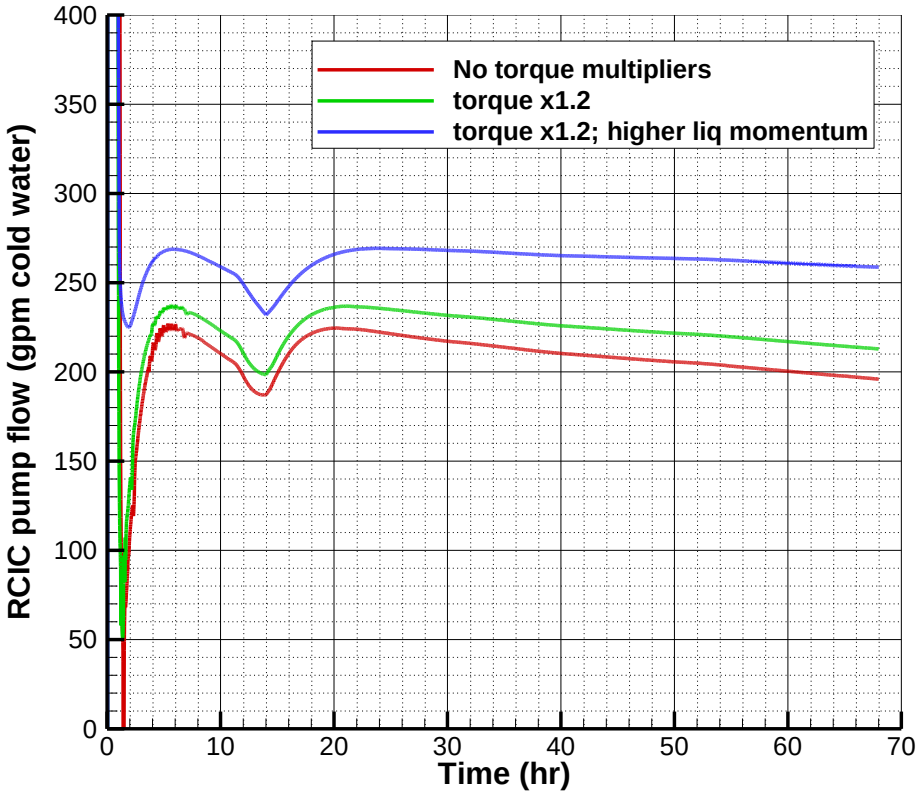

Figure 4.9. RCIC pump flow in equivalent cold water

Figure 4.8 shows that the long-term Terry torque, calculated using Equation 4.1, is 60% to 85% of the design values, which is near 500 to 540 ft-lb at higher RPV pressures; the design values are rated for normal operation of the governor valve that is usually only open a small fraction at high pressure [4.4]. Thus, the current RELAP system model predicts continuous degraded performance of the Terry turbine during uninhibited (by operators) two-phase operation, instead of discrete cyclical (i.e. on/off) behavior. Because the governor valve is fully opened at high RPV pressure, the drive torque initially undergoes an excursion with turbine torque exceeding the rated values by a factor of 3 to 4, as shown in Figure 4.10.

Figure 4.10 shows the calculations with the 1.2 multiplier on the Terry torque (green and blue cases) initially exhibit higher torque values, as expected, but the subsequent feedback drives long-term turbine torque to be lower than the red case with no torque multiplier. Higher early torque leads to more water pumped to the RPV (Figure 4.11), thereby driving down RPV pressure (Figure 4.5) and producing lower void fraction after the RPV floods (Figure 4.12). Lower RPV pressure and lower void fraction (i.e. more liquid) yield less momentum flux and hence less turbine torque.

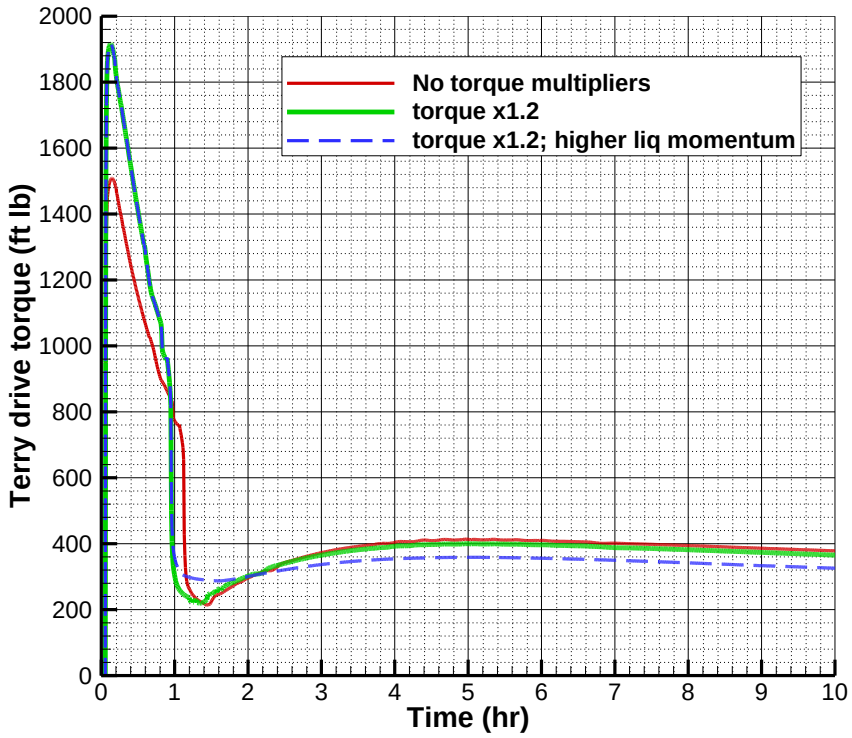

Figure 4.10. Terry turbine drive torque in RELAP calculations, 1-10 hours

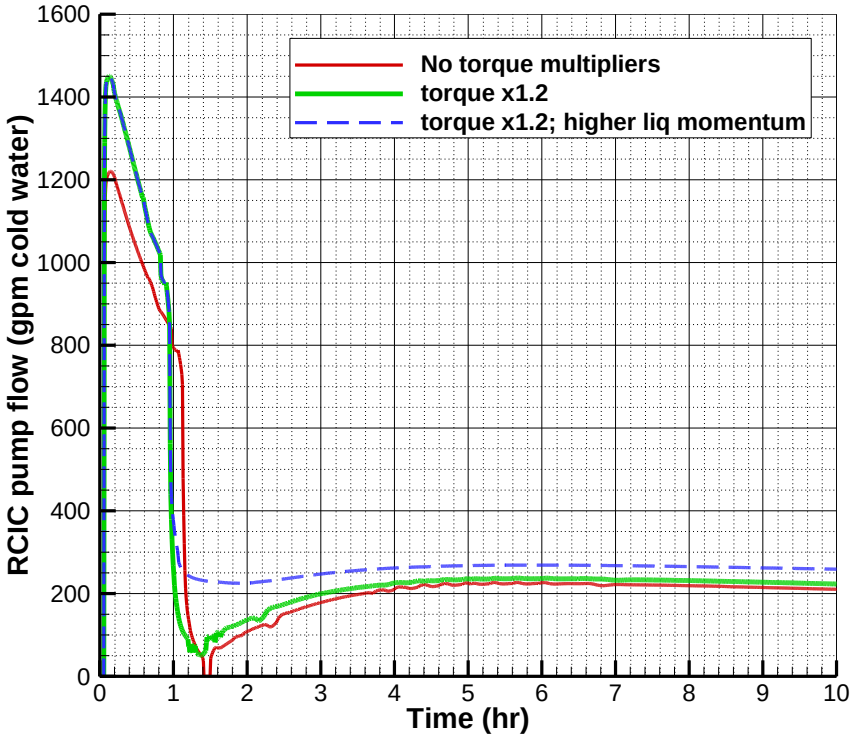

Figure 4.11. RCIC pump flow in equivalent cold water gpm, 1-10 hours

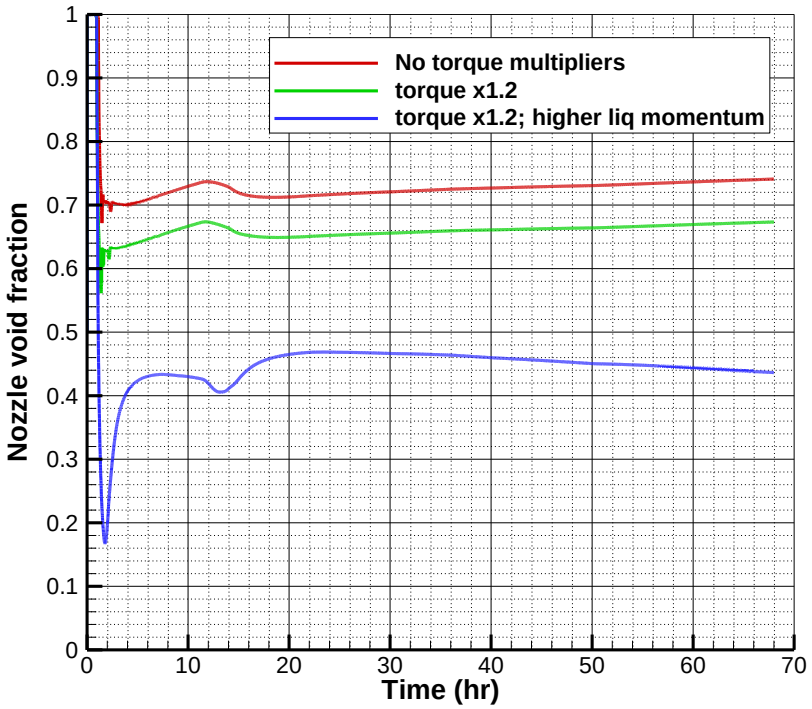

Figure 4.12. Void fraction at Terry nozzles in RELAP calculations

The RELAP calculations predict RPV flooding nears 2 hours, as shown by Figure 4.12, just like the original MELCOR preliminary test calculations from Section 2. However, void fraction in the RELAP models are significantly lower around 40% to 75% compared to the >90% void fractions in the MELCOR preliminary test model. The RELAP-calculated void fraction is also quite sensitive to the Terry turbine torque multiplier and the liquid momentum degradation multiplier. Both multipliers tend to increase pump flow rate (Figure 4.9 and Figure 4.11) which decreases the void fraction at the nozzles. Lower void fraction in the RELAP model is intuitive since it models the steam lines and RCIC steam piping that involve over 100 ft of elevation decrease from the RPV-MSL interface. However, the MELCOR preliminary test model neglects the majority of the steam piping and assumes that the nozzles are at the same elevation as the RPV-MSL interface. Therefore, it is rational that the RELAP model may predict water accumulation through the longer steam pipes that are at significantly lower elevation than the RPV-MSL connection. The different pump models are also of first-order importance for the calculation of the long-term void fraction at the nozzles.

Finally, it is interesting to note that RELAP does not predict identical flow regimes leading to the nozzles for each of the calculations; furthermore, flow regime for each case varies throughout the transient. Early in the transient, the flow regime at the nozzles is generally annular mist flow (perhaps similar to wet steam), later it may transition to bubbly flow, and it may end up as slug flow at the end of the transient. RELAP does not predict horizontal stratified flow at the nozzles, which is effectively how MELCOR simulates two-phase flow. Time-varying flow regimes at the nozzles might require a time-dependent (or flow-regime dependent) liquid degradation multiplier, since the magnitude of liquid flashing is dependent on the thermo-physical

characteristics of the liquid phase. Further system-level and CFD analysis of the flow regime entering the RCIC is warranted.

4.3.2 Interim MELCOR Calculations

With the use of homologous pump curves discussed in Section 4.1, RCIC pump performance curves provided by U.S. plants for calibration, and insights gained from the CFD analyses as discussed in Section 3, the MELCOR test model discussed in Section 2.3 was modified. As shown in Figure 4.13, results from the revision to the MELCOR test model trends similar to the Fukushima Unit 2 data but are offset. They similarly trend but offset results from the original test model presented in Section 2 (see Figure 2.4 for comparison). Reasons for the differences are being investigated. Both modeling uncertainties and uncertainties in the actions taken by operators during the accident look to be important. Some of the uncertainties are listed in Section 5.2.

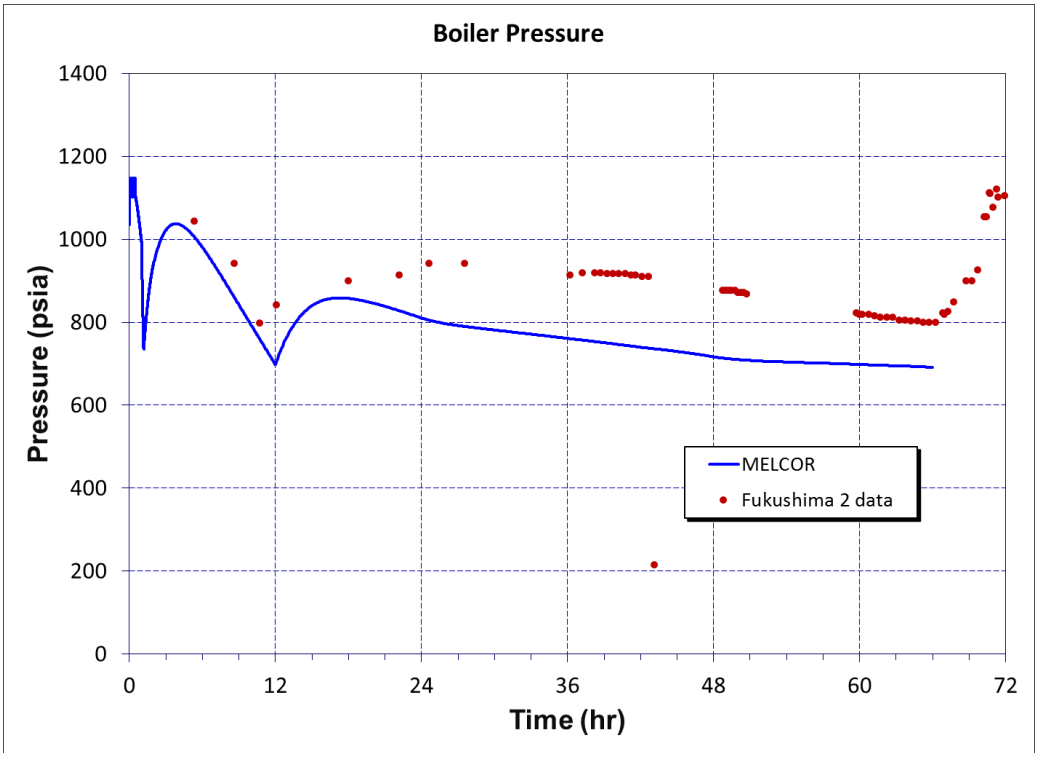

Figure 4.13. RPV pressure for revised MELCOR test model and Fukushima Unit 2 data

4.4 Section 4 References

[4.1] R.O. Gauntt, et al., SAND2012-6173, "Fukushima Daiichi Accident Study (Status as of April 2012)," SNL, Albuquerque, NM, 2012.

[4.2] D. Yamada, “TEPCO’s Investigation Activities on Unsolved Issues in Fukushima Dai-ichi Accident,” TEPCO, March 24, 2014.

[4.3] Nuclear Energy Agency, "NEA Benchmark Study of the Accident at the Fukushima Daiichi Nuclear Power Station (BSAF) Project," https://www.oecd-nea.org/jointproj/bsaf.html, accessed September 2015.

[4.4] J. Kelso et al., "Terry Turbine Maintenance Guide, RCIC Application," EPRI Technical Report, report number 1007460, Electric Power Research Institute, Palo Alto, CA, USA (2012).

5 SUMMARY AND CONCLUSIONS

Efforts are being pursued to develop and qualify a system-level model of a RCIC steam-turbine-driven pump. The model is being developed with the intent of employing it to inform the design of experimental configurations for full-scale RCIC testing. The model is expected to be especially valuable in sizing equipment needed in the testing. An additional intent is to use the model in understanding more fully how RCIC apparently managed to operate far removed from its design envelope in the Fukushima Daiichi Unit 2 accident.

RCIC modeling is proceeding along two avenues that are expected to complement each other well. The first avenue is the continued development of the system-level RCIC model that will serve in simulating a full reactor system or full experimental configuration of which a RCIC system is part. The models reasonably represent a RCIC system today, especially given design operating conditions, but lacks specifics that are likely important in representing the off-design conditions a RCIC system might experience in a beyond design basis situation such as a loss of all electrical power. A known specific lacking in the system model, for example, is the efficiency at which a flashing slug of water (as opposed to a concentrated jet of steam) could propel the rotating drive wheel of a RCIC turbine. To address this specific example, a second avenue is being pursued wherein CFD analyses of such a jet are carried out. The results of the CFD analyses will thus complement and inform the system modeling. The system modeling will, in turn, complement the CFD analysis by providing the system information needed to impose appropriate boundary conditions on the CFD simulations. The system model will be used to inform the selection of configurations and equipment best suitable of supporting planned RCIC experimental testing.

Preliminary investigations with the RCIC model indicate that liquid water ingestion by the turbine decreases the developed turbine torque; the RCIC speed then slows, and thus the pump flow rate to the RPV decreases. Subsequently, RPV water level decreases due to continued boiling and the liquid fraction flowing to the RCIC decreases, thereby accelerating the RCIC and refilling the RPV. The feedback cycle then repeats itself and/or reaches a quasi-steady equilibrium condition. In other words, the water carry-over is limited by cyclic RCIC performance degradation, and hence the system becomes self-regulating. The indications achieved to date with the system model are more qualitative than quantitative. The avenues being pursued to increase the fidelity of the model are expected to add quantitative realism. The end product will be generic in the sense that the RCIC model will be incorporable within the larger reactor coolant system model of any nuclear power plant or experimental configuration.

5.1 High Level Conclusions

In conjunction with a literature review of RCIC turbine design, a key conclusion is established that the simplicity and pure-impulse design of the turbine facilitates computational modeling using simplified (lumped-parameter) momentum methods. In Section 2, preliminary first-principle calculations are described that show promising initial results. The calculations demonstrate that the RCIC models have the capability to predict feedback between the RPV and RCIC for beyond design basis events without operator action. These results suggest that RCIC

may operate in a self-regulated regime for many hours, and this assertion agrees with the current state-of-knowledge for Fukushima Unit 2.

While the initial results from Section 2 are encouraging, they leave room for future development and improvement. The accuracy of a lump-parameter model is inherently dependent on the proper definition and quantification of several model parameters some of which require experimental derivation or computational models with higher spatial fidelity. Therefore, CFD models are developed and applied to the Terry turbine; these analyses are described in Section 3.

As discussed further in Section 3, the mass flow rate is accurately determined by two-phase critical flow models in MELCOR and RELAP, but the codes cannot predict the supersonic velocities developed by the nozzles. Therefore, the system code must be informed by more focused CFD analyses. There are several ways to go about this, however, an analytic formula fit of CFD results as a function of various plant variables was used for the initial application of the CFD insights into the system models. Analytical functions permit continuous relationships between the supersonic velocity and the plant variables.

Substantial CFD model development and analysis has been accomplished to support the development and improvement of system-level RCIC models. The CAD and CFD accomplishments described in Section 3 have critically informed the latest system-level model solution (i.e., the homologous-curve solution) with respect to:

- The approach angle of a steam jet to the RCIC turbine wheel, and
- The Mach number of a steam jet entering and leaving a bucket on a turbine wheel.

The CFD problems completed so far are the 'low-hanging fruit;' they have focused on the necessary first steps such as proper geometry creation, and the simulation of fundamental system behavior. Nozzle flow of dry saturated steam at various pressures has been studied in detail, and these analyses have produced several essential inputs that will improve the primary system-level modeling efforts. Nonetheless, there are several additional CFD analyses that will also improve the system model. CFD analysis of liquid flashing through the nozzles is probably the most important for understanding RCIC performance during beyond design basis scenarios.

As discussed in Section 4, a generic algorithm for pump curves allows the use of homologous definitions without a comprehensive knowledge of pump characteristics. Thus, a user can scale built-in curves by specifying problem-dependent design numbers such as rated pump speed, head, and brake horsepower. Given sufficient pump information, the user may also uniquely specify homologous curves. By taking advantage of these pump modeling features, homologous head and torque curves have been constructed from representative RCIC pump data and defined in the simplistic Unit 2 MELCOR test model. Important in considering the simplistic system-level model is to realize that it was designed to support key happenings and trends associated with the Unit 2 accident, but it is not a full representation of the reactor system. Exercising the new pump modeling features increases the realism of the model. The use of homologous pump curves has placed the responsibility of calculating RCIC pump dynamics on the system-level code, such as RELAP, MAAP, or MELCOR, rather than on the user.

Homologous pump models coupled to the Terry turbine relationships developed in Section 2 yielded a higher fidelity pump representation in the RCIC modeling framework. This benefitted the investigation of RCIC overspeed, which is of fundamental significance for the system during uncontrolled beyond design basis events. Updated system-level calculations also benefitted from incorporating the CFD results showing supersonic nozzle velocities. The updated calculations show good trends following of Fukushima Unit 2 data.

5.2 Future Endeavors

Further system modeling efforts will investigate enhanced numerical implementations for coupling the Terry turbine relationships to RELAP and MELCOR. This will improve stability and precision of these models. However, additional information needs in the ongoing RCIC modeling work, as an example, include:

- The number and size of the steam nozzles consistent with the performance information of a particular RCIC,
- The flow characteristics of a RCIC turbine governor valve and the minimum flow area of a fully open governor valve,
- The state of the CST recirculation valve(s) in the Fukushima Unit 2 accident after switchover of RCIC suction to the wetwell (e.g., were the valves closed at switchover?),
- System-level representations of the main steam line and RCIC steam piping,
- Additional Terry turbine parameters such as nozzle-bucket angle, and
- Addressing uncertainties in the CFD analyses such as supersonic velocities under varied two-phase flow regimes.

The system-level model RCIC solution utilizing the new homologous pump features are intended to be the solution carried forward in future RCIC modeling work. The solution is expected to add needed realism to Fukushima Unit 2 accident simulations and will inform the design of full-scale testing configurations.

However, it is apparent that without validated experimental testing data, the only data for these system-level RCIC models is from Fukushima Unit 2, which is limited. This further makes the case for some level of experimental testing to assure within validated boundary conditions these RCIC models will properly predict and inform the nuclear industry in updating emergency operating procedures, establishing a technical basis for operational changes that can prevent progression to core damage (i.e., reduce core damage frequency), and simplifying plant operations by increasing the time available for implementation of FLEX.

APPENDIX A: INVESTIGATION OF PUMP FAILURE MODES

The RCIC pump is unlikely to fail from cavitation. Figure A-1 contains a plot of the estimated net positive suction head (NPSH) margin ratio for an RCIC system in upset similar to that experienced at Fukushima Daiichi Unit 2. The margin ratio, as shown in the figure, is consistently greater than 50%. Recommendations based on experience are that the NPSH margin should exceed 15% of required NPSH, p_{NPSHR} [1].

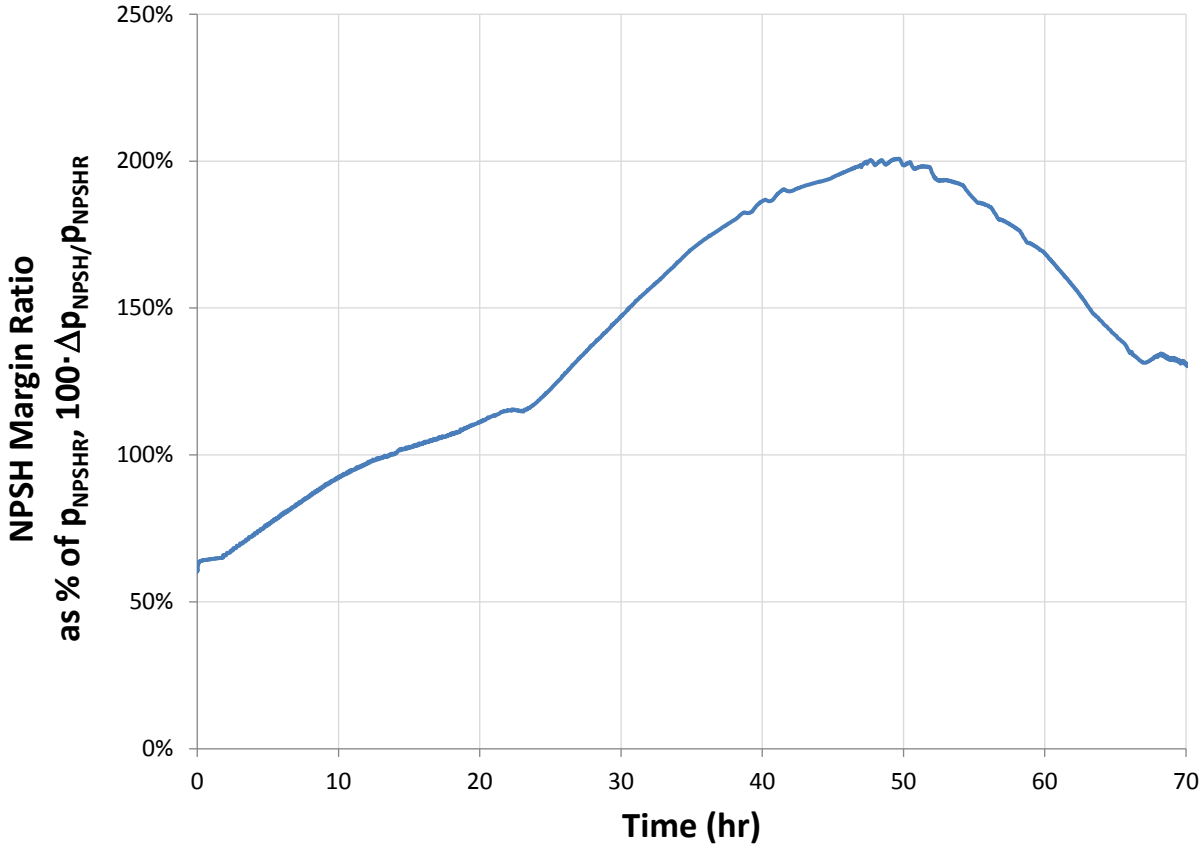

Figure A-1: Estimated NPSH Margin Ratio RCIC Pump System during Upset

A centrifugal pump's tendency for cavitation depends on the difference between the net positive suction head required by the pump, p_{NPSHr} , and the net positive suction head available from the pump/piping system, p_{NPSHa} . If we define this difference as the NPSH margin, Δp_{NPSH} , then:

$$\Delta p_{NPSH} = p_{NPSHa} - p_{NPSHr} \tag{A.1}$$

If a pump installation has a value of Δp_{NPSH} greater than zero, then no cavitation occurs. The overpressure tending to keep the fluid from flashing, p_{NPSHa}, exceeds the pressure droop the pump sees at its inlet, p_{NPSHr}. Conversely, if the pump requirement exceeds what the pump/piping system can deliver then Δp_{NPSH} will be negative and the pump will experience cavitation.

In this case, as illustrated in the figure, NPSH margin stays well above zero and the pump should not cavitate. As a consequence, it is unlikely that the RCIC pump experienced cavitation during the upset following the 2011 tsunami. The absence of evidence of cavitation also removes the possibility that the pump vapor locked as a result of cavitation.

As with any numerical model, the algorithm behind the information plotted in Figure A-1 contains assumptions. Most are routine and will be discussed as the development below progresses. However one assumption bears identification now. The model supporting Figure A-1 assumes that the wet well water is well stirred. The wet well consists of a ring, or torus containing the water and connected to the rest of the containment vessel. This torus contains a significant amount of equipment, including the intake to the RCIC pump and the release line where steam from the RCIC turbine discharges to the sump. Water in the immediate vicinity of the RCIC turbine discharge will be hotter and therefore more volatile than waters further away. This paper assumes that the pump intake is sufficiently far away from the turbine discharge that this increase in volatility is averaged out to the overall condition of water in the torus.

We make this assumption for the following reasons:

1. We do not yet have construction information in the form of drawings or personal observation regarding the relative location of these two piping fixtures.

2. It is reasonable to assume designers would take precautions to separate these two piping fixtures as much as possible.

3. Even with more physical information, a definitive answer will require either CFD modeling or a well-constructed experiment.

A.1 Model Development

Starting with Equation A.1, the NPSH available is a function of:

1. The ambient pressure on the system, in this case the containment pressure, p_{con},

2. Static head generated by the column of liquid between the surface of the wet well water and the pump suction, $\Delta p_{s,}$

3. Any friction losses imposed by flow through suction piping, Δp_f and

4. The vapor pressure of the water, pv_w.

Mathematically, this looks like:

$$p_{NPSHa} = p_{con} + \Delta p_s - \Delta p_f - pv_w \tag{A.2}$$

The containment pressure as a function of time was recorded during the upset and is discussed in more detail in Section A.2. The static head depends on density, which will vary with temperature and on the geometry of suction piping. The issues of temperature and density variation will be discussed in Section A.4 while a full discussion of pump static pressure occurs in Section A.5. Friction losses are discussed in Section A.6. Water vapor pressure varies with containment pressure and water temperature and is discussed in some detail in Section A.3.

At this time, we do not have RCIC pump curves. Consequently, the NPSH required by the RCIC pump was estimated using pump affinity rules and data for known pumps. This development is discussed in Section A.7.

The NPSH Margin ratio plotted in Figure A-2.1 is calculated as:

$$NPSH\ Margin\ Ratio = \frac{\left(p_{con} + \Delta p_s - \Delta p_f - pv_w\right) - p_{NPSHr}}{p_{NPSHr}} \cdot 100 \tag{A.3}$$

A.2 Containment Pressure

This section also addresses steam concentrations in the containment atmosphere. Figure A-2 contains a plot of the containment pressure data taken in the hours after the tsunami. This is actual data obtained from the reactor operations crew.

Pressure builds steadily from initial pressure close to 1 atmosphere to approximately 4.6 bara at 70 hours post tsunami when the RCIC pump stops working. At this point, the pressure drops before it begins rising again, increasing to approximately 7.5 bara at which the containment begins venting its atmosphere. The period of interest to this paper is the period between event start and 70 hours. This is the period in which the RCIC system is operational.

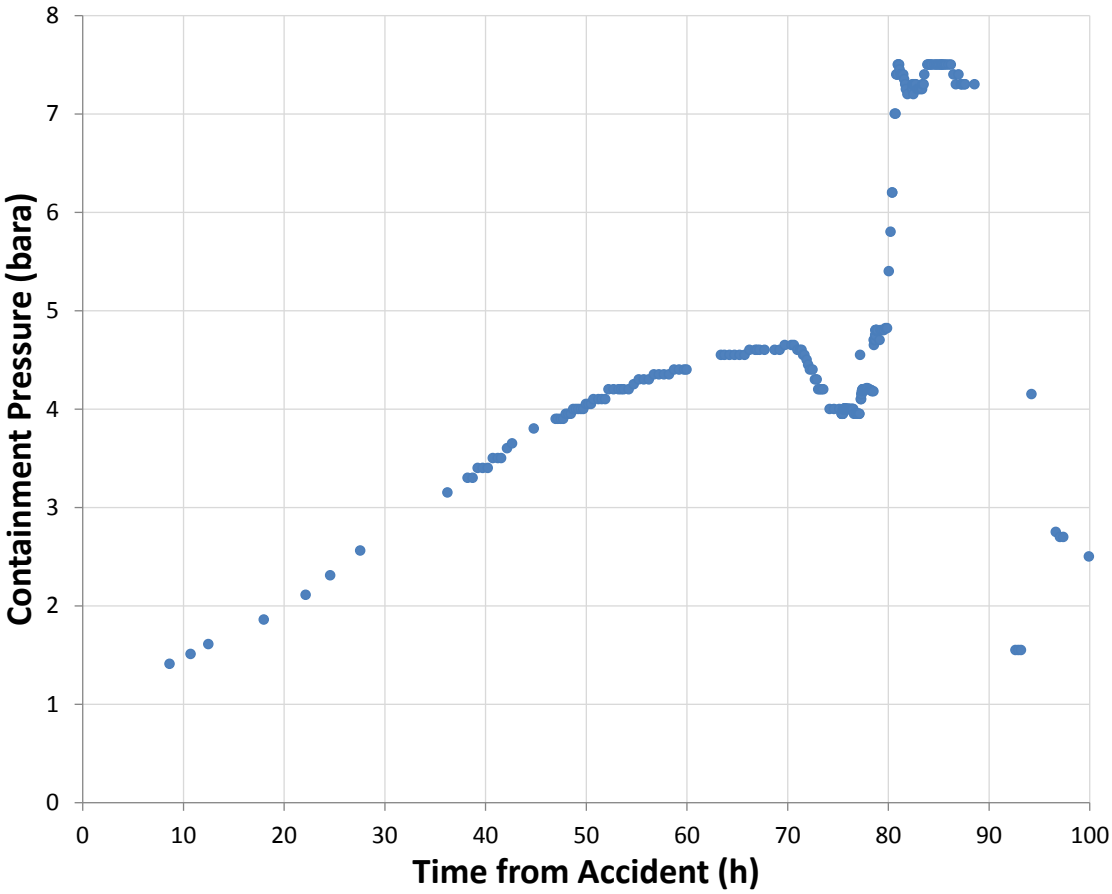

Figure A-2: Containment Pressure Data

Figure A-3 contains a plot of estimated mole fraction of steam in the containments atmosphere, x_w, as a function of time after the tsunami. This data was extracted from Fukushima Unit 2 MELCOR runs as part of follow-on analysis to Reference [1].

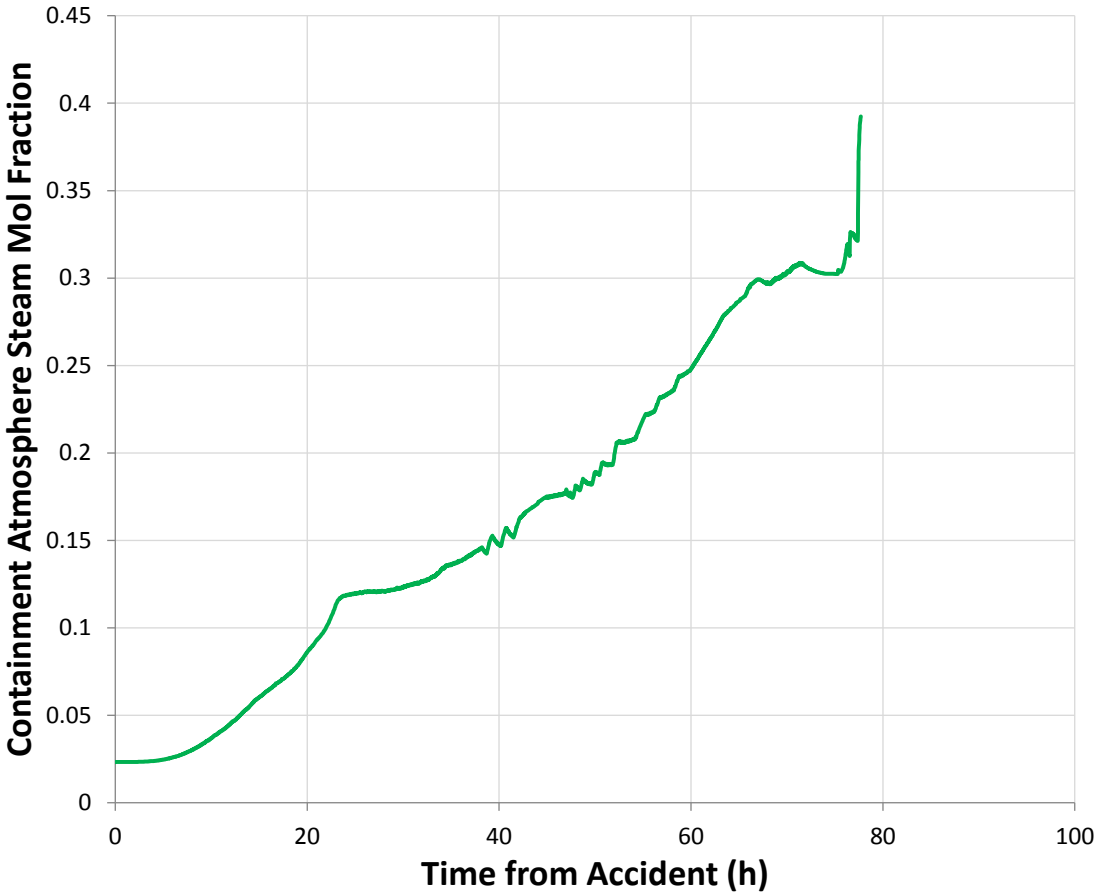

Figure A-3: Mole Fraction of Steam in Containment Atmosphere

A.3 Water Vapor Pressure

Assume the wet cell water is well stirred, or the water properties can be represented by an average value. The average vapor pressure of the water, pv_w, equates to the average partial pressure of steam in the atmosphere above it.

$$pv_w = x_w p_{con} \tag{A.4}$$

Mole fraction of water vapor in the containment atmosphere, x_w, and containment atmosphere pressure are discussed in the previous section.

Figure A-4 contains a plot of the vapor pressure with time as determined from Equation A.4.

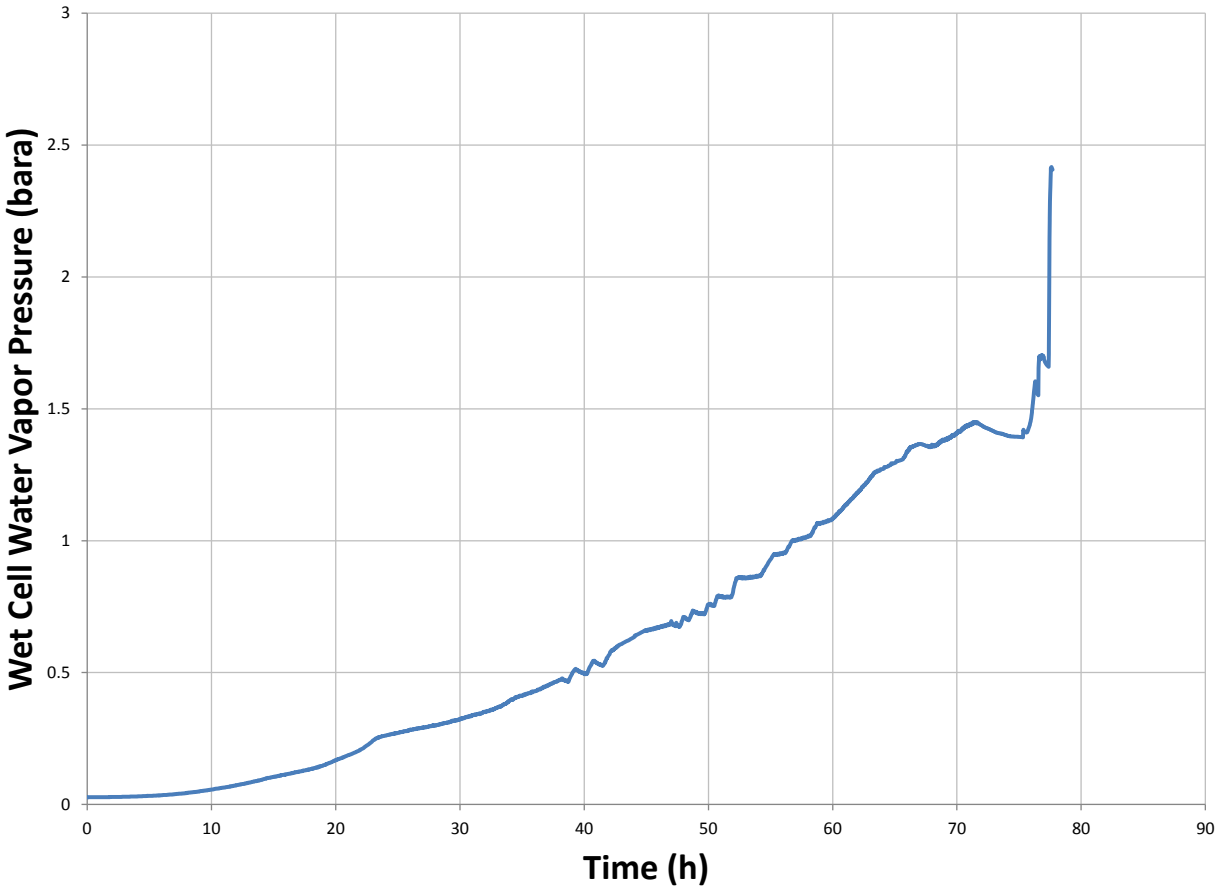

Figure A-4: Wet Cell Vapor Pressure

Water and Steam properties used in the paper come from the NIST Standard Reference Database 23 which uses the revised 1995 Formulation for Thermodynamic Properties of Ordinary water [3][4].

A.4 Containment Temperature and Density

This section assumes that wet cell liquid water properties are homogeneous. This is probably not true. For example, water evaporates from the pool only at the surface. As it leaves, more volatile water must migrate from within the pool to get to that surface. This leads a vapor pressure, and therefore a temperature gradient within the pool. Nonetheless, for the purposes of this first order analysis, homogeneous properties are assumed.

Water in the wet cell is saturated at the vapor pressure of the liquid. From this saturation point, one can extract temperature and pressure. Figure A-5 contains plots of these two parameters versus time for the duration of RCIC operation after the tsunami.

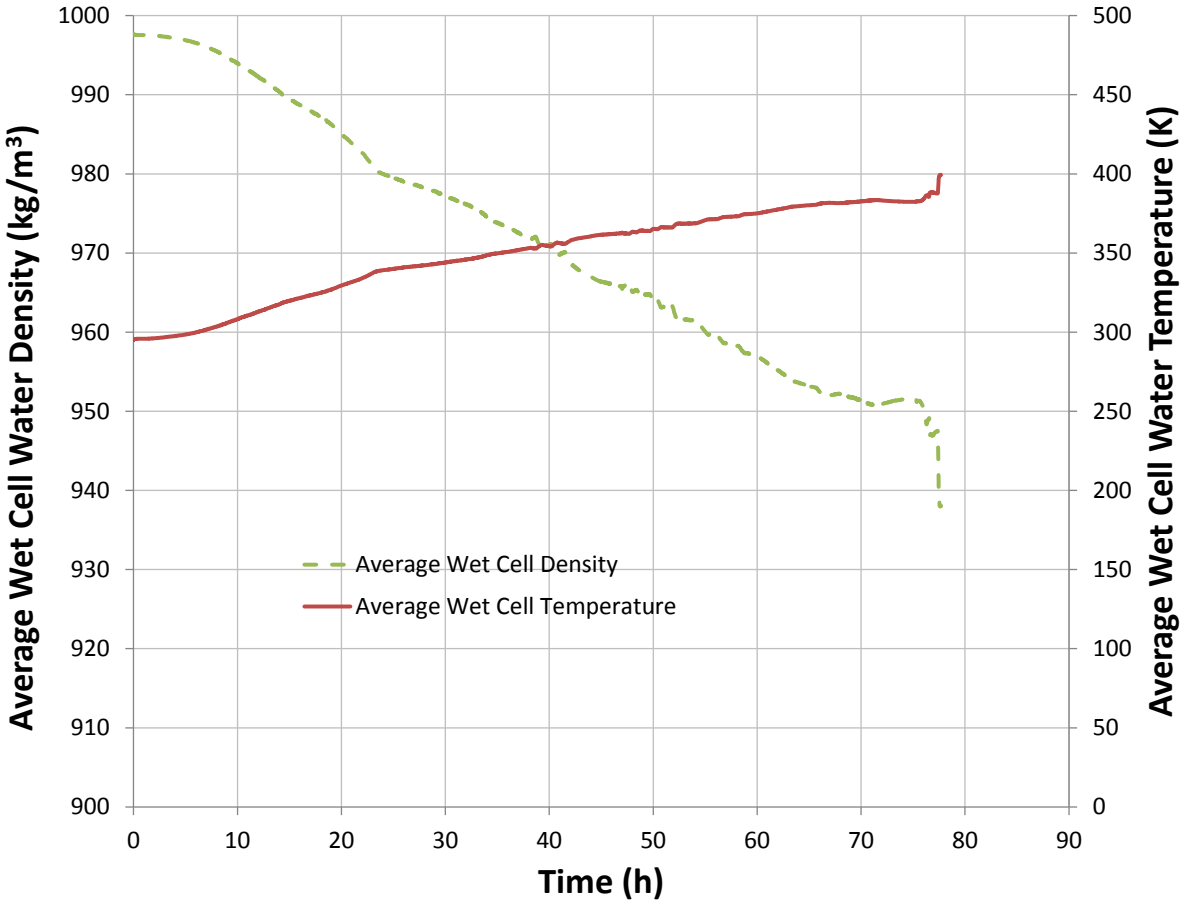

Figure A-5: Average Wet Cell Temperature and Density

Wet cell temperature ranges for an initial value of 295 *K* (72 *ºF*) to a high of 383 K (230 *ºF*) at 72 hours into the event. Since pressures are rising with temperature, water at 383 *K* is not yet a full boil.

A.5 Static Pressure at Pump Suction

From elementary hydrostatics:

$$\Delta p_s = \bar{\rho}_w g h_w \tag{A.5}$$

Density, $\bar{\rho}_w$, is discussed in the previous section. The bar above the symbol denotes that this is a value averaged over the height of the liquid column. This averaging is consistent with the density properties presented above. The acceleration due to gravity, *g*, is assumed constant at 9.81 m/s^2. The height of the liquid column, h_w, was obtained from piping and mechanical drawings for the Peach Bottom Nuclear Power Station, a power plant of similar design to Fukushima. At Peach Bottom, water in the torus is normally at the midpoint at elevation 110 ft while RCIC pump suction is at elevation 91.5 feet. Both elevations are measured from an arbitrary datum and were

extracted from Peach Bottom construction drawings. The net difference is 18.5 feet, or 5.64 meters. The choice of midpoint for the water level in the wet cell is conservative. The RCIC process consists of dumping water and steam into the torus throughout the event, probably raising water level above the normally specified midpoint.

The only parameter in Equation A.5 that varies with time is density and it varies only slightly. The net result is that static pressure ranges between 0.552 *bar* initially to 0.526 *bar* at 73 hours into the event.

As is typical for analyses such as this, the atmosphere was assumed to behave as an ideal gas. Occasionally, these blanket assumptions deserve verification. As a check, gas compressibility was estimated for water/air mixes based on the mole fraction data in Figure A-3. Compressibility factors were estimated using the Lee-Kesler equation of state with Plöcker mixing rules. The results are plotted in Figure A-6 [5].

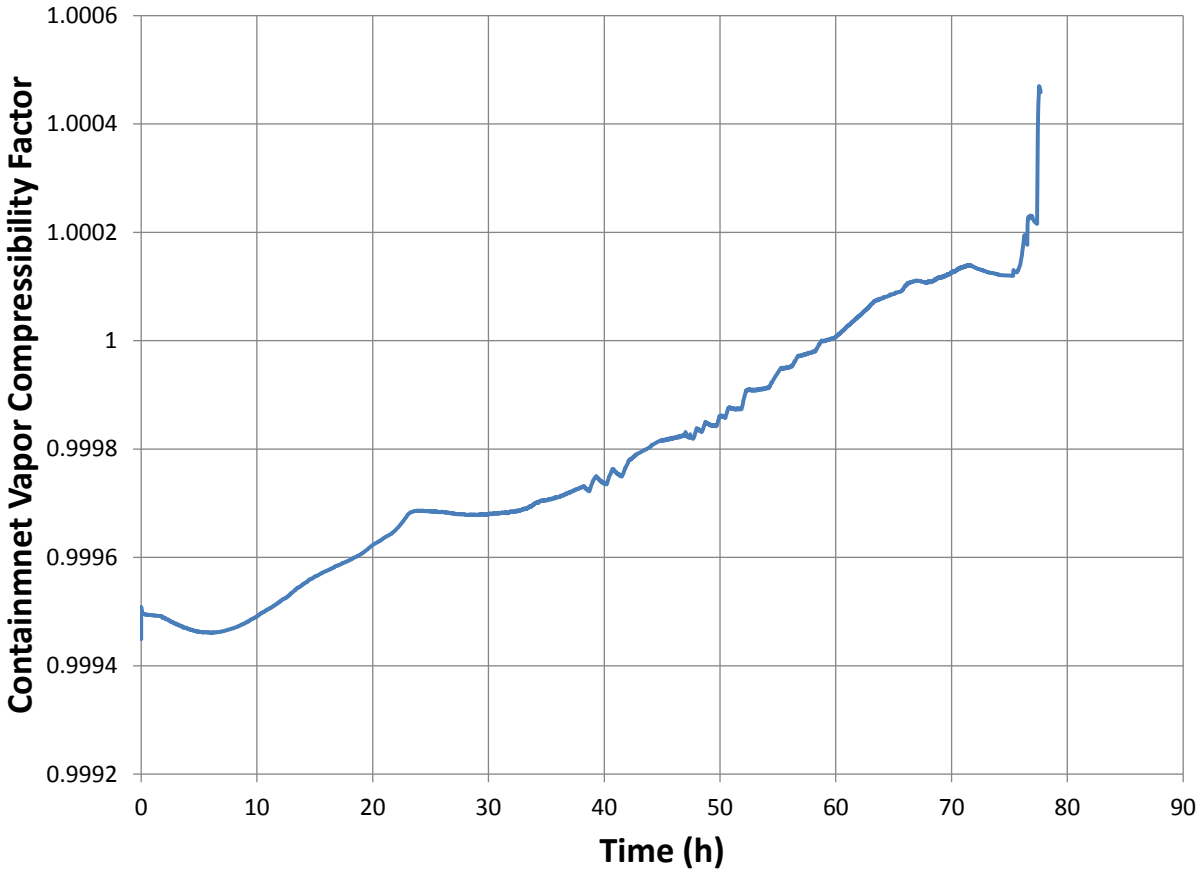

Figure A-2.6: Containment Atmosphere Compressibility

The information in Figure A-6 was plotted to four decimal places. In fact, the equation of state used is good to only 3 decimal places. Without the additional decimal place the data would all round to 1.000. The additional digit was added to illustrate the high degree to which atmosphere behaves as an ideal gas.

A.6 Friction Loss

Friction loss is a function of flow rate and pipe geometry and is typically small compared to other contributions to the NPSH margin. In this particular case, it was calculated to vary slightly around 0.0459 bar, an order of magnitude smaller than the contribution from static head.

Friction loss is calculated using the following relationship:

$$\Delta p_f = f\left(\frac{L}{D}\right)\rho_w \frac{V^2}{2} \tag{A.6}$$

From Peach Bottom Atomic Power Station piping and instrumentation drawings, the RCIC pump suction piping is 6" nominal. This equates to a 6.065" (0.154m) internal diameter, *D*. The pump's nominal 425 *gpm* rate equates in metric units to 0.0268 m^3/s. In pipe of this diameter such a volumetric rate corresponds to a velocity, *V*, of 1.44 *m/s*.

In this pipe, the Reynolds Number, ***Re***, is of order of magnitude 9E+05. For steel pipe after years of operation, absolute roughness, ε, would be approximately 0.3 mm, giving a relative roughness, ε/D, of 0.0019. At this Reynolds number and relative roughness, friction factor, *f*, would be approximately 0.0235 as shown in Figure A-7.

Density, ρ_w, has already been discussed and varies between 950 and 1000 kg/m3. Note that Equation A.6 does not use average density. Since the previous section provides average values some small uncertainty will occur in this calculation

The most uncertain variable in Equation A.6 is flow path length, *L*. Peach Bottom piping and mechanical drawings were too poor quality to extract lengths from them and no isometrics were available. As a consequence, Length was conservatively assumed to be 100 ft. (30.5 m). This length includes allowance for increased equivalent length due to bends and other fittings.

Combining all of the above results in an estimated flow loss of between 0.0444 to 0.0476 bar. At the midpoint this equates to 0.0459 *bar* or about 0.66 *psi* per 100 *ft*. Industry typically uses 0.5 psi/100 *ft* as a rule of thumb for allowable pressure drop. So while slightly conservative, values are in the right ballpark.

As initially discussed this range, 0.0444 to 0.0476 bar drop, is such a small contributor and the range is so small that subsequent analyses uses a constant of 0.046 bar drop for friction loss.

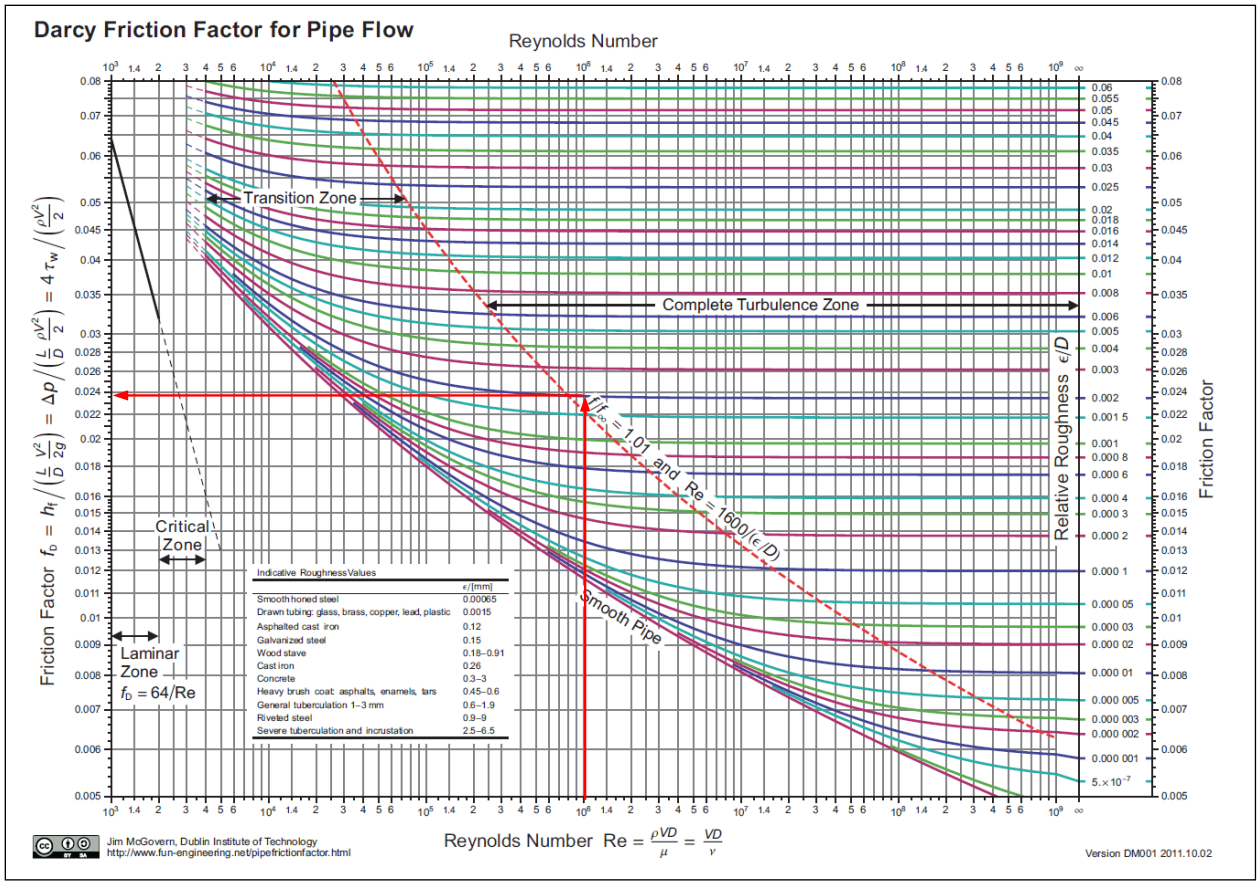

Figure A-7: Standard Moody Diagram [6]

A.7 NPSH Required by Pump

At the present time, we do not have pump curves for the RCIC pump. As a consequence, we have to estimate p_{NPSHr} from pump affinity rules. The following is based on emails exchanged with Ron Adams of Sulzer Pump. Mr. Adams' emails used US customary units. The following discussion stays with that set of units [7]. The operating conditions for the RCIC pump are shown in Table A-1.

Table A-1: RCIC Pump Operating Conditions

Pump Speed, N	4500 rpm
Nominal Capacity, Q_{Nom}	425 gal/min
Stages	5
Pumped Fluid	water
Pressure Rise, dp	1100 psi

Method 1: Based on Adjusted pump speeds
Adjust pump capacity to known pump with speed of 3560 rpm:

$$\dot{Q}_{adj} = Q_{Nom}\left(\frac{N_{adj}}{N}\right) = 425\left(\frac{3560}{4500}\right) = 336 \tag{A.7}$$

Pump head per stage:

$$h_s = \frac{dp}{\rho\frac{g}{g_c}} = \frac{1100\cdot 144}{62.34}\frac{1}{5} = 508\ ft \tag{A.8}$$

In US customary units, acceleration from gravity, g has a value of 32.2 ft/s^2 and g_c has a value of 32.2 $lb\cdot ft/lb_f\cdot s^2$. Pump head per stage adjusted for pump speed:

$$h_{s,adj} = 508\left(\frac{3560}{4500}\right)^2 = 318 \tag{A.9}$$

Figure A-8 contains a pump curve for a typical multistage pump. The solid red lines identify adjusted operating conditions. Based on the adjusted conditions, pump NPSH required, p_{NPSHr}, is 10.1 *ft*. At actual speed, p_{NPSHr} will be:

$$p_{NPSHr} = 10\left(\frac{4500}{3560}\right)^2 = 16.1\,ft \tag{A.10}$$

This would be the p_{NPSHr} for a modern pump. Recall that the Terry turbine-driven pump was designed circa 1900.

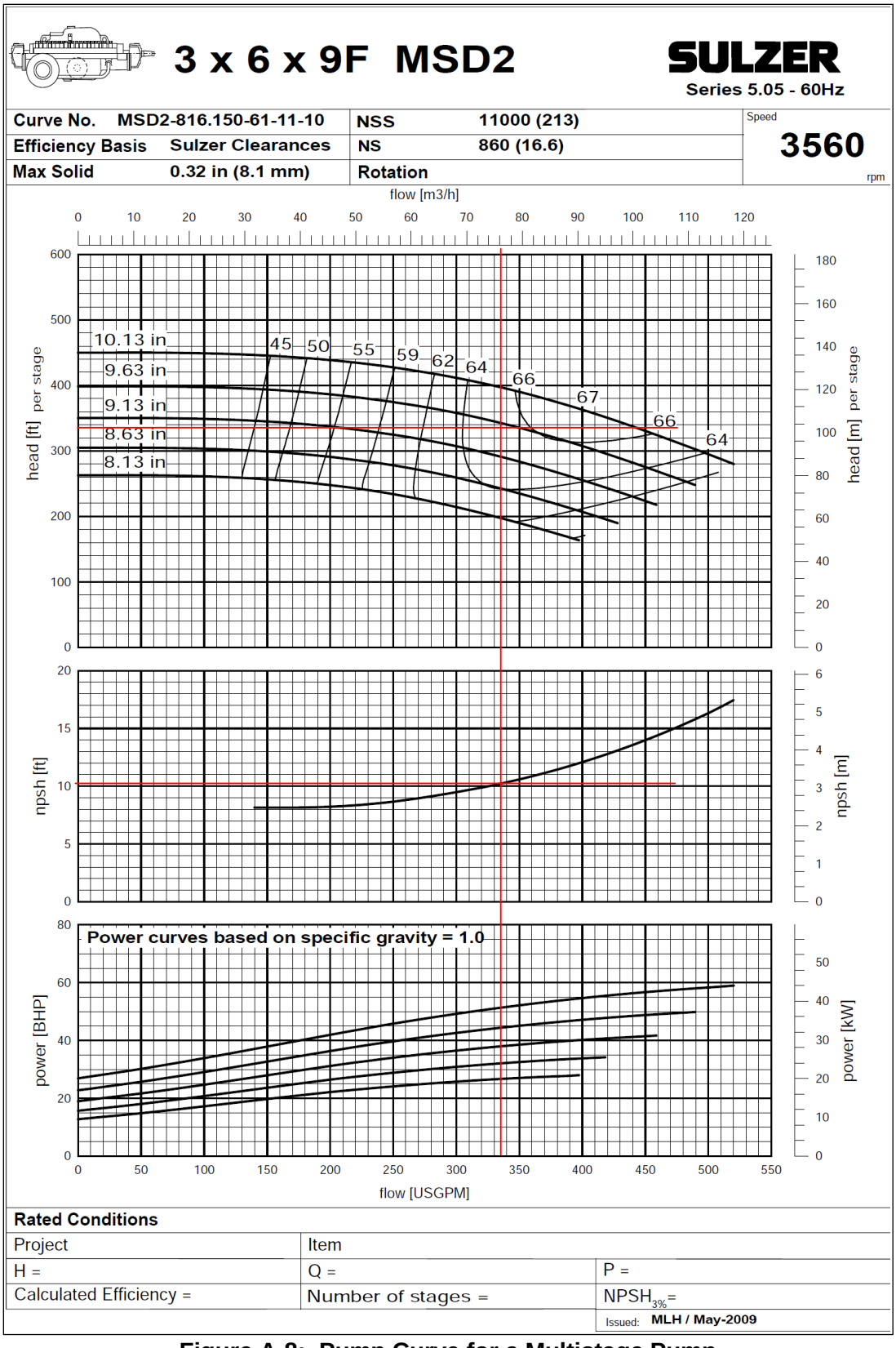

Figure A-8: Pump Curve for a Multistage Pump

Method 2 Specific Pump Speed
Specific pump speed, *Ns*, can be calculated per the following formula:

$$Ns = \frac{NQ^{0.5}}{h_s^{0.75}} = \frac{4500 \cdot 425^{0.5}}{508^{0.75}} = 867 \tag{A.11}$$

Value should be > 700 for the following to apply. The suction specific pump speed, *Nss*, is given by the formula:

$$Nss = \frac{NQ^{0.5}}{p_{NPSHr}^{0.75}} \tag{A.12}$$

Using the value for p_{NPSHr} calculated above using Method 1, at 16.1 ft, Nss = 11400. This is too high. Values should be around 8500. This preferred value for *Nss* corresponds to a p_{NPSHr} = 24.2. Given previously stated reservations concerning the age of the RCIC pump design, it is probably more reasonable to use the higher number. This higher number equates to 0.724 *bar* for p_{NPSHr}.

Because of the higher than normal level of uncertainty associated with this number. Calculations of NPSH margin will use a value for p_{NPSHr} rounded up to 1.0 bar. This higher value of net positive suction head requirement results in a suction specific speed, Nss, of 6670, a value on the low range of acceptable. This rounded up number is the value for p_{NPSHr} used in the development of Figure A-4.

A.8 Appendix A References

[1] McGuire, J.T., *Pumps for Chemical Processing*, 1990 Marcel Dekker, Inc. ISBN 0-8247-8324-7.

[2] R.O. Gauntt, et al., SAND2012-6173, "Fukushima Daiichi Accident Study (Status as of April 2012)," SNL, Albuquerque, NM, 2012.

[3] Lemmon E.W., Huber M.L., McLinden M.O., *NIST Reference Fluid Thermodynamic and Transport Properties REFPROP User's Guide*, Version 9.1; April, 2013, National Institute of Standards and Technology Standard Reference Data Program, Gaithersburg Maryland.

[4] IAPWS, "Revised Release on the IAPWS Formulation 1995 for the Thermodynamic Properties of Ordinary Water Substance for General and Scientific Use," June 2014.

[5] Poling B.E., Prausnitz J.M., O'Connell J.P., *The Properties of Gases and Liquids*; 5th ed.; 2001; ISBN 0-07-011682-2; McGraw-Hill.

[6] McGovern, J.: Technical Note: Friction Diagrams for Pipe Flow. Dublin Institute of Technology, 2011.

[7] Adams, R.; Email discussions; R. Adams, Global Portfolio Manager – Petroleum, Sulzer Pumps; Spring, TX USA.

APPENDIX B: VELOCITY TRIANGLES FOR TERRY TURBINE

A velocity vector analysis of the turbine buckets is necessary to characterize the RCIC system using a lumped-parameter approach. The angular momentum equation that determines the RCIC turbine motion depends on the tangential component of the outlet velocity; this quantity must be resolved from the nozzle jet velocity and the flow angles of the bucket. Figure B.1 depicts velocity triangles for one-way flow through an arbitrarily shaped bucket. The solid arrows with bold variable names represent velocity vectors, and the dotted lines represent the scalar components of these vectors. Red lines with '1' subscripts are for the inlet flow, and blue lines with '2' subscripts represent the outlet flow. The 'z' variables represent the axial components of the flow velocities, which is not in the imposed direction of the turbine motion. The 'y' variables signify horizontal (i.e. tangential, radial) components of the velocities, which are in the direction of turbine motion (i.e. the same direction as the bucket velocity). Because the bucket is also in motion, the y-components of the velocity have absolute magnitude with respect to the coordinate system and relative magnitude (subscript 'r') with respect to the bucket velocity. Since the bucket width is small compared to the radius of the turbine, the bucket velocity at the inlet and outlet is treated as being identical. Figure B.2 shows the approximate placement of the relative fluid velocities as they enter a preliminary CAD model of the Terry turbine.

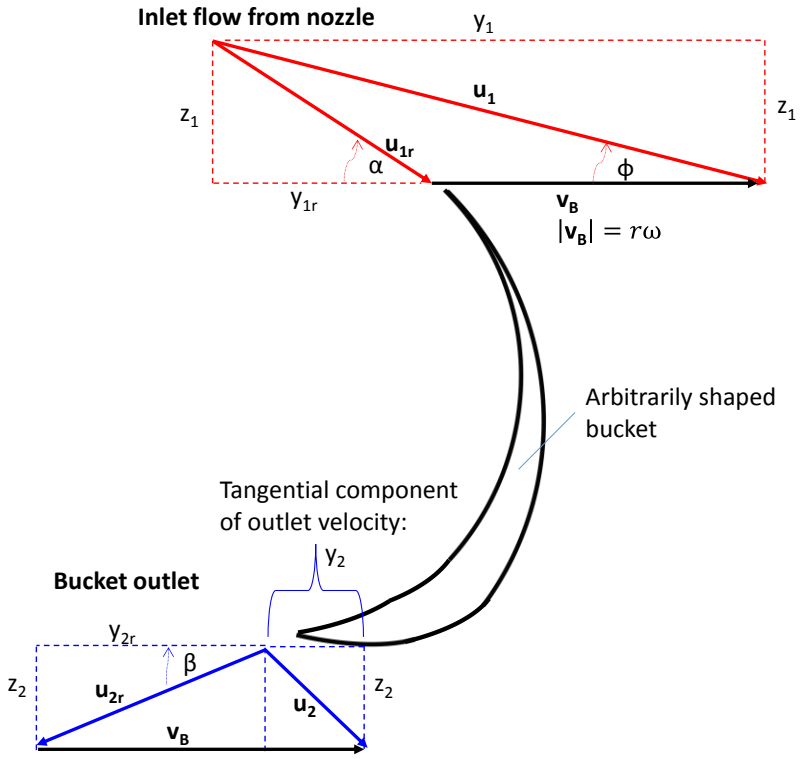

Figure B.1. Velocity diagram for one-way flow through arbitrary impulse bucket

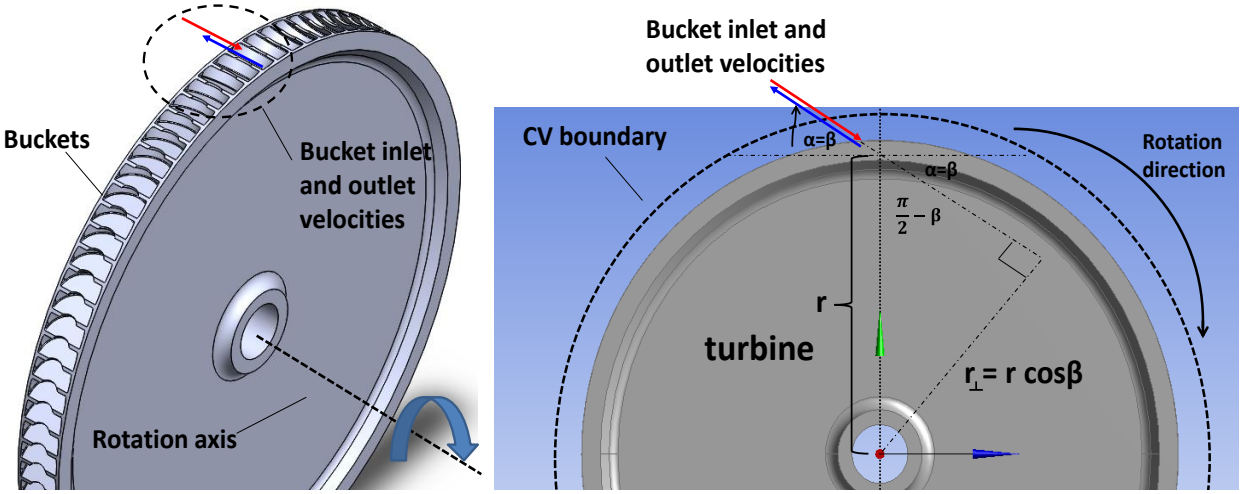

Figure B.2. Orientation of flow velocities for Terry turbine

There are a few pertinent relationships that are necessary to resolve the tangential component of the outlet velocity (y_2 in Figure B.1 and u_θ in Equation 2.1 in Section 2.2). These formulas are simple trigonometry expressions based on Figure B.1 and statements of the known input conditions for the problem. The formulas for the bucket inlet are:

$$|\mathbf{u}_1| = V_j, \text{ the jet velocity magnitude} \quad \text{(B.1)}$$

$$|\mathbf{v}_B| = r_\omega, \text{ the bucket velocity magnitude} \quad \text{(B.2)}$$

$$\alpha \approx \beta, \text{ angle between relative inlet/outlet velocities and bucket velocity} \quad \text{(B.3)}$$

$$\phi = \text{angle between absolute inlet velocity and bucket velocity} \quad \text{(B.4)}$$

$$y_1 = |\mathbf{u}_1|\cos\phi \quad \text{(B.5)}$$

$$y_{1r} = y_1 - |\mathbf{v}_B| \quad \text{(B.6)}$$

$$|\mathbf{u}_{1r}| = |\mathbf{u}_1 - \mathbf{v}_B| = \sqrt{z_1^2 + y_{1r}^2} = \sqrt{(|\mathbf{u}_1|\sin\phi)^2 + (y_1 - |\mathbf{v}_B|)^2} \quad \text{(B.7)}$$

Using the relationship $sin^2x + cos^2x = 1$ and the assumption that $\cos\phi \approx 1$, Equation B.7 reduces to:

$$|\mathbf{u}_{1r}| = \sqrt{V_j^2 - 2r\omega V_j + r^2\omega^2} = |V_j - r\omega| \quad \text{(B.8)}$$

The Terry turbine has roughly equivalent inlet (α) and outlet (β) bucket angles. Preliminary CAD models suggest that this angle may be near 45 degrees ($\pi/4$ radians). The assumption that $\cos\phi \approx 1$ is reasonable considering the magnitudes of the V_j and the fact that the bucket speed is comparable to the jet speed at rated conditions. It is also known that the system is designed such that V_j is always larger than the bucket speed ($r\omega$); hence $V_j - r\omega$ is always greater than zero.

The bucket outlet relationships are:

$$|\mathbf{u}_{2r}| = C_B|\mathbf{u}_{1r}| \quad \text{(B.9)}$$

$$y_{2r} = |\mathbf{u}_{2r}|\cos\beta \quad \text{(B.10)}$$

$$y_2 = |\mathbf{v}_B| - y_{2r} \quad \text{(B.11)}$$

C_B is the bucket velocity coefficient. The approximation of C_B=1 is sufficient for the scoping analyses. It is now possible to solve for y_2, the tangential component of the outlet velocity (i.e. u_θ in Equation 2.1 in Section 2.2):

$$y_2 = r\omega - (V_j - r\omega)\cos\beta \tag{B.12}$$

APPENDIX C: TIME-DERIVATIVE IN ANGULAR MOMENTUM EQUATION

This appendix shows that:

$$\frac{\partial}{\partial t}\iiint ru_\theta \rho dV = \frac{\partial}{\partial t}\iiint r(r\omega - \left(V_j - r\omega\right)cos\beta)\rho dV = I(1+cos\beta)\frac{d\omega}{dt}$$

First, the integral is expanded:

$$\begin{aligned}\frac{\partial}{\partial t}\iiint r(r\omega - \left(V_j - r\omega\right)cos\beta)\rho dV &= \frac{\partial}{\partial t}\iiint (r^2\omega(t) - rV_j cos\beta + r^2\omega(t)cos\beta)\rho dV \\ &= \frac{\partial}{\partial t}\iiint r^2(1+cos\beta)\omega(t)\rho dV - \frac{\partial}{\partial t}\iiint rV_j cos\beta \rho dV \\ &= (1+cos\beta)\frac{d\omega}{dt}\iiint \rho r^2 dV + (1+cos\beta)\omega(t)\frac{d}{dt}\iiint \rho r^2 dV\end{aligned}$$

Defining the moment of inertia to be:

$$I = \iiint \rho r^2 dV$$

The moment of inertia is treated as a constant (hence its time derivative is zero), so it is apparent that:

$$\frac{\partial}{\partial t}\iiint r(r\omega - \left(V_j - r\omega\right)cos\beta)\rho dV = I(1+cos\beta)\frac{d\omega}{dt}$$

APPENDIX D: HAND CALCULATION EXAMPLE FOR STEAM NOZZLE

Appendix D describes a simple, zeroth-order method for calculating the supersonic velocity of a converging-diverging nozzle. This analysis is consistent with historical methods for analyzing steam nozzles, and is mainly adopted from the techniques in Reference [1].

D.1 Analysis

Assuming frictionless, adiabatic, isentropic flow and neglecting inlet velocity, the outlet velocity of the nozzle can be estimated using [1]:

$$v_{out} = \sqrt{2(h_{in} - h_{out})}$$

The nozzle flow is isentropic with no shocks in the diverging section if the pressure drop over the nozzle is sufficiently large.

Picking two representative pressures that are easy to look up on a Mollier chart on hand:

- **Nozzle inlet pressure = 725 psi (50 bar); assume dry steam inlet**
- **Nozzle outlet pressure = 29 psi (2 bar)**

Specific enthalpies are taken from online interpolating tables [2] and corroborated by published steam data [3]. These values are sufficiently accurate for the example calculation:

h_{in} = h_g (dry inlet) at 725 psi = 2794.2 kJ/kg

$h_{out} = xh_g + (1 - x)h_f$ with specific enthalpy values at 29 psi; *x*=steam quality, which is unknown

At 29 psi, h_g= 2706.2 kJ/kg; and h_f= 504.67 kJ/kg

Steam quality exiting the nozzle is estimated via the use of a Mollier chart (enthalpy-entropy diagram for water). This chart could also give rough estimates for the enthalpy values for the dry inlet and the two-phase outlet. There are more accurate methods of assessing the two-phase composition, such as solving of an entropy conservation equation (i.e. $s_{in} = s_{out}$), but a quick examination of the Mollier chart is the simplest. The use of the chart is as follows:

1. Find blue pressure curve for inlet at 50 bar (725 psi),

2. Find intersection of this blue curve and bold red saturation curve of water with quality equal to one (dry steam inlet),

3. Assuming isentropic flow (entropy doesn't change), drop straight down until intersection with the outlet pressure curve at 2 bar (29 psi),

4. Examine red curves that give steam quality and estimate appropriate value.

For the assumed pressures here, the exit quality looks to be very close to 80%. Thus 20% of the flow by mass is now saturated liquid at the nozzle exit. [There is no guarantee that the liquid hangs around all the way to the turbine discharge; it may very well evaporate as the CFD calculations suggest.] The specific enthalpy of the nozzle outlet mixture is:

$h_{out} = xh_g + (1-x)h_f$ = 0.8 • 2706.2 + 0.2 • 504.6 = 2265.88 kJ/kg

Note that outlet enthalpy is significantly lower than it would be if it were purely dry saturated steam. The nozzle velocity can now be calculated:

$$v_{out} = \sqrt{2(h_{in} - h_{out})} = \sqrt{2 * (2794.2\text{x}10^3 - 2265.88\text{x}10^3)} \approx \mathbf{1028\ m/s}$$

Fluent calculations compare very well to the simple hand calculation. For 725 psia (dry steam) to 29 psia, the peak velocity predicted by Fluent is 1048 m/s, and the peak condensate mass fraction is 19.7%. These values are close to those obtained from the isentropic hand calculation. The area-averaged velocity entering the bucket is around 800-900 m/s. The Fluent calculations account for friction that will tend to heat the fluid and reduce condensation.

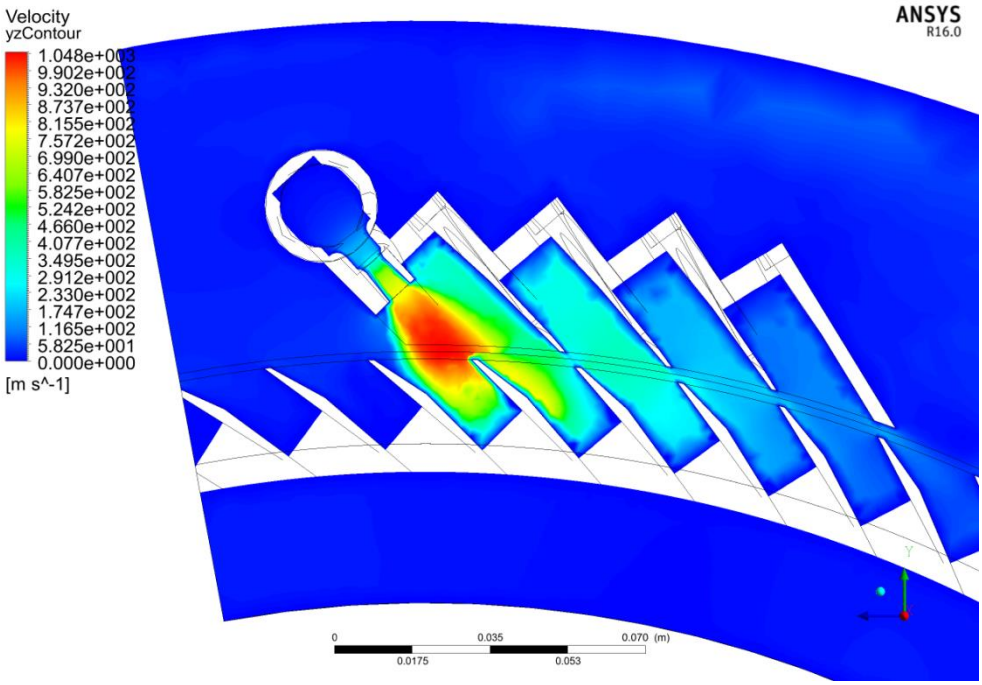

Figure D.1. Velocity contour through mid-plane of Terry nozzle for 725 psia inlet

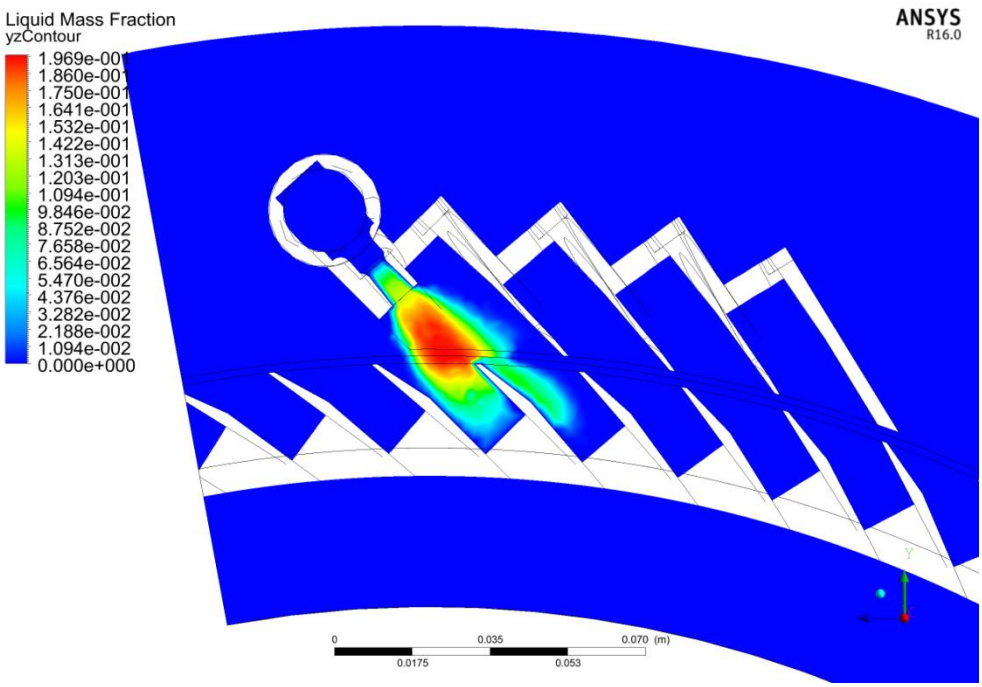

Figure D.2. Liquid fraction contour through mid-plane of Terry nozzle for 725 psia inlet

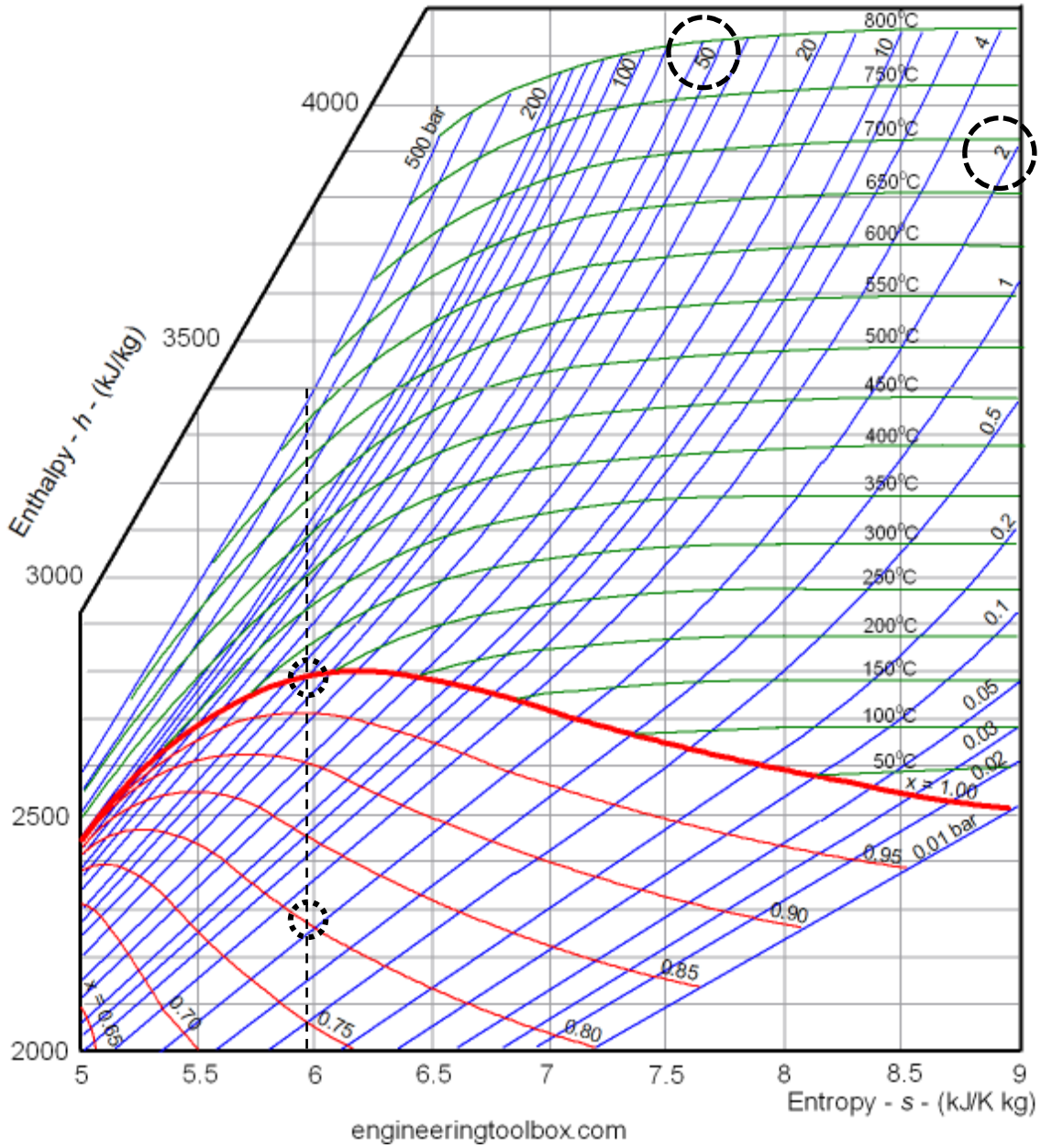

Figure D.3. Mollier diagram [4]

D.2 References for Appendix D

[1] J. A. Moyer, *Steam Turbines*, John Wiley & Sons, New York, NY (1914).

[2] http://www.efunda.com/materials/water/steamtable_sat.cfm

[3] R. C. Weast, *Handbook of Tables for Applied Engineering Sciences* 2nd Edition, CRC Press, Cleveland, OH (1973).

[4] http://www.engineeringtoolbox.com/mollier-diagram-water-d_308.html

DISTRIBUTION

1 Richard A. Reister
U.S. Department of Energy (DOE-NE-72)
Federal Programs Manager
Germantown, MD

1 Kathryn A. McCarthy
DOE-NE-72 Director, Light Water Reactor Sustainability Technical Integration Office
Idaho National Laboratory
Idaho Falls, ID

1 Michael L. Corradini
DOE-NE-72 Reactor Safety Technologies Program Manager
University of Wisconsin
Madison, WI

1	MS1219	Chisom Wilson	5943
1	MS0747	Charles Morrow	6223
1	MS0748	Randall Gauntt	6232
1	MS0748	Kyle Ross	6232
1	MS0748	Jeff Cardoni	6232
1	MS0748	Doug Osborn	6232
1	MS0899	Technical Library	9536 (electronic copy)

(This page intentionally left blank)


Sandia National Laboratories